In vitro induction of the apoptotic intrinsic pathway via a new antimitotic agent

by

Elize Wolmarans

28023766

Submitted in partial fulfilment of the requirements for the degree **Master of Science (Physiology)**

at the Faculty of Health Sciences

University of Pretoria

2014

Supervisor:

Prof. A Joubert
Department of Physiology, University of Pretoria, South Africa

Co-Supervisors:

Dr. K Sippel
Department of Biochemistry and Molecular Biology, Baylor College of Medicine, Texas, USA

Prof. R McKenna
McKnight Institute, University of Florida, Florida, USA

Statement of original authorship

I hereby declare that this dissertation, which I hereby submit in fulfilment of part of the requirements for the degree Master of Science (Physiology) at the University of Pretoria, is my own work that has not been previously submitted for a degree at this or any other University.

Summary

Unique, *in silico*-designed compounds with possible anticancer properties were identified in our laboratory. 2-Ethyl-3-*O*-sulphamoyl-estra-1,3,5(10)16-tetraene (ESE-16), with potential carbonic anhydrase IX inhibiting activity, is capable of interfering with microtubule dynamics.

In this study, it was investigated whether ESE-16 is capable of inducing apoptosis *in vitro* in the esophageal carcinoma SNO cell line via the intrinsic pathway at a concentration of 0.2µM with an exposure time of 24 hours.

Qualitative results were obtained via polarization-optical transmitted light differential interference contrast microscopy, light microscopy, transmission electron microscopy and confocal microscopy. Results showed hallmarks of apoptosis in the ESE-16-treated cells. In addition, data revealed an increase in the number of ESE-16-treated cells blocked in metaphase. Cell death via apoptosis in the ESE-16-treated cells was confirmed by studying the internal ultrastructure of the cells via transmission electron microscopy, while confocal microscopy revealed abnormal spindle formation and condensed chromatin in ESE-16-treated cells, confirming metaphase block.

Quantitative results were obtained via flow cytometry and spectrophotometry. Cell death via apoptosis in ESE-16-treated cells were quantitatively confirmed by cell cycle progression analysis and the Annexin V-FITC apoptosis detection assay. Metaphase block due to ESE-16 exposure was confirmed by demonstrating an increase in cyclin B levels in the ESE-16-treated cells. In addition, flow cytometry and spectrophotometry revealed dissipation of mitochondrial membrane potential, an increase in superoxide levels, changes in the redox status and an increase in cytochrome *c* levels in the cytosol of the ESE-16-treated cells. Both initiator caspase 9 and effector caspase 3 activities were increased, which demonstrates that ESE-16 causes cell death in a caspase-dependent manner.

This was the first *in vitro* study conducted to investigate the action mechanism of ESE-16 on an esophageal carcinoma cell line. The results provided valuable information on the action mechanism of this potential anticancer agent. It can be concluded that the novel *in silico*-designed compound exerts an anti-proliferative effect on the esophageal carcinoma SNO cell

line by disrupting microtubule function resulting in metaphase block. This culminates in apoptotic cell death via the intrinsic apoptotic pathway. This research provided cellular targets warranting *in vivo* assessment of ESE-16's potential as an anticancer agent.

Key Words: 2-Ethyl-3-*O*-sulphamoyl-estra-1,3,5(10)16-tetraene, esophageal carcinoma, intrinsic apoptotic pathway

Research Outputs

Publications

- Nkandeu DS, Mqoco TV, Visagie MH, Stander BA, **Wolmarans E**, Cronje MJ and Joubert AM. *In vitro* changes in mitochondrial potential, aggresome formation and caspase activity by a novel 17-beta-estradiol analogue in breast adenocarcinoma cells. Cell Biochem Funct. 2013; 31(7):566-574.

- **Wolmarans E**, Mqoco TV, Stander A, Nkandeu SD, Sippel K, McKenna R and Joubert A. Novel Estradiol Analogue Inhibits Esophageal Carcinoma Proliferation. Cell Mol Biol Lett. 2014; [Epub ahead of print].

Conference Proceedings

- **Wolmarans E**, Mqoco TV, Stander A, Marais S and Joubert AM. Possible Induction of Autophagy and Apoptosis by a novel 17-Beta-Estradiol Analogue in Esophageal Carcinoma Cells. South African Magazine of Science and Technology. 2012; 31(1): 304.

Conferences

Oral Presentations

- **Wolmarans E**, Mqoco TV, Stander A, Marais S, Joubert AM. Possible Induction of Autophagy and Apoptosis by a novel 17-Beta-Estradiol Analogue in Esophageal Carcinoma Cells. South African Academy of Sciences, Johannesburg, South Africa, 2011.

- **Wolmarans E**, Joubert AM. 2-Ethyl-3-*O*-sulphamoyl-estra-1,3,5(10)16-tetraene Induces Cell Death via the Intrinsic Pathway of Apoptosis. Faculty Day, Faculty of Health Sciences, University of Pretoria, South Africa, 2012 and South African Academy of Sciences, Potchefstroom, South Africa, 2012.

- **Wolmarans E**, Joubert A, Sippel KH, McKenna R. *In vitro* induction of the apoptotic intrinsic pathway via a novel *in silico*-designed antimitotic agent. Faculty Day, Faculty of Health Sciences, University of Pretoria, Pretoria, South Africa, 2013 and South African Academy of Sciences, Pretoria, South Africa, 2013.

Poster Presentations

- **Wolmarans E**, Mqoco TV, Stander A, Marais S, Joubert AM. Possible Induction of Autophagy and Apoptosis by a novel 17-Beta-Estradiol Analogue in Esophageal Carcinoma Cells. Faculty Day, Faculty of Health Sciences, University of Pretoria, Pretoria, South Africa, 2011. **Won first prize for poster presentation.**

- **Wolmarans E**, Joubert A, Sippel KH, McKenna R. *In vitro* induction of the apoptotic intrinsic pathway via a novel *in silico*-designed antimitotic agent. The International Cell Death Society (ICDS) Conference, Malaga, Spain, 2013.

- **Wolmarans E**, Joubert A, Sippel KH, McKenna R. *In vitro* induction of the apoptotic intrinsic pathway via a novel *in silico*-designed antimitotic agent. Physiology Society of Southern Africa (PSSA) Conference, Pretoria, South Africa, 2013. **Won first prize for poster presentation.**

Acknowledgements

- Thank you to the following organisations for the funding which enabled me to complete this MSc: the National Research Foundation (NRF), the Medical Research Council of South Africa (MRC), the Cancer Association of South Africa (CANSA), the Struwig-Germeshuysen Cancer Research Trust of South Africa, the Institute of Cellular and Molecular Medicine (ICMM) and the Research Committee (School of Medicine) of the University of Pretoria.

- Thank you to Prof D van Papendorp, head of the Department of Physiology, for granting me the opportunity to conduct and complete my study in his department.

- Thank you to the Department of Pharmacology of the University of Pretoria, for the use of the flow cytometer.

- Thank you to the Electron Microscopy Unit of the University of Pretoria, for the use of their facilities and their friendly assistance.

- Thank you to Francinah for maintenance of the physiology laboratory.

- Thank you to the cellular research team of the Department of Physiology of the University of Pretoria for their support and assistance. I want to thank in particular: Ms M Visagie, Ms S Nkandeu, Ms L Repsold, Ms T Mqcoco, Mrs XX Stander and Dr A Stander. Thank you for always being there to lend a helping hand or give a word of advice.

- A special thank you to my supervisor, Prof A Joubert. Thank you so much for everything you have done for me. Your wisdom, knowledge, advice and unwavering support helped me more than you will ever know.

- Thank you to my friends and family for their love, support and encouragement.

- A very special thank you to my mom, dad and sister. You have been my pilars of strength, my safe haven and my inspiration. Thank you for always being there for me.

- Most importantly I wish to thank God. He has always guided me and gave me strength when I needed it most. To Him goes all the glory.

I wish to dedicate this work to the man that survived, Mr. David White and to the men who didn't: Mr. Dirk Nel, Ds. Robert Rottervield and my grandfather Ben Badenhorst.

Table of Contents

List of Abbreviations

2ME - 2-Methoxyestradiol

ΔΨm – Mitochondrial membrane potential

ADH - Alcohol dehydrogenase

AIF - Apoptosis-inducing factor

ALDH - Acetaldehyde dehydrogenase

ANT - Adenine nucleotide translocator

Apaf-1 - Apoptotic protease activating factor 1

APC/C - Anaphase-promoting complex/cyclosome

APO1 - Apoptosis antigen 1

Atg - Autophagy-related genes

ATM - Ataxia teleangiectasia mutated

ADP – Adenosine diphosphate

ATP - Adenosine triphosphate

BH - Bcl-2 Homology

CAII - Carbonic anhydrase II

CAIX - Carbonic anhydrase IX

CAD - Caspase activated deoxyribonuclease

CARDs - Caspase recruitment domains

Cdc20 – Cell division cycle protein

CDKs - Cyclin dependent kinases

CHK - Checkpoint kinase

CKIs - CDK inhibitors

CO_2 - Carbon dioxide

DAMPs - Damage-associated molecular patterns

DAPI - 4’,6-Diamidino-2-phenylindole

dATP - Deoxyadenosine triphosphate

DDT - Dithiothreitol

DISC - Death-inducing signaling complex

DMEM - Dulbecco's modified eagle medium

DMSO - Dimethyl sulphoxide

DNA - Deoxyribonucleic acid

DRs - Death receptors

E1 - Ubiquitin-activating enzyme

E2 - Ubiquitin-conjugating enzyme

E3 - Ubiquitin ligase

EA - Esophageal adenocarcinoma

EC - Esophageal cancer

EGFR - Epidermal growth factor receptors

EndoG - Endonuclease G

ESCC - Esophageal squamous cell carcinoma

ER - Endoplasmic reticulum

ESE-16 - 2-Ethyl-3-*O*-sulphamoyl-estra-1,3,5(10)16-tetraene

FACS - Fluorescence-activated cell sorting

FADD - Fas-associated death domain

FasL - Fas ligand

FB1 - Fumonisin B1

FCS - Fetal calf serum

FITC - Fluorescein isothiocyanate

G_0 - Quiescent phase

GDP - Guanosine diphosphate

GSH - Glutathione

GTP - Guanosine triphosphate

H_2O_2 - Hydrogen peroxide

HCO_3^- - Bicarbonate

HE - Hydroethidine

H&E - Haematoxylin and eosin

IARC - International Agency for Research on Cancer

IMM - Inner mitochondrial membrane

LC3 - Light chain 3

MAPK - Mitogen-activated protein kinase

MAPs - Microtubule-associated proteins

MCC - Mitotic checkpoint complex

MDM2 - Murine double minute 2

MFI - Mean fluorescent intensity

MMP - Mitochondrial membrane permeabilization

MIDs - Microtubule-interfering drugs

MOMP - Mitochondrial outer membrane permeabilization

MPF - Mitosis-promoting factor

MTOC - Microtubule-organizing center

NAD^+ - Nicotinamide adenine dinucleotide

NADH - Reduced nicotinamide adenine dinucleotide

$NADP^+$ - Nicotinamide adenine dinucleotide phosphate

NADPH - Reduced nicotinamide adenine dinucleotide phosphate

NCD - Nanocrystal dispersion

O_2 - Oxygen

O_2^- - Superoxide

OMM - Outer mitochondrial membrane

PARP - Poly(ADP-ribose) polymerase

PE - Phosphatidylethanolamine

PBS - Phosphate buffered saline

PI - Propidium iodide

PI3K - Phosphatidylinositol 3-kinase

PlasDIC - Polarization-optical differential interference contrast

*p*NA - *p*-Nitroanilide

pRb - Retinoblastoma protein

PS - Phosphatidylserine

PTP - Permeability transition pore

RIP1 - Receptor-interacting protein kinase 1

ROS - Reactive oxygen species

RNS - Reactive nitrogen species

Ser - Serine

SAC - Spindle assembly checkpoint

SCC - Sister-chromatid cohesion proteins

SCF - SKP1–CUL1–F-box

SMC - Structural maintenance of chromosome proteins

Thr - Threonine

TEM - Transmission electron microscopy

TNF - Tumour necrosis factor

TOR - Target of rapamycin

TRAIL - TNF-related apoptosis inducing ligand

UPS - Ubiquitinatin-proteasome system

VDAC - Voltage-dependent anion channel

VEGF - Vascular endothelial growth factor

WHO - World Health Organization

Graphical representation of biochemical pathways

All graphical figures representing biochemical pathways were designed by E Wolmarans using Microsoft® Powerpoint® for Mac 2011, version 14.3.6 (130613).

List of Figures

List of Tables

Chapter 1
Literature Review

1.1) Overview of cancer

According to the World Health Organization (WHO), cancer is a generic term for a large group of diseases that can effect any part of the body (1). This disease arises from a single normal cell, which undergoes transformation into a tumor cell via a multi-stage process (1). The transformation normally results from a interaction between a person's genetic factors and external agents such as physical, chemical and biochemical cancer causing agents or carcinogens (1). This disease is increasing due to population aging and the adoption of cancer-associated lifestyles which include smoking, alcohol consumption and physical inactivity (2-4).

Cancer is the second leading cause of death in economically developing countries (2). Jemal and colleagues published statistics in 2011 derived from the International Agency for Research on Cancer (IARC), GLOBOCAN 2008, which estimates the worldwide incidence and mortality of cancer (2,5). Incidence data were obtained from population-based cancer registries, while the total number of cancer deaths per country was made available by the WHO (2). The report stated that about 12.7 million cancer cases were diagnosed and 7.6 million cancer deaths were estimated to have occurred in 2008 worldwide (2). Deaths from cancer are projected by the WHO to continue rising worldwide, with an estimated 13.1 million deaths in 2030 (1).

1.2) Incidence and causes of esophageal cancer

Esophageal cancer (EC) is the 8th most common incident cancer in the world and due to its high fatality rate, ranks 6th among all cancers in mortality (3,4,6,7). An estimated 482 300 new EC cases and 406 800 deaths occurred in 2008 worldwide (2). The highest incidence rates in both males and females were found in Eastern Asia and Eastern - and Southern Africa (2,3,8). Occurrence of EC increases with age with the highest incidence found in the age group of 50–70 years (6,9) with EC 3 to 4 times more common in males than in females (2,3).

Typically, EC involves malignancy which arises from the epithelium of the esophagus (7). EC can be classified histologically into two main types: esophageal squamous cell carcinoma (ESCC), which occurs in the upper one-third or middle of the esophagus and esophageal adenocarcinoma (EA), which occurs in the lower one-third of the esophagus or at the esophagus and stomach junction (2,4,10). EA is primarily associated with gastric reflux and Barret's esophagus, while ESCC is mainly associated with smoking and alcohol consumption (8). They also differ in incidence trends with EA dominating the western world, while ESCC dominates the rest of the world (4). In recent years ESCC incidence decreased in more developed countries, but remains the same in high risk areas such as China, Iran and South Africa (2,3,8,10).

Risk factors that may lead to ESCC can be divided into two groups: changeable and unchangeable risk factors (Table 1.1). Changeable risk factors frequently includes chronic exposure to irritants, hot drinks, smoking and alcohol consumption, whereas unchangeble risk factors include age, sex and hereditary factors (4,6).

The two most common risk factors for ESCC is chronic smoking and alcohol consumption (2,6-8), having been shown to account for up to 90% of the total cases of ESCC (2,3,11). It has been reported that smoking and drinking can have a synergistic effect, increasing the risk of EC up to a 100-fold (7).

Carcinogenesis due to smoking is believed to occur due to the presence of a large number of carcinogens in minute quantities such as polycyclic aromatic hydrocarbons, nitrosamines and acetaldehydes having a cumulative effect over several years (4,7,9). Nitrosamines have been confirmed as one of the most powerful and stable carcinogenic factors in EC (7). Nitrosamines are metabolized to a chemically active alkylating agent that produces alkylating intermediates that can form O^6-alkylguanines from deoxyribonucleic acid (DNA) guanine (9). Guanine mispairs with thymine rather than cytosine, possibly initiating carcinogenesis (9).

Alcohol, in excessive amounts, has almost universally been associated with the elevated risk of ESCC (4). Alcohol's conversion to acetaldehyde, or its ability as a highly active solvent, especially of fat-soluble compounds, may play a role (4,7,11). Acetyldehyde metabolized from ethanol is highly carcinogenic by forming DNA adducts which causes mutations in

tumor suppressor genes (11). Ethanol is converted to acetaldehyde by alcohol dehydrogenase (ADH) enzymes and then to acetate by acetaldehyde dehydrogenase (ALDH) enzymes (4,11).

The role of acetyldehyde in carcinogenesis has been shown *in vitro,* with acetaldehyde causing point mutations (where adenine is substituted for a guanine at adenine/thymine base pairs) in the HPRT reporter gene (12). In addition, genetic polymorphisms in ADH genes and ALDH2 (the key enzyme in ethanol metabolism) that favor the accumulation of acetaldehyde have been observed to increase ESCC risk, adding to the evidence of acetaldehyde carcinogenicity in humans (4,11).

One of the possible mechanisms in which smoking and alcohol bring about their synergistic effects may be the ability of hazardous material, such as benzo-a-pyrene, in tobacco to quickly invade esophagus epithelia due to ethanol being a highly active solvent (11). Ethanol also inhibits cell metabolic activity and detoxification functions of the epithelial cells (7). Another possible mechanism may be poor oral hygiene caused by heavy smoking and drinking (11). Poor oral hygiene causes changes in bacteria in the oral cavity which may result in higher acetyldehyde production from ethanol in saliva (11). The activation of cytochrome P450 2E1 also appears to be important in the synergistic effect of tobacco and alcohol (11). Chronic alcohol consumption activates cytochrome P450 2E1, which primarily metabolizes ethanol to acetaldehyde in the liver (11). Its activation leads to the generation of reactive oxygen species (ROS), reactive nitrogen species (RNS) and increases the activation of nitrosamines from tobacco smoke into active carcinogens (11).

Infectious agents also play a role in the development of EC. Fungi contaminating wheat and maize has been associated with EC (6). Epidemiologic studies have shown a strong association between the consumption of fumonisin B1 (FB1)-contaminated maize and the incidence of ESCC in regions with a very high frequency of EC such as the Henan Province of China and the Transkei region of South Africa (8,9,13). This may explain the high incidince rate of EC in South Africa.

The mycotoxin FB1 occurs in high concentrations in maize in the above-mentioned high risk areas due to a soil-borne fungus named *Fusarium verticillioides* (8,9,13). Research has suggested the FB1 is a slow-acting carcinogen since it is poorly absorbed and only becomes cytotoxic after accumulation over time, which may explain the late onset of EC (50–70 years)

in humans (6,9).

Fumonisins have been shown to have tumour promoting and cell cycle dysregulating abilities (8). The carcinogenic characteristics of FB1 may be due to the presence of an amino group and the location of the hydroxyl on the C14/C15 position, which facilitates the conjugation of FB1 via gluteraldehyde to protein carriers (9). It is believed that FB1 may act as a promotor or initiator of carcinogenesis in synergy with certain co-carcinogens such as nitrosamines found in tobacco (9).

Table 1.1: Changeble and unchangeble risk factors which may cause the development of esophageal cancer.

Changeable Risk Factors	
Habits	Alcohol consumption (3,4,6,8)
	Tobacco use (3,4,6,8)
	Opium use (4)
	Drinking maté (4,6)
Diet	Pickled vegetables (4,6)
	Low consumption of fruit and vegetables (3,4,6,8)
	Vitamin and mineral deficiencies (4,6)
Infectious Agents	Human papillomavirus (4,8)
	Fungi (4,6,8)
Chemical Carcinogens	Polycyclic aromatic hydrocarbons (4)
	N-Nitroso compounds (4,6)
	Acetaldehyde (4)
	Fumonisins (4)
Predisposing Conditions	Obesity (4)
	Poor oral hygiene (4)
Occupational Exposure (4)	
Socioeconomic Status (4,6)	
Unchangeable Risk Factors	
Age (6)	
Sex (6)	
Hereditary	Tylosis (6)
	Plummer – Vinson syndrome (6)

1.3) Overview of esophageal cancer treatments

The prognosis of EC is generally unfavourable, with an approximated long-term survival rate of only 5% (6). Patients (10–20 %) survive 5 years if they undergo radical esophagectomies; if the cancer is inoperable, the average survival time is 13–29 months (6-8). Reasons for the low survival rate are multiple: it can be due to ineffective screening tools, late detection of the cancer, unreliable non-invasive tools to accurately measure response to chemotherapy and the possibility of cancer recurring after surgery and chemotherapy (14).

Treatment decisions are often made based on the individual, taking into account the stage of the cancer and underlying comorbidities (14). During the early stages, surgery is still the mainstay treatment for EC (15). The optimal treatment for locally advanced EC is controversial. Currently, the best two options is a coin-toss between cisplatin-based chemoradiation and surgery; both treatments offering similar rates in local control, survival and mortality (14). Patients with bulky advanced tumors, unlikely to be cured surgically, are first treated with preoperative chemoradiation, followed by salvage surgery (14). Metastatic or unresectable EC remains incurable, with chemotherapy only improving quality of life and dysphagia in 60%–80% of patients (14).

Advances in nonsurgical therapies have arisen out of a need to treat patients that do not have a surgical option due to cancer stage or comorbid illness (16). Surgery has been challenged with less invasive approaches such as limited resection, organ-preserving treatment and endoscopic therapies which include endoscopic mucosal resection, radiofrequency ablation, and cryotherapy (15,16).

Another well-known therapy for EC is chemotherapy, which can be administered as a single agent or in combination (14). Despite significant progress, cancer treatments have not met expectations and cancer research is focused on innovation to address bioavailability and delivery methods of anticancer compounds.

The drug development field has been transformed by targeted treatments and their ability to direct treatment at specific molecular targets (14). These targets include proteins related to growth regulation, such as epidermal growth factor receptors (EGFR), proteins related to

angiogenesis, such as vascular endothelial growth factor (VEGF), proteins related to apoptosis (p53, bax, and Bcl-2) and proteins related to cell cycle control (p16, p21) (10,14).

1.4) Overview of the cell cycle

The cell cycle is the complex process involved in the growth and proliferation of cells and can be morphologically subdivided into interphase and the mitotic (M) phase (Figure 1.1) (17,18). Interphase consists of the G_1, S and G_2 phases. G_1 (the first gap) phase allows for protein synthesis in preparation for DNA replication which occurs during S phase and the G_2 (the second gap) phase prepares the cell for the M phase (17,19).

Cell cycle progression is controlled on three levels. The first level controls the general functions of the cell such as DNA synthesis and chromosome seperation via phosphorylation and dephosphorylation (20). The second level controls the movement of the cell through the cell cycle which is dependent on cyclin dependent kinases (CDKs) (17,18,20). The CDKs are controlled by the heterodimeric protein kinases (cyclins) and CDK inhibitors (CKIs) (20). The third level controls protein levels of cell cycle-related regulators such as cyclins and CKIs, which is done by ubiquitylating enzymes (20).

Most signaling pathways inside the cell are regulated by protein phosphorylation and dephosphorylation, which are controlled by the activities of both protein kinases and protein phosphatases (21). Protein phosphatases have been classified into two major families: the protein serine/threonine (Ser/Thr) phosphatases, which remove the phosphoryl group from Ser/Thr residues and the protein tyrosine phosphatases which dephosphorylate tyrosine residues in phosphoprotein substrates (21).

The second level of control of the cell cycle is regulated by cyclins and their catalytic subunits, CDKs (18,22,23). CDKs are Ser/Thr protein kinases which are activated at certain points of the cell cycle and are critical for cell cycle progression (17,18,20). Their function is to phosphorylate target proteins on critical Ser/Thr sites which allows the cell cycle to continue (17,24). Each CDK is dependent on a particular cylin which are needed to activate and guide the CDKs by binding to them and phosphorylating certain protein residues of the CDKs (17,20,24). In addition to activating the CDKs, cyclins also help to target the CDKs to the nucleus of the cells with the assistance of their nuclear localization signals (17).

The levels of CDKs are relatively constant throughout the cell cycle while the levels of the cyclins vary (20,24). Varying cyclin levels can be explained by the presence of PEST sequences, present in cyclins (17,20,22). These sequences contains peptides proline (P), glutamic acid (E), serine (S) and threonine (T), which targets them for degedation at certain times via the ubiquitinating-proteasome system (UPS) (17,20,22). This results in the degradation and synthesis of cyclins during certain stages of the cell cycle with the CDKs only being active during the time that their corresponding cyclin is present (17,18,24). There are a variety of cyclin/CDK complexes that are formed during the distinct phases of the cell cycle (18,24).

The third level of control is maintained by ubiquitylating enzymes which forms part of the UPS. Contrary to reversible modifications done via phosphorylation or association with CKIs, ubiquitin-mediated proteasomal degradation is an irreversible mechanism which plays an essential role in the strict unidirectionality and regulation of the cell cycle (25).

The UPS consists of two steps: the covalent attachment of the small 76-amino-acid polypeptide ubiquitin protein to the protein substrate (ubiquitylation) and the degradation of the polyubiquilated protein by a proteosome complex (20). The first step occurs through a three-stem enzymatic cascade: the ubiquitin-activating enzyme (E1), the ubiquitin-conjugating enzyme (E2) and the ubiquitin ligase (E3) (20,25). Ubiquitin is first bound and activated by E1 in an adenosine triphosphate (ATP)-dependent manner and is subsequently transferred to E2 before being covalently attached to the target protein by E3, leading to the formation of a polyubiquitin chain (20,25). The polyubiquitylated protein is recognized by a proteasome, and is destroyed in an ATP-dependent manner (20). This process is known as the ubiquitin-proteasome pathway.

E3 is defined as a protein or protein complex that facilitates the transfer of ubiquitin from E2 to the substrate thereby coordinating the ubiquitylation of the selected protein substrate (20). Two major classes of ubiquitin ligases which have a central role in cell cycle regulation is the SKP1–CUL1–F-box-protein (SCF) complex and the anaphase-promoting complex/cyclosome (APC/C) (20,25). SCF ligases drive cell cycle progression throughout the cell cycle, while APC/C orchestrates exit from mitosis and establishes a stable G_1 phase (25).

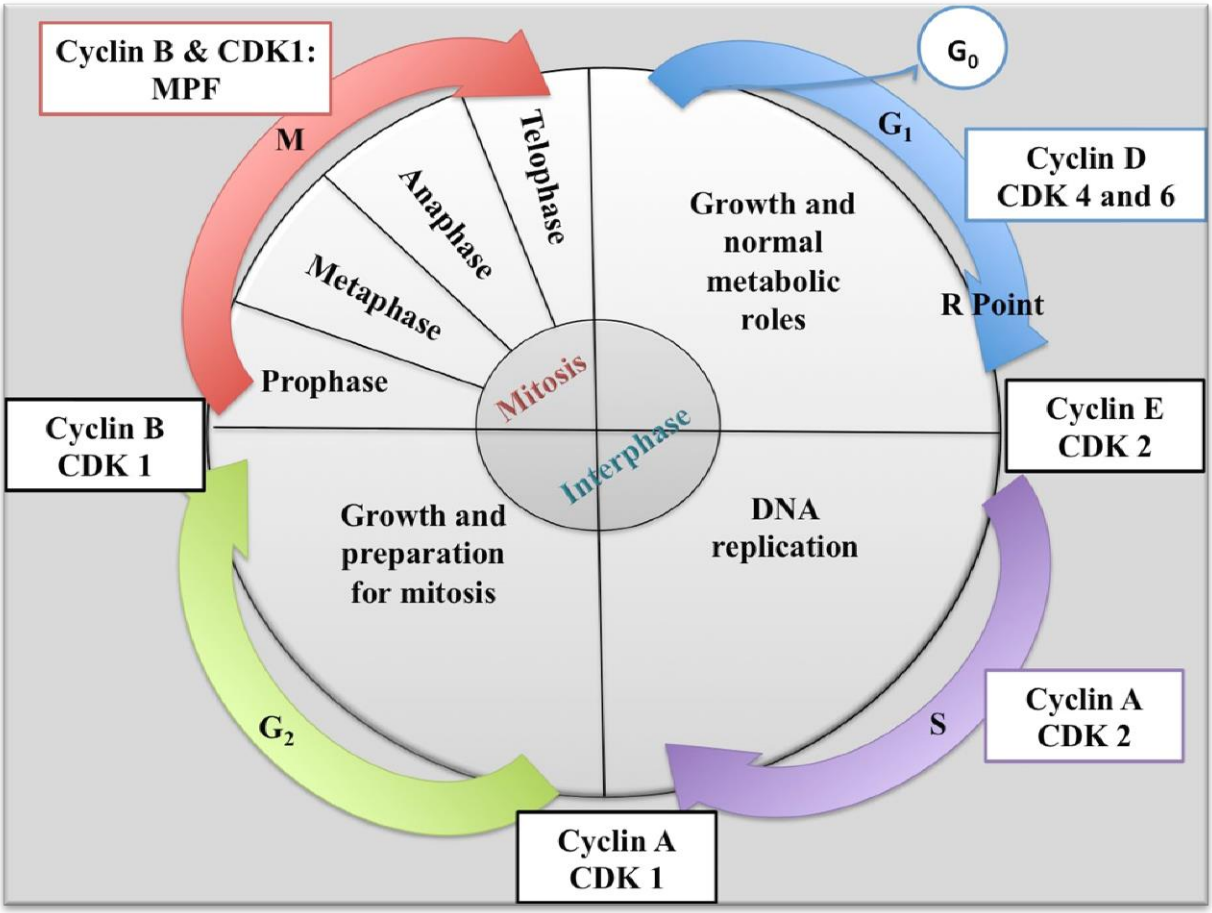

Figure 1.1: Graphical representation of the cell cycle. The cell cycle can be subdivided into interphase and the M phase. Interphase consists of the G_1, S and G_2 phases. The cell cycle is controlled by cyclins and their catalytic subunits, CDKs. There are a variety of cyclin/CDK complexes that are formed during the distinct phases of the cell cycle with cyclins associating with specific CDKs at specific times during the cell cycle.

Interphase consists of the G_1, S and G_2 phases (17). As mentioned previously, there are a variety of cyclin/CDK complexes that are formed during the distinct phases of the cell cycle (18,24). Cyclins are associated with specific phases of the cell cycle: cyclin D is associated with G_1, cyclins E and A with the S phase and cyclins B and A with the M phase (26).

During G_1, protein synthesis within the cell occurs (27). This phase is regulated by Cyclin D and CDKs 4 and 6 (17,23,24). One of the most important targets for the activated cyclin/CDK complex in the G_1 phase is the retinoblastoma protein (pRb) which serves as the decision point at the end of the G_1 phase termed the restriction point (17,24). At this point the cell decides to commit itself to continue with the cell cycle or enter the quiescent phase (G_0) (24). With sufficient mitogen stimulation and cell growth, the cells commits to cell division and the cyclin/CDK complex catalyzes the phosphorylation and the inactivation of pRb which is bound to and inhibiting E2F transcription factors (17,25). With the phosphorylation of pRb,

E2F is released and participates in the transcription of proteins such as dihydrofolate reductase, thymidine kinase and DNA polymerase which is needed for the cell cycle to continue (Figure 1.2) (17,22).

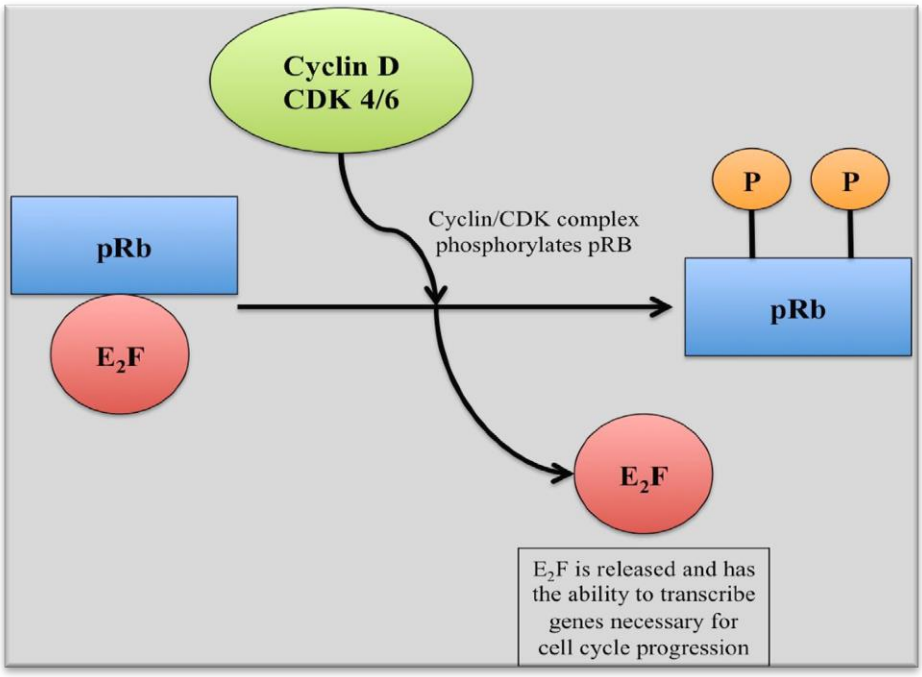

Figure 1.2: Phosphorylation of the retinoblastoma protein. The cyclin/CDK complex catalyzes the phosphorylation and the inactivation of pRb which is bound to E2F transcription factors. Once pRb is inactivated E2F is released and able to start the transcription of proteins needed for the continuation of the cell cycle.

In mid to late G_1 phase, Cyclin E is synthesized and forms complexes with CDK2 which is essential for the cell to enter the S phase (18,22,24,25). Before the activation of the cyclin E/CDK2 complex, the CKI proteins, providing additional control to the cell cycle, must be broken down (22). These CKIs include $p21^{Waf1}$, $p27^{Kip1}$ and $p57^{Kip2}$ and their breakdown is catalyzed by the ubiquitin-conjugating enzyme Cdc34 and the Cdc53-dependent ubiquitin-ligase SCF (22). After the degradation of the inhibitors, the complex becomes activated and the cell cycle continues. As the cell transitions from the G_1 to the S phase, the two centrioles of the centrosome separate and start to duplicate (28).

During the S phase, DNA replication occurs (27). Cyclin E/CDK2 and cyclin A/CDK2 are the two main cyclin/CDK complexes in the S phase and mediate the initiation of DNA and centrosome duplication (25). Cyclin A appears along with the onset of DNA replication and is required for both S phase progression and the early steps in mitosis (22,24). Cyclin A associates initially with CDK2 and later with CDK1, where it remains bound until cyclin B

appears late in the G_2 phase (24,25). In late G_2, the two centrioles, still remaining together as a single complex, grow in size and reach the appropriate dimensions (28).

CDK1, also known as the cell division cycle protein (Cdc20), is essential for driving the cell from G_2 phase into the M phase (23,29). Apart from it becoming active only when bound to the appropriate cyclin (26), CDK1 is also inhibited when bound to CKIs which includes members of the $p21^{Cip1}$ family (30). CDK1 function is also inhibited by the phosphorylation of the location Tyr15 by Wee1 kinase (30). In late G_2, $SCF^{\beta\text{-}TrCP}$ promotes activation of CDK1 by mediating the degradation of Wee1 (25).

The M phase consists of nuclear division (mitosis) and cytoplasmic division (cytokinesis) (28,29). Mitosis is the process where the cell's condensed chromosomes segregate into two identical daughter cells, each containing a full set of chromosomes and a single centrosome (18,19,29). During cytokinesis, the cytoplasm and its contents are partitioned into two daughter cells (29). Mitosis can be further subdivided into prophase, prometaphase, metaphase, anaphase and telophase (17,27,29).

Cyclin B and CDK1 form the mitosis-promoting factor (MPF) that allows the cell to enter the mitotic phase (18,22,24,31). Phosphorylation reactions catalyzed by the MPF orchestrates essential steps in early mitosis including chromosomes condensation, nuclear envelope breakdown and the assembly of the mitotic spindle apparatus (22,25,29,31,32).

During prophase, the majority of chromatin condensation occurs (19). The sister chromatids are tightly coupled by large multisubunit cohesin protein complexes at a specific point known as the centromere (19,33). The cohesin complex consists of two structural maintenance of chromosome (SMC) proteins, SMC1 and SMC3, and two sister-chromatid cohesion (SCC) proteins, SCC1 and SCC3 (33). The centromere is the place where the chromosome develops specializations, known as kinetochores, for the attachment to the machine that will effect seggregation (19). Kinetochores are made up of about 30 scaffold proteins which create a solid link between the chromatin and the mitotic spindle (31,34). The breakdown of the nuclear envelope also occurs during prophase. The envelope consists of a double membrane adjoining the endoplasmic reticulum (ER) and lies over the lamina, a shell made from polymers of the nuclear lamin proteins (26). As cells enter mitosis, the lamins are phosphorylated by the cyclin B/CDK1 complex and becomes depolarized (26). Also during

prophase, two radial array of microtubules, called asters, move to opposite sides of the nucleus to initiate the formation of the two poles of the mitotic spindle (28). Prophase ends when the condensed chromosomes begin to interact with the segregtion machine – the mitotic spindle (19).

The mitotic spindle is a very dynamic cytoskeletal structure made up of microtubules and hundreds of associated proteins (18,19,28). The spindle formation initiates the prometaphase mitotic stage, during which chromosome organization takes place (19). During prometaphase, the chromosomes attach to the mitotic spindle microtubules via their kinetochores (28) and migrates to the equator of the cell (19). At metaphase, the chromosomes are aligned at the equator of the mitotic spindle, forming the metaphase plate (19,28).

During anaphase, the cohesins that have been holding the sister chromatids together are cleaved by proteases and the chromosomes separate to the two poles of the spindle via a shortening of the kinetochore microtubules (19,28). Mitosis is complete by the end of telophase when the two sets of daughter chromosomes reach the poles of the spindle and decondense and a new nuclear envelope reassembles around each chromosome set, forming two nuclei (19,28).

1.4.1) Overview of the cell cycle checkpoints

Cell cycle checkpoints regulate the progression of the cell cycle to ensure accurate duplication, segregation and distribution of chromosomes and will delay or prevent cell cycle progression if there is any fault with cellular processes or cellular proteins (18,22,28,35,36). According to K.A Schafer, the checkpoints can be defined as: “the biochemical pathways which ensures that unrelated biochemical processes are dependent on one another and can trigger cell cycle arrest in the different phases” (17).

1.4.2) Spindle assembly checkpoint

The spindle assembly checkpoint (SAC) is a kinetochore-associated sensor that monitors the correct attachment of chromosomes to the microtubules and ensures accurate segregation of the chromosomes (Figure 1.3) (19,22,28). It is comprised of a signal transduction cascade which delays the onset of anaphase until all spindle microtubules are correctly attached to the

kinetochores of each individual chromosome (22,37). Kinetochores, creates attachments between the chromosomes and the microtubules (34) and plays a key role in sensing defects in the spindle architecture and in allowing the cell cycle to progress (28). SAC uses information about the interaction between the chromosomes and the microtubules to regulate APC/C, the target of the checkpoint (26).

As mentioned earlier, APC/C orchestrates the exit from mitosis and establishes a stable G_1 phase (25). Its activation is required for separation of sister chromatids (22,23,28). Two activators of the APC/C are Cdc20 and Cdh1 (20). Cdc20 targets securin and mitotic cyclins for degradation, promoting sister-chromatid separation, while Cdh1 facilitates exit from M phase and maintains G_1 phase by mediating the degradation of mitotic cyclins, non-CDKs, mitotic kinases and some regulators of the formation of pre-replicative complexes (20).

After complete kinetochore attachment by all chromosomes, the APC/C subunits are phosphorylated (catalyzed by activated CDK1) and bound to Cdc20 (22). The activated APC/C^{Cdc20} complex then assists in cell cycle progression by degrading cyclin A during prometaphase and during metaphase/anaphase transition (25). The activated APC/C^{Cdc20} complex then initiates anaphase by targeting securin for degradation (22,25).

During metaphase, the sister chromatids are tightly coupled by large multisubunit cohesin protein complexes (19,25,33). Securins (such as Pds1) are chaperones that bind and inhibit separase, enzymes capable of cleaving cohesin (25). With the degradation of securin, separase (such as Esp1) is released and cohesin is cleaved, leading to sister chromatid segregation (22,25). Esp1-dependent proteolysis of SCC1, an important component of the cohesin complex, directly facilitates segregation of sister chromatids (22,33).

The APC/C^{Cdh1} complex is activated late in mitosis and facilitates the exit from mitosis and the entrance into G_1 phase by targeting a variety of proteins involved in DNA replication, cycle progression and mitosis (22,25). Among the targets that promote DNA replication is Cdc6, which binds to the origin recognition complex to form pre-replication complexes (25). APC/C^{Cdh1} also regulates pro-proliferative signal transduction by targeting Ets2, a transcription factor involved in Ras–Raf–mitogen-activated protein kinase (MAPK) signaling pathway that induces the expression of cyclin D, thus allowing the continuation of the cell cycle (25).

However, until all kinetochores are correctly attached to the spindle fibers and the chromosomes are properly aligned on the metaphase plate, the SAC inhibits APC/C activation and prevents the continuation of the cell cycle (25). The key step in the SAC appears to be the interaction of two complexes at the kinetochore (26). The complexes consist of mitotic checkpoint proteins such as Bub1, Bub3, Mad1 and Mad2 (26,28,37). The one complex, consisting of the Bub1, Bub3, and Mad3 proteins, is thought to reside at the kinetochore, whereas the other complex, consisting of Mad1 and Mad2 proteins are soluble (22,26). At kinetochores without attached microtubules, the complexes interact and generate a new complex containing Mad2, Mad3/BubR1and Bub3 which binds to Cdc20 to form the mitotic checkpoint complex (MCC). This leads to sequestering of Cdc20 and direct inhibition of APC/C^{Cdc20} (25,26,37). Inhibition of APC/C prevents cyclin B and securing degradation, which will lead to the arrest of cell division in metaphase (22,28,37-39).

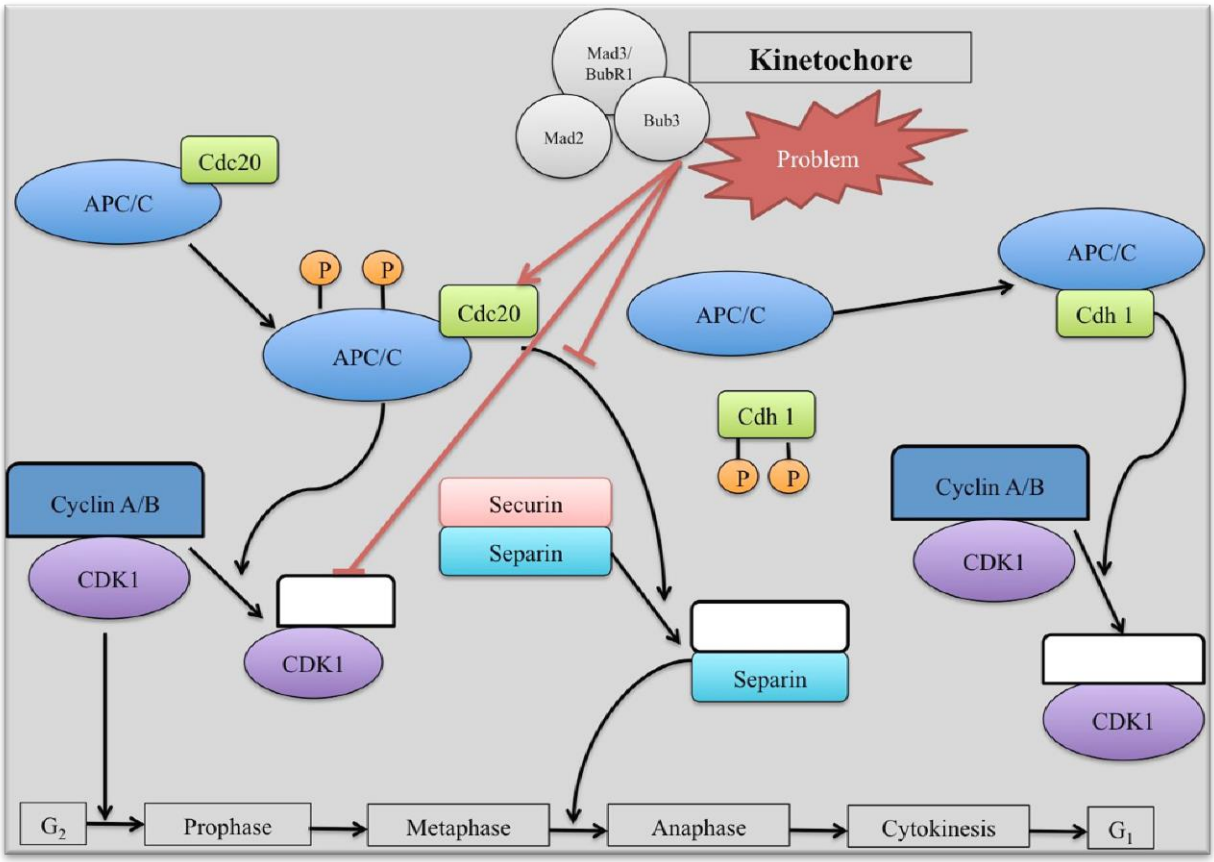

Figure 1.3: Schematic representation of the spindle checkpoint. The activation of APC/C allows for the separation of the sister chromatids, exit from mitosis and establishing a stable G_1 phase. The two activators of the APC/C are Cdc20 and Cdh1. Cdc20 targets securin and mitotic cyclins for degradation, promoting sister-chromatid separation. Cdh1 facilitates exit from M phase and maintains G_1 phase by mediating the degradation of mitotic cyclins, non-CDKs, mitotic kinases and some regulators of the formation of pre-replicative complexes. If the SAC is activated due to abnormal spindle formation, the APC/C complex is inhibited preventing the continuation of the cell cycle. The APC/C complex inhibition is due to the interaction of complexes at the kinetochore generating a new complex containing Mad2, Mad3/BubR1and Bub3 that binds to Cdc20 to form the MCC, which sequesters Cdc20 and directly inhibits APC/C^{Cdc20}.

1.4.3) DNA damage checkpoint

The DNA damage checkpoint (Figure 1.4) of the cell is reponsible for stopping the cell cycle in case of DNA damage (29,40). These checkpoints contain sensor proteins that scan chromatin for partially replicated DNA, DNA strand breaks, or other abnormalities such as hypoxia, genotoxic compounds or spindle damage and translate these stimuli into biochemical signals that modulate the functions of specific downstream target proteins (22,36). DNA damage activates a number of molecules that will promote cell cyle arrest; the most noteworthy of these molecules is the tumor-suppressing transcription factor p53 protein (29,36).

When DNA of a cell is damaged, there is an accumulation p53, a response that is mediated primarily through an increase in this protein's stability (36,41). The p53 protein, in turn, has the ability to induce cell cycle arrest or cell death (22,40).

There are two main proteins that play a significant role in the stabilization of p53. The sensory molecule ataxia teleangiectasia mutated (ATM), which establishes multiple regulatory contacts with p53 (29,36) and the murine double minute (MDM2), a key regulator of p53 stability by acting as an ubiquitin ligase which targets p53 for polyubiquitination-mediated proteolysis (22,40).

Once activated, ATM can affect p53's stability in numerous ways such as activating checkpoint kinases (CHK) 1 and -2, which, in turn, phosphorylates Cdc25C – one of the proteins responsible for activating CDK1 (29). Phosphorylated Cdc25C associates with the p53 target molecule 14-3-3σ, resulting in CDK1 inactivation and cell cycle arrest between G_2 - and M phase (22,29).

ATM can also target the p53-MDM2 interaction by modifying the MDM2 protein (36). The MDM2 protein is a ubiquitin E3 ligase and key mediator of p53 protein stability by targeting p53 for polyubiquitination-mediated proteolysis once its bound to the amino-terminal transactivation domain of p53 (22,25). MDM2 contains a carboxy-terminal motif containing Ser395 in the S-Q target sequence, identified as a phosphorylation site for ATM (36). Ser395 phosphorylation favors stabilization of p53 by interfering with the shuttling activity of MDM2, which normally exports p53 out of the nucleus for proteosomal degradation in the cytoplasm (22,36).

Another mechanism for p53 stabilization involves an intermediate protein kinase, hCHK2, which relays ATM-dependent signals to p53 and many other downstream target proteins (36). ATM activates hCHK2 by phosphorylating its amino terminal Thr68, in turn; hCHK2 phosphorylates Ser20 in p53 (36). Phosphorylation at Ser20 interferes directly with the binding of p53 to MDM2, favoring p53 accumulation in response to DNA damage (36).

After stabilization and accumulation of p53, there are posttranslational modifications that regulate the transcriptional activating functions of certain proteins (36). One of the targets of p53 is the CKI protein p21 that prevent the cell from continuing the cell cycle (22). The p53-dependent increase in p21 expression suppresses cyclin E- and cyclin A-associated CDK2

activities, and thereby prevents G_1-to-S phase progression (22,36). Direct inhibition of transcription factors of the E2F family by $p21^{Waf1}$ may be another mechanism involved (22). The inhibition of the E2F will prevent the transcription of proteins needed for the cell cycle to continue (17,22). In addition to p21, p53 stimulates the expression of a large panel of genes, which, depending on the cellular context and type of initiating insult, may modulate intracellular redox status, or induce the cell to undergo cell death (36).

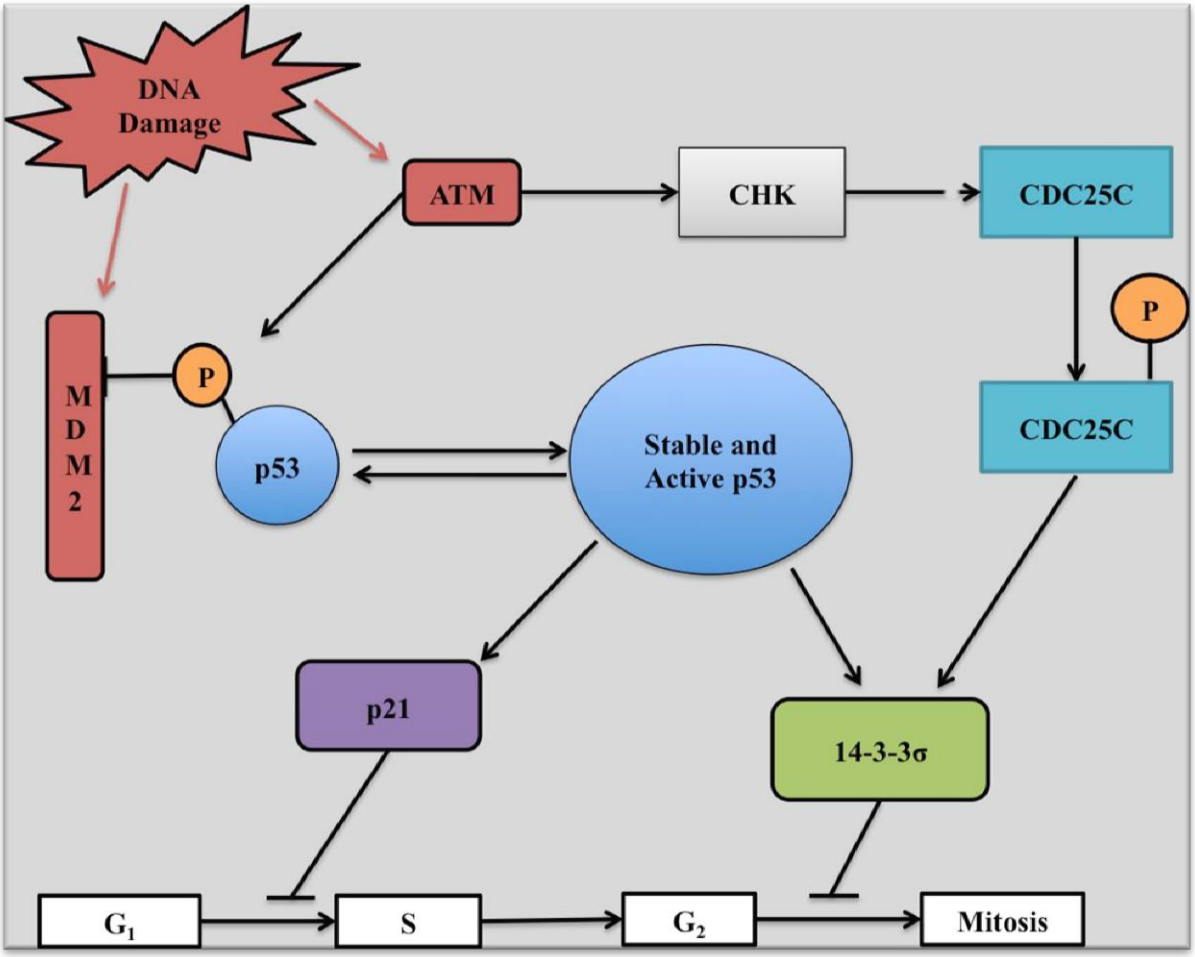

Figure 1.4: Schematic representation of the DNA damage checkpoint. With DNA damage, the p53 protein becomes stable and starts accumulating. The two main proteins that play a significant role in the stabalization of p53 is ATM and MDM2. Once activated, ATM affects p53 stability in numerous ways. ATM can activate CHK1 and -2 which in turn phosphorylates Cdc25C. Phosphorylated Cdc25C associates with the p53 target molecule 14-3-3σ, resulting in CDK1 inactivation and cell cycle arrest between G_2 - and M phase (22,29). ATM can also target the p53-MDM2 interaction by modifying the MDM2 protein (36). The MDM2 protein is an ubiquitin E3 ligase and key mediator of p53 protein stability by targeting p53 for polyubiquitination-mediated proteolysis (22,25). After stabilization and accumulation, p53 targets various proteins including the CKI protein p21 to prevent the cell from continuing the cell cycle. The p53-dependent increase in p21 expression suppresses cyclin E- and cyclin A-associated CDK2 activity and prevents G_1-to-S phase progression (22).

1.5) Types of cell death

Cell death is an evolutionarily conserved, genetically regulated process and is a major component of both normal development and pathogenesis (42-44). Cells choose to die as part of normal development or due to damage or infection (45). Different cell death pathways has been characterized and includes apoptosis, autophagy and necrosis (45,46).

Apoptosis is established as an evolutionarily conserved pathway, regulating programmed cell death (45). It is a fundamental homeostatic mechanism essential for normal growth, development and maintenance of every tissue and organ, but also plays a prominent role in pathological and therapeutic settings (47,48).

Autophagy, on the other hand, plays an essential role in cellular development and differentiation (49). Its dysregulation is implicated in various diseases including cancer, infectious disease, obesity, aging and neurodegenerative disorders such as Alzheimer's, Parkinson's and Huntington's diseases (49).

Another type of cell death commonly found under pathological conditions is necrosis (45). Programmed necrosis or necroptosis has been found to contribute to a wide range of pathologic cell death paradigms including ischemic brain injury, myocardial infarction and chemotherapy-induced cell death (50).

1.5.1) Autophagy

Autophagy is defined as a highly regulated process with a lysosome-dependent degradation of intracellular macromolecules and organelles (49,51,52). It is characterized by the appearance of double membrane cytoplasmic vesicles engulfing bulk cytoplasm, proteins and organelle components which are then sequestered into lysosomes and degraded (29,42,53,54).

Cells in early stages of autophagy contain several autophagic vacuoles with the mitochondria and the ER sometimes being dilated and the Golgi apparatus often enlarged (42). The plasma membrane loses specializations and blebbing may occur (29,42). During the late stages of autophagy the number and size of vacuoli increases, many of which are filled with lipids (42).

There are different forms of autophagy including macroautophagy, microautophagy and chaperone-mediated autophagy (49,51). Macroautophagy (referred to as autophagy from here on) is the sequestration and degradation of the cytoplasm in a process that uses specialized cytosolic vesicles (autophagosomes) that ultimately fuse with lysosomes (51,52). Microautophagy involves the direct uptake of the cytoplasmic material at the lysosome surface via membrane rearrangement (49,51). Chaperone-mediated autophagy allows for direct import into the lysosome of unfolded, soluble proteins containing a particular pentapeptide motif (49,51).

Autophagy (Figure 1.5) consists of several sequential steps including induction, autophagosome formation, docking and fusion with the lysosome and degradation (49). At the induction of autophagy an expanding membrane sac, termed the phagophore, enwraps portions of the cytoplasm and forms double-membrane-bound, sequestering autophagic vesicles called autophagosomes (29,42,51-53). The double membrane is derived from ribosome-free areas of the rough ER (42). The autophagosome encapsulates the cytosolic materials to be degraded and subsequently fuses with lysosomes (29,42,51,53). Lysosomes are cellular compartments enriched with hydrolases which has the ability to cleave proteins, lipids, nucleic acids and carbohydrates (42,51). After the fusion with the lysosomes, the inner membrane of the autophagosome, together with the enclosed cargo, is degraded and the resulting macromolecules are released into the cytosol through lysosomal membrane permeases for recycling (51).

On the molecular level, the autophagy-related genes (Atg), phosphatidylinositol 3-kinase (PI3K) and the kinase target of rapamycin (TOR) play important roles in the signaling pathways which leads to autophagy (29,42,51). TOR kinase is believed to be the gatekeeper for initiation of the autophagic pathway by negatively regulating autophagosome formation (29,53). In addition, TOR kinase acts as a sensor for amino acids and ATP and acts as an integrator for growth factor-induced signals (53). Under nutrient-rich conditions, TOR phosphorylates Atg13 which causes it to have a low affinity for Atg1 (52,53). This, in turn, leads to reduced Atg1 kinase activity (52,53). During starvation, TOR activity is blocked, Atg13 is dephosphorylated and associates with Atg1 kinase promoting its activation (52,53). Atg1 kinase activation then leads to autophagy induction (52,53).

Autophagosome formation is a process which includes isolation membrane nucleation, elongation and completion (49). The PI3K complex (consisting of Atg6, Atg14, myristylated

serine kinase Vsp15 and Vsp35) plays an essential role in isolation membrane nucleation (42,49,53).

The ubiquitin-like protein systems plays a role in the elongation and completion of the autophagosomes (49,53). One of the systems consists of an Atg12/Atg5 complex created by Atg12 being conjugated to Atg5 by a covalent bond between the carboxyterminal glycine of Atg12 and the lysine residue in the central part of the Atg5 (49,53). The Atg12/Atg5 complex becomes functional when it binds to Atg16 (53). The Atg12/Atg5/Atg16 complex is localized on the outer membrane forms larger protein complexes via the oligomerization of Atg16 (53).

Another ubiquitin-like protein system, essential for the formation of the autophagosome, is the modification of light chain 3 (LC3) protein by the phospholipid phosphatidyl-ethanolamine (PE) (49). LC3 is cleaved by Atg4 and then conjugated with PE by Atg7 and Atg3. The lipidated LC3-II associates with newly forming autophagosome membranes and remains on the mature autophagosomes until fusion with lysosomes (49).

Autophagy's role in the execution of cell death is controversial. It is described as the general response to cell stress such as starvation due to, for example, decreased extracellular nutrients (42,46,52). Its response can protect the cell from death, or it can mediate cell death, depending on the circumstances (42,46,52).

Cell death via autophagy can occur in two ways. The cell can be destroyed via mass autophagy where large portions of the cytosol and organelles are destroyed with subsequent collapse of vital cellular functions (52). The second way is where autophagy is the first response to cellular stress and then either apoptosis or necrosis is triggered (52).

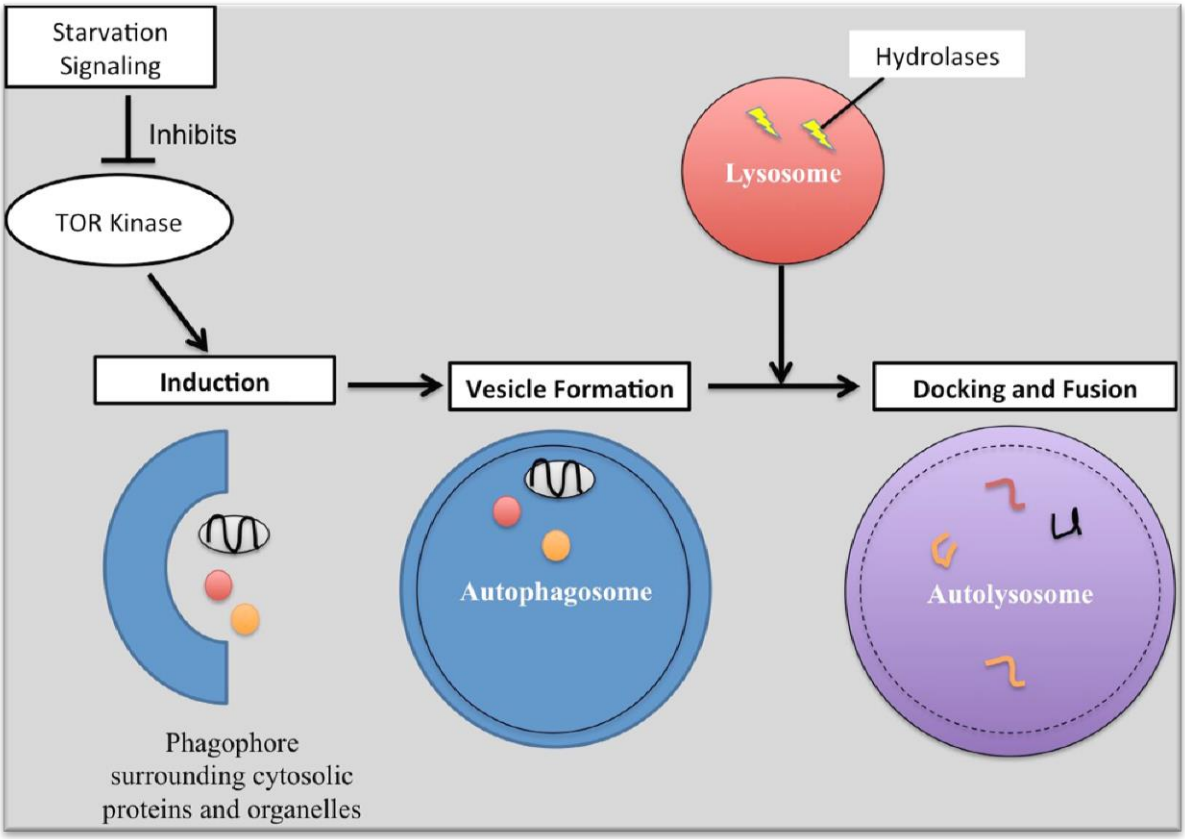

Figure 1.5: Schematic representation of autophagy. An expanding membrane sac, termed the phagophore, enwraps portions of the cytoplasm and forms double-membrane-bound, sequestering autophagic vesicles called autophagosomes, which occurs when a portion of the cytoplasm is engulfed by a double membrane vacuole. The autophagosome encapsulates the cytosolic materials to be degraded and subsequently fuses with lysosomes enriched with hydrolases. The inner membrane of the autophagosome, together with the enclosed cargo, is degraded and the resulting macromolecules are released into the cytosol.

1.5.2) Necrosis

Necrosis is defined as passive cell death caused by overwhelming stress (50). It is characterized by cellular swelling, chromatin condensation, destruction of organelles and disruption of the plasma membrane; leading to cellular and nuclear lysis and inflammation (27,29,42,43,46).

Necrosis is known to occur under a variety of pathological conditions and has long been believed to be an uncontrolled form of cell death, with some researchers believing that it was not a form of cell death at all, but rather the end stage of any cell death process (27,43,50). However, mounting evidence shows that necrotic cell death is carried out by complex signal transduction pathways and execution mechanisms (43,50,55).

One particular type of programmed necrosis has been termed "necroptosis" (50,55). This regulated mechanism depends on the Ser/Thr kinase activity of receptor-interacting protein kinase 1 (RIP1) (50,55). RIP1 is a death-domain containing kinase, associated with the death receptors (DRs) and found in the complex containing Fas-associated death domain (FADD) and caspase 8 (45,50). RIP1 is activated via autophosphorylation on Ser161 within the activation loop of the kinase (45).

Once activated RIP1 is believed to induce necroptosis (50,55). There are a number of suggested ways in which RIP1 initiates necrosis, one of which is the possible promotion of mitochondrial membrane permeabilization (MMP) via the activation of poly(ADP-ribose) polymerase (PARP) proteins, which stimulates the release of apoptosis-inducing factor (AIF) from the mitochondria (55). The implication of PARP proteins in programmed necrosis has been substantiated by Hitomi *et al.* whose findings revealed PARP-2 as one of the core regulators of necroptosis. It is believed that excessive activation of PARP proteins causes a decrease in ATP levels and a depletion of NAD^+ levels which may lead to excessive ROS production and rapid mitochondrial dysfunction (45,55).

In addition, apoptotic cells that are not recognised and phagocyted have been found to show several of the above-mentioned necrotic features (27,47). Apoptosis is known to cause cell death which is always followed by cell elimination, normally carried out by scavenger cells such as phagocytes (56). It is believed that apoptotic cells, in the absence of phagocytes, may undergo secondary necrosis (27,46,56), where the plasma membrane ruptures and the intracellular contents are released in a disorganized manner (46,56). Intracellular contents released include damage-associated molecular patterns (DAMPs) which are cellular constituents normally exposed to the innate immune cells when released from dying cells (47). Cell surface sensors on immune cells are believed to interact with DAMPs which then leads to the activation of signaling pathways resulting in a nonpathogen-induced sterile inflammatory immune response (47).

It has been postulated that in the absence of scavengers cells (such as when cells are grown *in vitro*), the phased transition from apoptosis to secondary necrosis is a self-sufficient process leading to self-elimination (47,56).

1.5.3) Apoptosis

Apoptosis is defined as a regulated programmed cell death pathway: a fundamental homeostatic mechanism essential for normal growth, development and cell maintenance (45,47). It is characterized by specific biochemical and morphological changes. Biochemical changes include: mitochondrial changes (leading to the collapse of the transmembrane electrochemical potential), the activation of caspases, the activation of endonucleases, DNA cleavage and segregation of nucleoli (57).

Morphological changes include cellular and nuclear shrinkage and fragmentation, chromatin hypercondensation, cell membrane blebbing and formation of apoptotic bodies (27,42,43,46,48,58,59). Blebs are formed from the plasma membrane when it delaminates from the cortical cytoskeletal network and expand due to increased hydrostatic pressure within the cell (47). These blebs may break away from the cell body to form membrane-clad apoptotic bodies (47).

There is also the loss of the phospholipid asymmetry on the plasma membrane (46). The plasma membrane is composed of a variety of phospholipids including choline phospholipids and aminophospholipids such as phosphatidylserine (PS) (57,59). In the normal cellular state, the cell maintains an asymmetry of the phospholipid contents between the inner and outer leaflet of the plasma membrane by actively translocating PS from the outer to the inner leaflet of the membrane (59). During apoptosis, the asymmetry is lost as PS equilibrates between the inner and outer leaflets, in a process facilitated by a Ca^{2+}-dependent flip-flop (59). Accumulation of PS on the outer leaflet of the membrane acts as a sign for neighboring cells and macrophages to remove the apoptotic cells (59).

Apoptosis can be divided into three stages: The first stage (initiation) is when the cell receives apoptotic signals from various stimuli, internal or external to the cell (48,59). In the second stage (integration/decision), the cell integrates the various signals via several signal transduction pathways which may, or may not, commit the cell to apoptotic death (48,59). The final decision to undergo apoptosis depends upon several factors including: the relative levels of apoptotic and survival factors within the cell, the metabolic state of the cell and at what stage of the cell cycle the cell is in (59). The third (execution) stage involves the degradation of the cellular proteins and the manifestation of morphological changes indicative of apoptotic cell death (48).

There are two main pathways which lead to caspase-dependent apoptosis: the extrinsic and intrinsic pathways. The extrinsic pathway is mediated by DRs on the cell surface while the intrinsic pathway is mediated by the mitochondria (41).

1.5.3.1) Extrinsic apoptotic pathway

The extrinsic apoptotic pathway (Figure 1.6) is triggered from receiving lethal signals from the extracellular environment, detected by DRs on the plasma membrane (48,58). DRs are members of the tumor-necrosis factor (TNF) receptor superfamily and comprise a sub-family, which is characterized by an intracellular death domain (41). The DRs are activated by their natural ligands, the TNF family (41).

Death ligands include the Fas ligand (FasL), TNF-α and TNF-related apoptosis inducing ligand (TRAIL) (27,29,48,58,59). They interact with their respective DRs and are responsible for transducing signals which leads to apoptosis (27,29,48,58,59). TRAIL binds to DR4 and DR5 while FasL binds to the death receptor Fas also known as apoptosis antigen 1 (APO1) (40).

When the ligands bind to their respective DRs, the death domains recruits adaptor molecules such as FADD, which in turn recruits inactive proforms of certain members of the caspase protease family (initiator procaspases 8 and 10), creating the death-inducing signaling complex (DISC) (27,40,41,48,58,59). DISC then triggers the cleavage and activation of the initiator caspases which will lead to the activation of the effector (execution) caspases 3, 6 and 7 resulting in apoptosis (29,48,58,59).

1.5.3.2) Intrinsic apoptotic pathway

The intrinsic apoptotic pathway (Figure 1.6) can be activated via a wide variety of extracellular and intracellular stimuli including DNA damage, gamma radiation and chemotherapeutic drugs, leading to the activation of the central death machinery located at the mitochondria (58-61).

The key step in the intrinsic pathway is believed to be MMP, an event that is regulated by members of the Bcl-2 protein family (39,58,60-62). MMP leads to the release of several pro-

apoptotic proteins such as AIF and cytochrome *c*, found in the mitochondrial intermembrane space (27,48,58,60,61,63).

Once released into the cytoplasm of the cell, cytochrome *c* binds to apoptotic protease activating factor 1 (Apaf-1), allowing deoxyadenosine triphosphate (dATP) to bind onto Apaf-1 inducing conformational changes which causes the oligomerization of Apaf-1 into the Apaf-1 apoptosome (27,48,58-61). This apoptosome subsequently recruits the initiator procasapase 9 through caspase recruitment domains (CARDs) present in the N-termini of both Apaf-1 and procaspase 9 (61). Once bound to the apoptotsome, caspase 9 is activated and in turn activates downstream effector caspases such as caspase 3, leading to the execution phase of apoptosis (27,48,58-61).

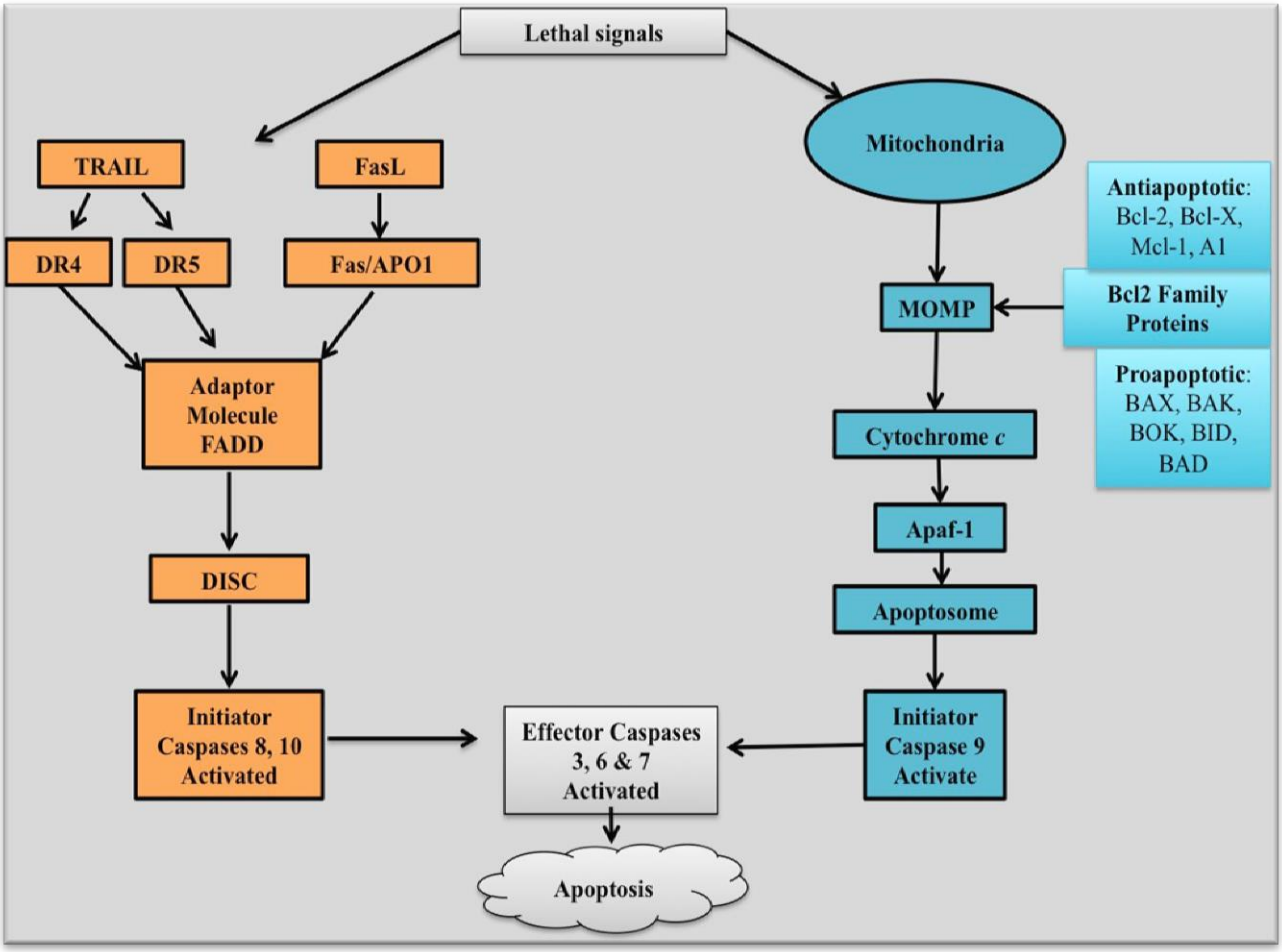

Figure 1.6: Schematic representation of the intrinsic and extrinsic apoptotic pathways. The extrinsic pathway depicted in orange: Death ligands interact with their respective DRs (27,29,48,58,59). The death domains of the DRs recruit adaptor molecules, which in turn recruits inactive proforms of the initiator caspases 8 and 10, creating DISC (27,40,41,48,58,59). DISC activates the initiator caspases which will leads to the activation of the effector caspases 3, 6 and 7 resulting in the execution phase of apoptosis (29,48,58,59). The intrinsic pathway depicted in blue: MMP leads to the release of several pro-apoptotic proteins such as AIF and cytochrome *c* into the cytoplasm (27,48,58,60,61,63). Cytochrome *c* binds to Apaf-1 and helps to form the apoptosome (27,48,58-61). This apoptosome recruits the initiator procasapase 9 (61). Once bound, caspase 9 is activated which in turn activates downstream effector caspases leading to the execution phase of apoptosis (27,48,58-61).

1.5.3.2.1) Bcl-2 protein family

The Bcl-2 family of proteins, many of whom reside at the membranes of the ER, nucleus and mitochondria, play a pivotal role in apoptosis (28,59). The family members have been grouped into three classes depending on their activities and the particular Bcl-2 Homology (BH) domains within the protein (60). The first class is the anti-apoptotic proteins such as Bcl-2, Bcl-X, Mcl-1 and A1 (39,59,61,64). The anti-apoptotic proteins contain BH domains 1,

2, 3 and 4 (60). The second class is the pro-apoptotic proteins such as Bax, Bak and Bok (39,59-61,64). These proteins contain BH domains 1, 2, and 3 (60). The third class is also pro-apoptotic proteins, but only contain BH domain 3 and are often referred to as BH3-only proteins (60). These include Bad, Bik, Noxa, and Puma (60).

The Bcl-2 protein family controls apoptosis through the regulation of mitochondrial processes and the release of mitochondrial pro-apoptotic molecules, located in the mitochondrial intermembrane space, critical for the cell death process (28,61,64). It is believed that the pro-apoptotic members of the Bcl-2 protein family, induces MMP which results in the release of the above mentioned pro-apoptotic molecules (65).

A range of BH3-only proteins acts as 'death sensors' in the cytosol or cytoskeleton (41,52). Following a death signal, they stimulate MMP by interacting with Bax and/or Bak (52). Bax exists as an inactive monomer in the cytosol and its activation requires conformational change, mitochondrial translocation and oligomerization (60,65). Bak on the other hand is already located on the outer mitochondrial membrane (OMM) (60). Bak oligomerization and activation is mediated by the exposure of the BH3 domain to a Bak protein, leading to the insertion of the exposed BH3 domain into the groove of another Bak molecule, resulting in a symmetric dimer essential for its pro-apoptotic function (60).

Once activated, they form protein-permeable channels in the OMM, allowing the escape of the pro-apoptotic proteins from the intermembrane space of the mitochondria (41,52). These channels may also cause dissipation in the mitochondrial membrane potential ($\Delta\Psi m$), which may lead to the further breakdown of the mitochondria and cell death (41).

1.5.3.2.2) Mitochondria

As mentioned above, the mitochondria is considered to be the central death machinery in the intrinsic apoptotic pathway (58-61).

In its normal state, the mitochondria is an oblong structure with a inner and outer phospholipid membrane (59). The inner membrane defines the central matrix space where mitochondrial DNA can be found and where protein synthesis, respiration and steroid hormone biosynthesis occurs (59). Between the inner and outer membranes, there is the intermembrane space which contains several pro-apoptotic proteins such as cytochrome *c* and AIF (59).

The mitochondria normally maintains a voltage and pH gradient across the inner membrane with the help of the proton pump via the electron transport chain, which is used by the F_1F_0- ATPase in the formation of ATP (59,66). In its normal state, the mitochondria carries out a wide range of metabolic functions which include ATP synthesis, fatty acid oxidation and amino acid metabolism (66,67).

The mitochondria's role in the regulation of cell death is well established (44). The key step in the intrinsic apoptotic pathway is believed to be MMP, an event that is regulated by members of the Bcl-2 family as dicussed above (39,58,60-62). MMP is generally considered as the "point-of-no-return" in the sequence of events leading to apoptotic cell death and effects the inner mitochondrial membrane (IMM) and the OMM (27,48).

The IMM is almost completely impermeable to ions, which is essential for maintaining the ion gradient, required for oxidative phosphorylation in the mitochondria (48). The permeabilization of the IMM can occur due to the opening of pre-existing permeability transition pores (PTP) (44,48,65). PTP is a multiprotein complex primarily made up of the voltage-dependent anion channel (VDAC) in the outer membrane, adenine nucleotide translocator (ANT) in the inner membrane and cyclophilin D in the matrix (41,65). The permeabilization of IMM causes disruption in mitochondrial ion and volume homeostasis, which wil lead to the dissipation of the $\Delta\Psi m$ and cause an influx of fluid into the matrix, resulting in swelling and rupturing of the OMM and the release of pro-apoptotic proteins from the intermembrane space (44,48,58,59,65).

Apart from the rupturing of the OMM due to IMM permeabilization, the protein permeable channels formed by Bak or Bax, mentioned above, also plays a role in MMP (41,52). Another theory is that these Bcl-2 pro-apoptotic proteins could also interact with and regulate PTPs (44,48,65). In normal conditions, VDAC would mostly exist in a low conductance state within the PTP, flickering between open and closed conformations allowing diffusion of molecules through the OMM (48). It is believed that with pro-apoptotic signals, Bax or Bak interact with the PTP, causing increased conductance in the VDAC, resulting in long-lasting openings of the PTP, $\Delta\Psi m$ dissipation, mitochondrial outer membrane permeabilization (MOMP) and the release of pro-apoptotic proteins from the intermembrane space (48).

1.5.3.2.3) Reactive oxygen species

Mitochondria are the main source of ROS production in cells (44,67). ROS play a regulatory role in cellular metabolic processes by activating various enzymatic cascades and several transcription factors (44). ROS are also a major cause of cellular oxidative stress and is implicated in a wide variety of pathologies such as type II diabetes, atherosclerosis and several neuro-degenerative diseases (44,68). Oxidative stress is defined as an imbalance that favors the production of ROS over antioxidant defenses (44).

ROS are by-products from the production of ATP which occurs in the mitochondrial matrix via the oxidative phosphorylation pathway (44,68-70). Approximately 1-2% of oxygen (O_2) consumed during normal cellular respiration is converted to superoxide (O_2^-) via one-electron reduction (44,67). This is catalyzed by nicotinamide adenine dinucleotide phosphate (NADPH) oxidase (44,67,71-74).

The mitochondrial electron transport chain serves as the primary source of O_2^- due to several redox centers in the transport chain that may leak electrons to O_2 (44). The electron transport chain consists of a series of electron carriers and is arranged into four complexes (75). Most O_2^- is believed to be generated by complex I (reduced nicotinamide adenine dinucleotide (NADH):ubiquinone oxidoreductase) and complex III (ubiquinol:cytochrome *c* oxido-reductase) (61,69,75,76).

This superoxide anion can be regarded as the precursor of most ROS (44). For instance, O_2^- once generated can rapidly converge into hydrogen peroxide (H_2O_2) by Mn-dependent superoxide dismutase, present in the mitochondrial matrix (44). O_2^- toxicity causes oxidation and inactivation of iron-sulphur proteins which may cause simulataneous release of iron and H_2O_2 within the mitochondria (44). Subsequent interaction of O_2^- and H_2O_2 can generate highly reactive and toxic hydroxyl radicals, which in turn can oxidize mitochondrial proteins, DNA, and lipids, amplifying oxidative damage (44).

The mitochondria are both the major source of intracellular ROS and, at the same time, targets of ROS (61,67,68). The accumulation of ROS may lead to oxidative damage to mitochondrial proteins and mitochondrial DNA, causing loss of electron transport, decrease in ATP production and $\Delta\Psi m$ dissipation (44,67). In addition, ROS accumulation is believed

to act as signaling molecules which initiates MMP via PTP (discussed above), causing the release of the pro-apoptotic proteins found in the intermembrane space (47,67).

1.5.3.2.4) Redox status

The pyridine nucleotides such as nicotinamide adenine dinucleotide (NAD^+), NADH, nicotinamide adenine dinucleotide phosphate ($NADP^+$) and NADPH have essential roles in ATP production, metabolic processes and redox regulation (77-81).

Both NAD^+ and $NADP^+$ are subjected to a two-electron reduction in the nicotinamide ring to be converted to NADH and NADPH respectively (80). They are all involved in many biological reactions as electron carriers; NAD^+ and NADH participate mainly in ATP production while $NADP^+$ and NADPH participate in modulating the redox status of the cell (80).

The redox status is a term used to describe the oxidation and reduction status of the cell and is also commonly used to describe the balance of NAD^+/NADH and $NADP^+$/NADPH within the cell (77,78,80). When the intracellular redox balance shifts towards oxidation, the cell undergoes oxidative stress, due to increased production or insufficient degradation of ROS and may lead to oxidative damage to mitochondrial proteins and DNA, causing loss of electron transport, decrease in ATP production, $\Delta\Psi m$ dissipation and cell death (44,67,77). Cumulating evidence has suggested that the NAD^+/NADH and $NADP^+$/NADPH ratios may also change during oxidative stress (79).

NAD^+ and NADH play a role in combatting oxidative stress in several ways (79). The NAD^+/NADH ratio is an index of cellular reducing potential, since the redox couple plays key roles in numerous redox reactions (79,81). In addition, studies have suggested that NADH may have a direct antioxidation effect on the cell while NAD^+ can inhibit ROS generation from α-ketoglutarate dehydrogenase and pyruvate dehydrogenase (79,81).

NADPH is one of the most important factors in cellular antioxidation (79). $NADP^+$ is converted into NADPH by the pentose phosphate pathway, an alternative glycolytic pathway (80). The electrons derived from NADPH are then transferred to glutathione (GSH) (79-81). GSH is a small antioxidant protein composed of a L-γ-glutamyl-L-cysteinyl-glycine

tripeptide and is essential for the function of several key antioxidation enzymes such as glutathione peroxidase and glutathione *S*-transferase (79,80).

In contrast to the above two paragraphs, evidence has also suggested that electrons derived from NADH and NADPH can contribute to oxidative stress (79,80). With the cell undergoing oxidative stress, there will be an increase in NADH, which will dramatically alter the NAD^+/NADH ratio which, in turn, would affect numerous oxidoredutive reactions (78). It is believed that inhibition of the respiratory chain in the mitochondria via damage, mutation or loss of cytochrome *c* will cause a build up of NADH which will increase the NAD^+/NADH ratio and lead to increased O_2^- formation (67). In addition NADH – and NADPH oxidases also contribute to oxidative stress by catalyzing the generation of ROS (44,71,79,80).

Several studies have also suggeted that the pyridine nucleotides may be directly involved in cell death (79,81). Due to their critical role in oxidative stress, NAD^+/NADH and $NADP^+$/NADPH can effect cell survival by influencing oxidative stress and the antioxidation systems of the cells (81). It is also believed that the NAD^+/NADH and $NADP^+$/NADPH ratios can modulate PTP openings, significantly influencing the ΔΨm and MMP (79,81,82). In addition, it is interesting to note that it is believed that NADH and NADPH are oxidized at the early stages of cell, before cell shrinkage and PS exposure, thus NADH/NADPH depletion has been reported to be is an early event in apoptosis (79,81,82).

1.5.3.2.5) Cytochrome *c*

Cytochrome *c* is a critical apoptogen that plays an important role in the intrinsic apoptotic pathway (58,59,63). It is found primarily within the cristae of the mitochondria (61) and is required for protein import, mitochondrial biogenesis and plays an important role in the production of ATP (60). By transporting electrons from complex III to complex IV of the electron transport chain, cytochrome *c* generates an ΔΨm across the mitochondrial inner membrane (60). This potential is used by complex V to generate ATP from adenosine diphosphate (ADP) via aerobic respiration (60).

When cytochrome *c* is lost from the mitochondria, the electron transport chain is disrupted, causing ROS production and loss in ΔΨm, which may play a role in MMP (60,61). In addition, when released into the cytosol, cytochrome *c* binds to an adapter molecule (Apaf-1),

allowing dATP to bind onto Apaf-1 inducing conformational changes and causing Apaf-1 to oligomerize into the Apaf-1 apoptosome (27,48,58-61).

1.5.3.2.6) Caspases

Caspases are cysteine proteases produced in the cell as catalytically inactive zymogens (27,44,59,83). They become activated when cleaved at internal aspartate residues and will subsequently start the caspase cascade (27,84).

Caspases are central in both the intrinsic and extrinsic apoptotic pathways and are among the most specific of proteases as they require recognition of specific peptide sequences and cleave only after an aspartic acid residue (41,58,59,84). The specificity of the target sites for caspases are believed to be determined by a four-amino-acid recognition motif and other three-dimensional structure aspects of the targeted protein (84).

Apoptotic caspases constitute two general classes. The one class are those with long N-terminal domains and are labelled as initiator caspases, such as caspase 2, -8, -9 or -10, while the second class are those with short N-terminal domains and are known as effector (executioner) caspases, such as caspase 3, -6 and -7 (44,83-85). The activation of initiator and subsequently effector caspases will start the caspase cascade and induce cell death through the coordinated cleavage of a specific collection of protein substrates including structural elements, nuclear proteins and signaling proteins (59,83,85).

The initiator caspases are activated first via a series of poly-protein complexes and are mediated by various apoptotic-signaling pathways (27,44). The long prodomains of the initiator caspases provide them with the ability of binding to activator molecules, such as Apaf-1, or adaptor molecules associated with membrane receptors, such as Fas (84). Once activated they, in turn, activate the effector caspases, initiating the caspase cascade (59).

The extrinsic and intrinsic apoptotic pathways converge at the execution phase of apoptosis mediated by the effector caspases 3, 6 and 7 (41,48). The effector caspases are specifically responsible for initiating the degradation phase of apoptosis which includes DNA fragmentation, cell shrinkage and membrane blebbing (59,62).

DNA breakdown can occur in two stages; the first stage being large-scale DNA cleavage, followed by a second stage of oligonucleosomal DNA fragmentation or DNA laddering (65).

This is achieved by endonucleases capable of inducing both chromatin condensation and DNA fragmentation (41,65). One such endonuclease is DNase caspase activated deoxyribonuclease (CAD) (41,65). CAD requires cleavage of its inhibitor by effector caspases causing its release where it subsequently travels to the nucleus to fragment DNA (41,65). The dramatic morphological alterations seen during apoptosis (cell fragmentation, blebbing and the formation of apoptotic bodies) can be associated with the cleavage of the structural proteins such as actin, plectin and gelsolin by the effector caspases (41,59).

1.5.4) Caspase-independent cell death

Caspases are known for their central role in the intrinsic and extrinsic apoptotic pathways as discussed above. However, it should be mentioned that cell death can also occur in a caspase-independent manner (65,86).

Various proteins have been identified of having the capability of inducing cell death without caspase activation. Some reside within the intermembrane space of the mitochondria and include AIF and endonuclease G (endoG) (60,65,86). They are released from the mitochondria due to the permeabilization of the OMM, which is controlled by the Bcl-2 protein family (60,65).

AIF is first expressed as a 67kDa precursor, addressed and compartmentalized in the mitochondria by two mitochondrial localization sequences located within the N-terminal prodomain (86). The full-length AIF is then processed and the prodomain removed, giving rise to a mature 57kDa mitochondrial flavoprotein, consisting of three structural domains: the FAD-binding domain, the NAD-binding domain, and the C-terminal domain (65,86). It is believed that after an apoptotic stimulus, AIF is released from the mitochondria into the cytosol and translocates to the nucleus where it triggers chromesome condensation and large-scale DNA fragmentation leading to cell death (48,60,65,86).

Another mitochondrial enzyme believed to induce caspase-independent cell death is endoG (60,65). EndoG belongs to an important Mg^{2+}-dependent nuclease family, synthesized as a precursor, which, after being imported into the mitochondria, is matured, with the removal of the N-terminus (86). EndoG, normally found in the mitochondrial intermembrane space, is activated by a change in subcellular localization, such as when it is released from the

mitochondria after apoptotic signals (65). EndoG, like AIF, translocates to the nucleus after being released into the cytosol and also generates oligonucleosomal DNA fragmentation (48,60,65).

1.6) Microtubules

The microtubule cytoskeleton is one of the major targets in cancer treatments (87). Microtubules are hollow, cylindrical, dynamic polymers distributed within the cell in length, composed of α/β tubulin heterodimers (28,87). They play key roles in a large number of cellular functions, including controlling organelle positioning, directing intracellular trafficking and the pulling apart of chromosomes during mitosis (28,35,39,87). Many of these functions are associated with the dynamic restructuring ability of the microtubule cytoskeleton, which is continuously growing (assembling) and shinking (disassembling) (28,87,88).

Microtubules consists of protofilaments which associates in parallel to form the cylindrical wall of microtubules (88). The protofilaments are, in turn, made up of alternating α and β tubulin monomers, the basic building blocks of the microtubule (87,88). Each monomer (α or β tubulin) can be divided into three domains: The N-terminal domain (residues 1–206), forming the nucleotide binding site, the central domain (residues 207–384) involved in the contacts between the monomers, and the C-terminal domain, which is mainly involved in the binding of microtubule-associated proteins (MAPs) and plays a significant role in various tubulin activities (87,88).

Because the protofilaments of microtubules are arranged in parallel, the microtubules have distinct polarity with a minus end, normally associated at the microtubule-organizing center (MTOC) and/or centrosome, capable of slow-growth, and a plus end, constantly exploring the cytoplasm and capable of rapid growth (28,39,88). Microtubules are capable of growing and shortening via reversible non-covalent association and disassociation of the α/β tubulins at the two ends (35).

Guanosine triphosphate (GTP) hydrolysis plays a pivotal role in microtubule dynamics (28). Each monomer (α or β tubulin) binds to a GTP molecule (87,88). The α tubulin is bound to GTP non-exchangeably at the N-terminal domain while the β tubulin, found to cap the plus end of the microtubule, binds to GTP and hydrolyses it to guanosine diphosphate (GDP)

(35,87,88).

Microtubules containing non-hydrolysable GTP analogues are highly stable; with bound GDP, they are unstable (88). Thus, when the microtubule is growing, a new subunit containing GTP is added into the microtubule structure (28). If there is a low rate of subunit addition, it provides enough time for the GTP to hydrolyze into GDP (28). If the rate of subunit addition is high (which will normally be found at the plus end of the microtubule), a new GTP-containing subunit is added on the microtubule polymer before the GTP molecule of the previously added subunit is hydrolyzed, leading to the accumulation of GTP-containing subunits at the tip of the microtubule, known as the GTP cap, which will ensure the stability of the microtubule (28,87,88). If the cell's conditions allow either GDP-tubulin to be added or time for the hydrolysis of GTP to GDP, the cap can be lost, and the microtubule can enter a phase of depolymerization, which will lead to the shortening of the microtubule (88). The unique GTP binding and hydrolysis property of the α/β tubulin provides the microtubule with unique dynamic instability, allowing the microtubules to switch between episodes of growth and shortening (28,87,88). A steady state is reached when the growth of the microtubule polymer due to α/β tubulin dimer addition is precisely balanced by its shrinkage due to disassembly into α/β tubulin subunits (28).

Microtubules go through a phase of rapid lengthening and shortening when the chromosomes attaches to the spindle during cell division (88). The crucial role of microtubules in the cell division for tumor cells has made microtubules a valuable target for cancer chemotherapy (28,87).

1.7) Microtubule interfering drugs

One of the most promising classes of cancer chemotherapeutic drugs available, with a high ability to induce apoptosis, are microtubule-interfering drugs (MIDs) (35,39,87).

MIDs target the cell cycle by binding to and interfering with the assembly and degradation of the microtubule machinery; inhibiting the normal function of the mitotic spindle and preventing hyperproliferation of cancer cells (22,28,35,89). Interference with the microtubule machinery can be done in a number of ways. MIDs can either cause stabilization of the microtubules or inhibit polymerization, both of which will lead to cell cycle arrest (87,88). Due to the therapeutic success of MIDs, intense search and development of new microtubule-targeting compounds are being conducted by pharmaceutical companies (39).

Currently, there are three classes of tubulin-binding drugs namely vincas, taxanes and colchicine analogues (28,35,39,87,88). They are all classified by their respective tubulin binding domains (Table 1.2).

Vinca alkaloids are destabilizing agents that bind to both tubulin and microtubules (35,87). The vinca domain is located adjacent to the exchangeable GTP binding site in β tubulin at the plus end (35). Their actions are highly dependent on the drug concentration (μM) (35,87). At relatively high concentrations, they cause microtubule depolymerization, dissolve spindle microtubules and arrest cells at mitosis (35). At even higher concentrations, they induce the aggregation of tubulin into paracrystalline arrays (35). In contrast, at low concentrations, the vinca alkaloids suppress microtubule dynamics without depolymerizing spindle microtubules, but remain able to arrest mitosis and induce apoptosis (35,87).

The taxane site, on the other hand, resides in a deep hydrophobic pocket at the lateral interface between adjacent protofilaments, within the lumen of the microtubule (35). At relatively high concentrations, taxanes promote microtubule polymerization and stabilize microtubules (23,35,39). At lower concentrations taxanes suppress microtubule dynamics, but retain their capability of inducing mitotic arrest and subsequent apoptotic cell death (35).

Colchicine is one of the earliest microtubule-targeting agents identified and its action mechanism has been extensively investigated (35). The colchicine site is located at the intra-dimer interface between β - and α tubulin (35). Colchicine forms a quasi-irreversible pre-equilibrium complex with the tubulin dimer, which induces conformational changes in tubulin and effectively inhibits cell growth, mitosis, cell elongation and cell motility (87). The binding process is slow and temperature-dependent (87). Drugs binding to this site typically induce microtubule depolymerization at high concentrations and suppress microtubule dynamics at low concentrations, similar to both vinca alkaloids and taxanes (35).

Several colchicine site-binding agents have been developed, such as 2-methoxyestradiol (2ME), which binds reversibly at the colchicine site and are used as an antiangiogenic agent (35,87). 2ME is registered as Panzem by Entremed Inc. (Rockville, MD) and are currently undergoing clinical trials (90-93).

Table 1.2: Three classes of microtubule interfering drugs

Type	Action	Binding Site	Examples
Vinca Alkaloids	Destabilizing Agent	Vinca domain on β tubulin	Vinblastine (35,87)
			Vinorelbine (35,87)
			Vinflunine (35,87)
Taxanes	Stabilizing Agent	Within lumen of microtubule	Docetaxel (35,87)
			Paclitaxel (35,87)
			Discodermolide (35)
			Epothilones (35,87)
Colchicine Analogues	Destabilizing Agent	Interdimer interface between	Colchicines (35,87)
		α and β tubulin	Combretastatins (35,87)
			2-Methoxyestradiol (35,87)

1.8) 2-Methoxyestradiol

2ME (Figure 1.7 A) is an endogenous metabolite derived from 17β-estradiol (38,89,94-98) which is naturally formed within the body by the enzyme catechol estrogen methyl trasferase (99). 2ME exerts antiproliferative, anti-angiogenic and pro-apoptotic characteristics *in vitro* and *in vivo* (38,89,94,100,101) independent of the estrogen receptor (89,98,102,103).

2ME's major target is the microtubule skeleton (38,89,97,98,101,103). The compound influences the SAC by interacting with the colchicine binding site situated between the α- and β-dimers of the tubulin protein (88,94,95,101,104). This causes abnormal spindle formation and activation of the spindle checkpoint, which leads to metaphase arrest, inhibition of further cell proliferation and the induction of cell death (32,89,96,97).

2ME, however, has been found to have low bioavailability in the human body due to rapid metabolic degradation by the enzyme 17β-hydroxysteroid dehydrogenase type 2 in the gastrointestinal tract and liver (94,99,100,105,106). The compound is currently undergoing clinical trials with an innovative nanocrystal dispersion (NCD) drug delivery system which may possibly overcome the rapid biodegradation problem (90-93). The NCD drug delivery system involves the reduction of the particle size of the drug substance to nanometer-size, thus enhancing dissolution (90-93).

Researchers have also attempted to create analogues of 2ME with improved bioavailability and potency. With the creation of these analogues it was shown that the 2-methoxy group on

the 2ME compound is of importance for drug activity, since it provides the compound with increased antiproliferative characteristics (89,107). Sulphamoylated analogues with modifications on the 3- and 17-position of the molecule revealed significant anticancer potency and prolonged half-life and bioavailability (89,97,100,106-108). Increased bioavailabilty is due to the ability of the sulfamoylated derivatives to reversibly bind to carbonic anhydrase II (CAII) found in red blood cells, thereby enabling them to journey through the liver without undergoing presystemic metabolism (94,99,100,108,109).

1.9) 2-Ethyl-3-*O*-sulphamoyl-estra-1,3,5(10)16-tetraene

The analogue being investigated in this research project is the latest *in silico*-designed 2ME derivative: 2-ethyl-3-*O*-sulphamoyl-estra-1,3,5(10)16-tetraene (ESE-16). ESE-16 (Figure 1.7 B) was developed when potential carbonic anhydrase IX (CAIX) inhibitors, capable of interfering with microtubule dynamics were identified in our laboratory with the use of bioinformatics software (94).

The bioinformation software used included the Chimera package from the Resource for Biocomputing, Visualization and Informatics at the University of California, San Francisco (supported by NIH P41 RR-01081), which was used for structure preparation and visualization (94). Docking studies were conducted with Autodock 4.0 and AutoDockTools4 (Scripps Research Institute, La Jolla, CA, USA) to evaluate the energy status for both the bound and unbound states of the compounds and uses a semi-empirical free energy force field by taking into account hydrogen bonding, electrostatic interactions, deviation from covalent geometry, internal ligand torsional constraints and desolvation effects (94).

Docking studies revealed that ESE-16 had a pronounced preference of CAIX over CAII binding (94). CAIX, an extracellular carbonic anhydrase isoenzyme, is over expressed in a variety of tumors and contributes to the acidification of the extracellular microenvironment of many tumors (109,110). It was also shown *in vitro* that ESE-16 was more potent than its source compound (2ME) having antiproliferative effects on a variety of cell lines at a concentration of between 1-2μM whereas ESE-16 showed antiproliferative activity at nanomolar values (94).

When the chemical structures of ESE-16 and 2ME are compared (Figure 1.7), an exchange of a sulphamoylated group for a hydroxyl group at position 3 and the removal of a hydroxyl

group at position 17 on the ESE-16 compound are noticed. As mentioned above, the sulphamoylated group increases the bioavailability of the compound since it allows the compound to reversibly bind to CAII, enabling them to journey through the liver without undergoing presystemic metabolism (94,99,100,108,109), while the modifications at position 3 and -17 increased the anticancer potency and prolonged half-life of the compound (89,97,100,106-108).

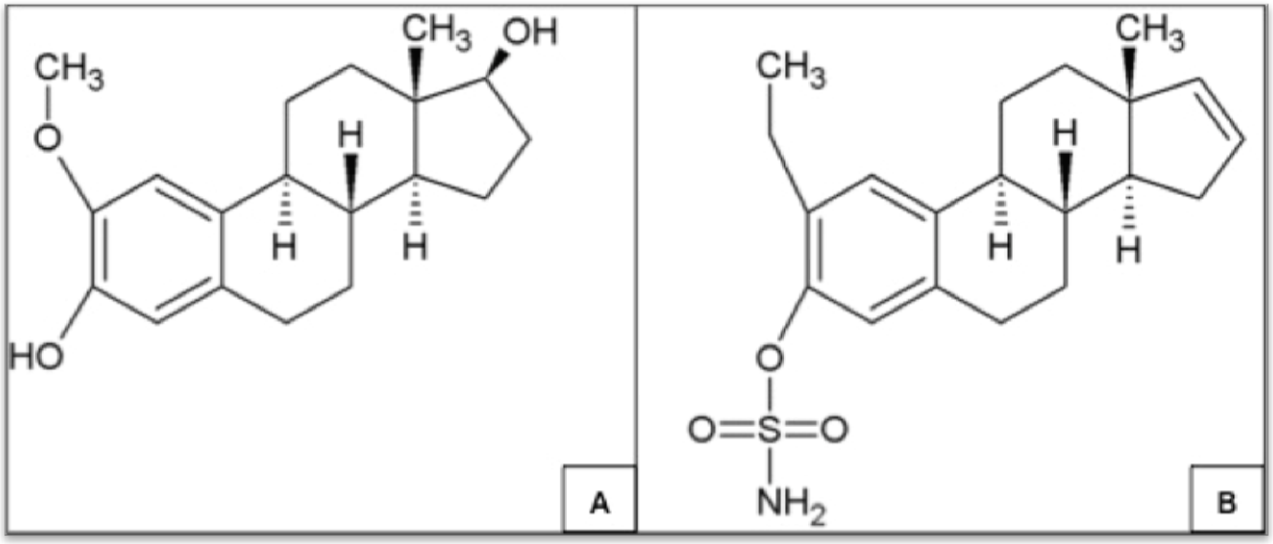

Figure 1.7 : Structural comparison between (A) 2ME and (B) ESE-16. When the two chemical structures are compared, an exchange of a sulphamoylated group for a hydroxyl group at position 3 and the removal of a hydroxyl group at position 17 on the ESE-16 compound are noticed. The sulphamoylated group increases the bioavailability of the compound (94,99,100,108,109), while the modifications at position 3 and -17 increases the anticancer potency and provides a prolonged half-life (89,97,100,106-108).

1.10) Carbonic anhydrases

Carbonic anhydrases are zinc enzymes that controls the carbon dioxide (CO_2)/bicarbonate ratio in the blood and thus the acid/base balance in the body (94,105,111-113). This family of enzymes can be divided into three structurally distinct classes: α, β and γ (113). The α–class is known to be present in vertibrates and plays an active role in respiration and pH homeostasis (113). CAIX, a membrane-associated glycoprotein, is a unique member of the human α–class CA (113,114). It is overexpressed in a variety of tumors and is implicated in the acidification of the extracellular environment (94,113,114).

Tumor hypoxia, caused by an inadequate supply of oxygen, appears to be strongly associated with tumor propagation, malignant progression and resistance to chemo- and radiotherapy (114). In hypoxic tumors, there is an increase in CO_2 concentration, believed to be a result of an increase in the penthose phosphate pathway (113,115). This serves to replenish the supply of NADPH and generate ribose-5-phosphate, necessary for nucleotide and coenzyme production (113). It is known that hypoxia is strongly associated with the overexpression of CAIX (94). CAIX converts the excess CO_2 to bicarbonate (HCO_3^-) and a proton, creating the significant increase in extracellular proton concentration and causing the acidification of the tumor microenvironment (113,114). The acidic environment, in turn, plays a role in promoting actions of growth factors and proteases involved in tumor progression (94).

Selective inhibition of CAIX provides thus a valuable strategy for curtailing the development of metastatic processes associated with acidotic microenvironmental conditions in tumors (94,113).

1.11) Significance of this study

EC is the 8th most common incident cancer in the world and ranks 6th among all cancers in mortality. The highest incidence rates in both males and females were found in Eastern Asia and Eastern and Southern Africa, making this a cancer of national importance. One of the reasons for the high incidence rate is believed to be the consumption of FB1-contaminated maize, which is frequently found in certain areas of South Africa. It is believed that FB1 may act as a promotor or initiator of carcinogenesis in synergy with certain co-carcinogens such as nitrosamines found in tobacco.

The prognosis of EC is generally unfavourable, with an approximated long-term survival rate of only 5%. Treatments for EC include surgery, radiation treatments and chemotherapy. Despite significant progress, cancer treatments have not met expectations and cancer research is focused on innovation to address bioavailability and delivery methods of anticancer compounds. The drug development field has been transformed by treatments with the ability to direct treatment at specific molecular targets.

This *in vitro* study delivered valuable information on the action mechanism of the novel ESE-16 compound Data from this study provided cellular targets for future *in vivo* studies to establish ESE-16'ss efficacy as a clinically usable anticancer agent.

1.12) Aims of this study

1. To study the morphological changes in SNO cells after exposure to 0.2µM ESE-16 with the use of polarization-optical differential interference contrast (PlasDIC) microscopy and light microscopy via haematoxylin and eosin (H&E) staining.
2. To study changes in the internal ultrastructure in SNO cells after exposure to 0.2µM ESE-16 with the use of transmission electron microscopy (TEM).
3. To determine the influence of 0.2µM ESE-16 on SNO cells on the cytoskeletal microtubule architecture via confocal microscopy.
4. To quantitatively confirm apoptosis taking place in SNO cells after exposure to 0.2µM ESE-16 by calculating the mitotic indices of the cells and using the apoptosis detecting assay (Annexin V-FITC) and cell cycle progression studies via flow cytometry.
5. To quantitavely confirm metaphase arrest by determining cyclin B1 activity in the SNO cells after exposure to 0.2µM ESE-16 via flow cytometry.
6. To study the redox status in the SNO cells after exposure to 0.2µM ESE-16 with the quantification of ROS via flow cytometry and the study of NAD^+/NADH and $NADP^+$/NADPH levels within the cells with spectrophotometry.
7. To study the changes in mitochondrial membrane potential and cytochrome *c* levels in the SNO cells after exposure to 0.2µM ESE-16 with the use of flow cytometry.
8. To study caspase 3 and 9 activity after exposure to 0.2µM ESE-16 with the use of spectrophotometry.

Chapter 2
Materials and methods

2.1) Type of study

This research project is regarded as a preclinical *in vitro* study and data cannot directly be extrapolated to an *in vivo* environment. Data gained from this investigation will establish the use of ESE-16 as a possible anticancer agent, paving the way for *ex vivo* and *in vivo* studies.

2.2) Materials

2.2.1) Esophageal carcinoma cell line

SNO esophageal carcinoma cells are non-keratinizing squamous epithelial cells (116) and was purchased from Highveld Biological (Pty) Ltd (Sandringham, SA). The cell line was derived from a well-differentiated squamous cell carcinoma, 6.5 cm in length and metastatic to the lymph nodes, from a Zulu male aged 62 in 1976 (116).

2.2.2) *In silico*-designed compound

The unique, non-commercially available ESE-16 compound was *in silico*-designed with the use of the Chimera package from the Resource for Biocomputing, Visualization and Informatics at the University of California, San Francisco (supported by NIH P41 RR-01081), which was used for structure preparation and visualization of the compound (94). Docking studies were carried out with Autodock 4.0 and AutoDockTools4 (Scripps Research Institute, La Jolla, CA, USA) (94). The ESE-16 compound was synthesized by iThemba Pharmaceuticals (Pty) Ltd (Modderfontein, Gauteng, South Africa).

2.2.3) General laboratory reagents and supplies

Dulbecco's Modified Eagle Medium (DMEM) and F-12 Nutrient Mixture, formulated from single-cell plating of Chinese Hamster Ovary (CHO) cells (HAM's-F12), was obtained from Sigma-Aldrich Co. (St. Louis, USA). Penicillin, streptomycin, fungizone, gentamycin and trypsin were obtained from Highveld Biological (Pty) Ltd (Sandringham, SA). Phosphate-

buffered saline (PBS) was purchased from Gibco-BRL (Invitrogen, Carlsbad, CA, USA). Dimethyl sulphoxide (DMSO), trypan blue, propidium iodide (PI), RNase A and actinomycin D was supplied by Sigma-Aldrich Co. (St. Louis, USA). Ethanol was purchased from Merck (Darmstadt, Germany). Fetal calf serum (FCS), sterile cell culture flasks, cell culture plates and syringe filters (0.22 μM) were obtained from Separation Scientific (Randburg, Johannesburg, SA). All other analytical grade chemicals were supplied by Sigma-Aldrich Co. (St. Louis, USA).

2.3) General laboratory procedures

2.3.1) Preparation of general cell culture maintenance reagents

(i) Dulbecco's modified eagle medium complete

DMEM with glucose, sodium pyruvate and L-glutamine was supplemented with 10% fetal bovine serum, 100μg/l penicillin, 100μg/l streptomycin and 250μg/l fungizone.

(ii) Phosphate buffered saline

A tenfold concentrated stock solution of PBS consisting of 80g/l NaCl, 2g/l KCl, 2g/l KH_2PO_4 and 11.5g/l Na_2PO_4 was prepared and the pH adjusted to 7.4. The solution was stored at 4˚C in aliquots of 500ml. One times solution was made and then autoclaved (120˚C, 15psi, 20 min) before being used.

(iii) **Freeze medium**

Freeze medium was made by adding 70% complete DMEM, 20% FCS and 10% DMSO to a 50ml sterile tube and stored at 4˚C.

2.3.2) General cell culture maintenance

(i) Maintenance and subculturing

The SNO cells were maintained in 25cm^2 tissue culture flasks within a water-jacketed CO_2 incubator (Forma Scientific Inc. Ohio, USA) at a humidified atmosphere of 37°C with 5% CO_2. They were allowed to proliferate in 5ml DMEM complete with glucose, sodium pyruvate and L-glutamine in 25cm^2 cell culture flasks. The growth medium was routinely replased with fresh growth medium. When the cells were confluent, they were dispersed by

trypsinization. This was done by removing the medium from the cell culture and washing the cells with 2ml PBS. Trypsin (1ml), derived from beef pancreas (0.125% Trypsin, 0.1% Versene EDTA) was added to the cells and the flask was incubated at 37°C for 2-3 min. Trypsin was removed and the cells were detached by gently hitting the flask. Cells were resuspendend in fresh medium and divided into subcultures or used in experiments. All solutions were filtered through a 0.22µm membrane filter and all procedures were conducted under sterile conditions.

(ii) Preservation

Cells were frozen at a concentration of 4×10^6 cells/ml in cell culture freeze medium. The freeze medium was prepared as stated above. A cell suspension of 1ml was transferred into 1.5ml cryovials which was then wrapped in cotton wool and placed in a polystyrene foam box. This ensured that the vials cool at a rate of 1˚C/min. The box was placed in a freezer (-70˚C) for a day or two, afterwhich the vials were transferred to liquid nitrogen for long term storage.

2.3.3) Experimental procedures

Experiments were conducted at a concentration of 0.2µM with a 24 hour seeding time to allow for attachment and a 24 hour exposure time in a humidified atmosphere (37°C with 5% CO_2). A stock solution of 10mM ESE-16 was dissolved in DMSO and diluted with medium to the desired concentration prior to exposure of the cells. The concentration of 0.2µM for ESE-16 was chosen since previous dose-dependent investigations conducted in our laboratory showed ESE-16 inhibiting cell proliferation to 50% from concentrations ranging from 0.18µM to 0.22µM (94).

Experiments were conducted in 6-well plates or $25cm^2$ cell culture flasks. For 6-well plates, cells were seeded on heat-sterilized coverslips at a density of 5×10^5 cells per well in 3ml of medium. For $25cm^2$ cell culture flasks, cells were seeded at 1×10^6 cells in 5ml of medium.

The number of cells was determined with the use of a haemocytometer. A 20µl cell suspension was resuspended in 80µl PBS; 20µl of that solution was then mixed with 20µl trypan blue. This method provides a cellular concentration with a dilution factor of 10. Trypan blue is an exclusion dye which can only penetrate cellular membranes of cells which

are no longer intact, staining the non-viable cells blue (117). The number of cells/ml was determined by the following equation:

$$\text{Cells/ml} = \text{Average count of viable cells in the four corner squares of haemocytometer x Dilution factor x } 10^4$$

Appropriate controls were included namely: cells propagated in complete medium only, a vehicle control which was composed of cells treated with DMSO, the final dilution never exceeding 0.02% (v/v) (102,118). Actinomycin D (0.1µg/ml in growth medium) was used as a positive control for the induction of apoptosis (118).

2.4) Methods

2.4.1) Polarization-optical differential interference contrast

PlasDIC microscopy is an improved polarization-optical transmitted light differential interference contrast method from Zeiss (Carl Zeiss MicroImaging GmbH, Göttingen, Germany) where linearly polarized light is only generated after the objective, thus providing images of outstanding quality (119,120). The technique utilizes a beam of polarized light that is split in two and takes slightly different pathways through the sample (97). The optical density of the sample causes the two beams to interfere with each other before recombining resulting in a three dimensional image indicating the variations in optical density of the samples (97). PlasDIC was used to observe morphological characteristics and cell density changes of SNO cells after exposure to ESE-16 and the appropriate controls and provided high-quality imaging of individual cells and cell clusters in plastic cell culture vessels. The images were viewed and captured at a magnification of ×40 using the Zeiss Axiovert-40 microscope (Zeiss, Göttingen, Germany).

2.4.2) Light microscopy

2.4.2.1) Haematoxylin and eosin staining

H&E staining allows for the quantitative comparison of the morphological characteristics of the cytoplasm and nuclear components (96). Hematoxylin has a deep blue-purple color and

stains nucleic acids while eosin is pink and stains proteins nonspecifically (121). Thus, during a general H&E staining experiment, the nuclei of the cells are stained blue, whereas the cytoplasm and extracellular matrix are stained varying degrees of pink (121).

In order to obtain quantitative data from the morphological study, mitotic indices were determined (122). One thousand cells were counted on each slide of the biological replicates and divided into their different phases (122,123). Identification of cells in interphase, the different mitotic phases and cells undergoing apoptosis were done based on their cellular and nuclear morphology (124). Cells that could not be categorized due to excessive fragmentation, unusual nuclear morphology or a lack of clear nuclear material were defined and counted as abnormal (97). The data are expressed as the percentages of cells in each phase.

(i) Materials

Haematoxylin, eosin, ethanol and xylol were purchased from Merck (Darmstadt, Germany). Bouin's fixative was purchased from Sigma-Aldrich Co. (Clubview, South Africa).

(ii) Method

SNO cells were seeded in complete growth medium at 5×10^5 cells per well in 6-well plates on heat-sterilized coverslips. Cells were exposed to ESE-16 and the appropriate controls discussed previously (2.3.3). After the 24 hour incubation period, coverslips were removed from the wells and transferred to a staining dish. Bouin's fixative was added to the staining dish until the entire sample slide was covered. Samples were incubated at room temperature for 30 min after which the Bouin's fixative was discarded and replaced with 70% ethanol for 20 min to dehydrate the cells. Excess fixative was removed and the staining dish was rinsed with tap water to remove excess ethanol. Haematoxylin was added until the entire sample slide in the staining dish was covered. Samples were incubated at room temperature for 20 min. The staining dish was rinsed with tap water for 2 min and then rinsed with 70% ethanol to remove any excess stain. Eosin (1%) was added to the staining dish until the entire sample slide was covered. Samples were incubated at room temperature for 2 min. The staining dish was rinsed twice for 5 min with 70% ethanol, twice for 5 min with 96% ethanol, twice for 5 min with 100% ethanol and twice for 5 min with xylol. Coverslips were mounted on microscope slides with resin and left overnight to dry. Samples were evaluated at a magnification of ×20 with Zeiss Axiovert MRc microscope (Zeiss, Oberkochen, Germany).

2.4.3) Electron microscopy

2.4.3.1) Transmission electron microscopy

TEM allows a beam of coherent electrons to be directed on to a sample under vacuum (125). Due to the scattering of electrons within the sample, small objects inside the cell can be viewed directly (125). This allows for the study and subsequent better understanding of biological structure-function relationships at cellular, subcellular and molecular levels (46,125,126). TEM was used to provide precise intracellular information of the SNO cells.

(i) Materials

Glutaraldehyde, osmium tetroxide, EMBED 812, uranyl acetate and Reynold's lead citrate were purchased from Merck (Darmstadt, Germany) and provided by the Electron Microscopy Unit of the University of Pretoria (Pretoria, South Africa).

(ii) Method

SNO cells were seeded in complete growth medium at 1.5×10^6 cells per $25cm^2$ flask and were subsequently exposed to ESE-16 and the appropriate controls. After the 24 hour incubation period, cells were trypsinized and the samples were resuspended in 1ml DMEM complete medium. Samples were fixed with PBS:2.5% gluteraldehyde (9:1) solution for 45 min at room temperature and then rinsed three times for 5 min each with PBS. Samples were fixed again with osmium tetroxide for 15 min and rinsed afterwards three times for 5 min each with PBS. The samples were dehydrated with increasing ethanol concentrations (30%, 50%, 70%, 90%, 100%) and left overnight in 100% ethanol. Samples were then infiltrated and embedded with 100% EMBED 812. Ultrathin sections of the samples were prepared using a microtome and were contrasted using 4% uranyl acetate for 5 min and Reynolds' lead citrate for 2 min, then rinsed with water and viewed at a scale bar of between 2-10µm with a Multi-purpose Philips 301 TEM (Electron Microscopy Unit, University of Pretoria, South Africa).

2.4.4) Confocal microscopy

2.4.4.1) Confocal-alpha (α)-tubulin assay

A confocal microscope creates sharp images by performing point-by-point image construction by focusing a point of light sequentially across a specimen, excluding most of the light from the specimen that is not from the microscope's focal plane (127). Confocal microscopy was employed to observe the effects of ESE-16 on the microtubule tubulin dynamics of SNO cells after 24 hours exposure time.

(i) Materials

Alpha-tubulin antibody, alexafluor 488 and 4',6-diamidino-2-phenylindole (DAPI) were purchased from BIOCOM biotech (Pty) Ltd (Clubview, South Africa).

(ii) Method

SNO cells were seeded in complete growth medium at 5×10^5 cells in 6-well plates on heat-sterilized coverslips and exposed to ESE-16 and the appropriate controls. After the 24 hour incubation period the samples were fixed with 1.5ml glutaraldehyde fixer for 10 min at 37°C and then permeabilized with 2ml permeabilization buffer for 15 min at room temperature. Samples were stained first with a 100µl mouse monoclonal antibody against human α-tubulin (Clone 2-28-33; 1:1000) for 1.5 hours at 37°C. After the incubation period, samples were washed with PBS for 5 min at room temperature and then stained with a secondary antibody, biotin-conjugated anti-mouse IgG 58 (Fab-specific, developed in goat) in fluorescein isothiocyanate (FITC)-conjugate diluent (100µl), for 1.5 hours at 37°C. After three 5 minute washes with PBS, coverslips were stained with DAPI (2ml), a nucleic stain that produces blue fluorescence for 10 min at room temperature. Samples were mounted with a glycerol-based mounting fluid on glass slides and viewed with a Zeiss LSM 510 META confocal laser microscope at the Electron Microscopy unit at the University of Pretoria (Pretoria, South Africa). Images taken by the microscope were visualized at 10µm with the use of ZEN 2009 software (Carl Zeiss (Pty) Ltd Johannesburg, South Africa).

2.4.5) Flow cytometry

Flow cytometry is a well-established technique in clinical diagnostics and biomedical research and a powerful discovery tool in biotechnology (128,129). It allows for accurate and multiparametric analysis of cell populations or single cells (128,129). Parameters that can be measured and studied include size, granularity, surface and intracellular protein expression and gene expression of cells (128-130).

Cell samples are placed in suspension and are drawn into a stream created by a surrounding sheath of isotonic fluid that creates laminar flow, allowing the cells to pass single file across one or more laser interrogation points (128,130). A beam of monochromatic light intersects the cells at the interrogation points (130). The forward scatter on the laser light is commonly used to approximate cell size, while the amount of side scatter generally correlates with the degree of granularity of a cell (126,130). Fluorescent dyes added to the cell may bind to or intercalate with different cellular components such as DNA or RNA (130). Additionally, antibodies conjugated to fluorescent dyes can bind to specific proteins on or inside cells (130). When such labelled cells pass by the interrogation point, the fluorescent molecules are excited to a higher energy state causing fluorochromes to emit light energy at higher wavelengths when returning to their resting states (130). Light emitted is collected and directed to a series of filters and dichroic mirrors that isolate particular wavelength bands which are detected by photomultiplier tubes and digitized for computer analysis (130).

2.4.5.1) Cell cycle progression

This flow cytometric technique was developed to take a single time-point cell measurement to study cell cycle progression and DNA integrity within a cell population (131). Single time-point measurement reveals percentage of cells in the different phases of the cell cycle (G_1, S, G_2/M) at a specific point in time (131). Cell cycle analysis was performed via PI staining (94) to study cell cycle progression and DNA integrity of the SNO cells.

(i) Materials

PI and RNase A were purchased from Sigma-Aldrich Co. (St. Louis, USA). Ethanol was purchased from Merck (Darmstadt, Germany).

(ii) Method

SNO cells were seeded in complete growth medium at $1x10^6$ cells per $25cm^2$ flasks and were exposed to ESE-16 and the appropriate controls. Samples were trypsinized and centrifuged at 400 x g. Supernatant was removed and the cell pellet was resuspended in 1ml ice-cold PBS. Samples were centrifuged at 400 x g and supernatant was removed. Samples were fixed in 200µl ice-cold PBS containing 0.1% fetal bovine serum. Ethanol (4ml) (70%) was added dropwise to the solution while vortexing. Samples were left at 4°C overnight.

After fixation, samples were centrifuged and the supernatant was removed. Samples were resuspended in PBS containing PI (40µg/ml), RNase A (100µ/ml) and 0.1% triton X-100 and incubated at 37°C for 40 min. Fluorescence was measured by using the FL3 channel of a fluorescence-activated cell sorting (FACS) FC500 system flow cytometer equipped with an air-cooled argon laser excited at 488 nm (Beckman Coulter South Africa (Pty) Ltd). This experiment was repeated three times with at least 10 000 to 30 000 events being counted for each repeat and analysis of the data were conducted by using the Cyflogic program created by Pertu Terho and Mika Korkeamäki from CyFlo Ltd (Finland).

2.4.5.2) Apoptosis detection assay

During apoptosis, the asymmetry between the phospholipid content of the inner - and outer leaflet of the plasma membrane is lost in order to attract macrophages to the apoptotic cells to engulf them (57,59,109). Thus, one of the earliest indications of apoptosis is the translocation of PS from inner to outer leaflet of the plasma membrane where it becomes exposed (57,94). Annexin V is a Ca^{2+}-dependent, phospholipid binding protein with a high affinity for PS (27,46,59) and is used when conjugated to a fluorochrome (FITC), as an indicator of early apoptosis (57,94).

(i) Materials

Annexin V-FITC Apoptosis Detection Kit was purchased from BioVision (Mountain View, California, USA).

(ii) Method

SNO cells were seeded in complete growth medium at $1x10^6$ cells per $25cm^2$ flasks and were exposed to ESE-16 and the appropriate controls. Samples were trypsinized, resuspended in

1ml 1x Binding Buffer and centrifuged at 300 × g for 10 min. Supernatant was removed and samples were resuspended in 100µl of the 1x Binding Buffer. Subsequently, 10µl of Annexin V-FITC was added and samples were incubated for 15 min in the dark at room temperature. After incubation, samples were washed with 1ml 1x Binding Buffer and centrifuged at 300 × *g* for 10 min. Supernatant was carefully pipetted off and samples were resuspended in 500µl 1x Binding Buffer solution. The FL1 channel was used to measure Annexin V-FITC fluorescence and was conducted with an FACS FC500 system flow cytometer (Beckman Coulter South Africa (Pty) Ltd) equipped with an air-cooled argon laser with an excitation wavelength of 488nm. This experiment was repeated three times with at least 10 000 to 30 000 events being counted for each repeat. Analysis of the data were conducted with the use of Cyflogic version 1.2.1 software (Peru Therho, Turko, Finland).

2.4.5.3) Cyclin B levels

Cyclin proteins bind to CDKs, resulting in the formation of an active cyclin-CDK complex that regulates the cell's journey through the cell cycle (18,22,23,27). Cyclin B and CDK1 form the MPF that allows the cell to enter the mitotic phase of the cell cycle (18,22,24,31).

Defects in spindle assembly or spindle-kinetochore attachment during the mitotic phase are sensed by the spindle checkpoint which will cause metaphase arrest by inhibiting cyclin B degradation (22,28,37-39). Elevated cyclin B levels are thus used as an indicator of metaphase arrest. An anti-cyclin B1-FITC conjugated antibody was used to quantify the cyclin B levels (110) in the SNO cells.

(i) Materials

The milli-mark anti-cyclin B1 clone GNS3 (8A5D12) was purchased from Millipore Corporation (Billerica, MA, USA).

(ii) Method

SNO cells were seeded at 1×10^6 cells per $25cm^2$ flask and exposed to ESE-16 and the appropriate controls. Samples were trypsinized and washed with 1ml ice-cold PBS. Samples were centrifuged at 15 000 x g and the supernatant removed. The pellet was resuspended in 200µl ice-cold PBS containing 0.1% FCS to prevent non-specific binding in subsequent steps. Samples were fixed with 10ml ice-cold 70% ethanol and stored at 4°C for 24 hours. After 24

hours, samples were centrifuged at 1000 x g and washed twice with 500µl PBS to remove excess ethanol. A working antibody solution was prepared by diluting the primary antibody (FITC-conjugated anti-cyclin B1) with PBS in a 1:5 ratio. Working antibody solution (10µl) was added per $1x10^6$ cell sample to provide a final volume of 100µl with 90µl PBS containing 0.1% triton X-100. Samples were incubated with the conjugated cyclin B1 antibody solution for 40 min at 37°C. Samples were washed twice with 1ml PBS and were resuspended in 600µl PBS. All procedures after the incubation with the antibody were performed in the dark. The FITC fluorescence was measured with an FACS FC500 system flow cytometer from Beckman Coulter South Africa (Pty) Ltd equipped with an air-cooled argon laser with a 488nm excitation wavelength. This experiment was repeated three times with at least 10 000 to 30 000 events being counted for each repeat. Analysis of the data were conducted with the use of Cyflogic version 1.2.1 software (Peru Therho, Turko, Finland).

2.4.5.4) Mitochondrial membrane potential

Under normal circumstances, the ΔΨm ranges from 120 to 180mV with the intramitochondrial side being electronegative (48). Lipophilic cations accumulate in the mitochondrial matrix, driven by the ΔΨm, causing the cations to be 2 to 3 logs more concentrated in the mitochondrial matrix than in the cytosol (48). Cationic lipophilic fluorochromes may be used to measure the ΔΨm (48).

The Mitotracker kit allows us to measure the ΔΨm by labelling the mitochondria with a cationic dye named 5,5',6,6'-tetrachloro-1,133'-tetra-ethylbenzimidazolyl-carbocyanine iodide, which passively diffuse across the plasma membrane and accumulate in active mitochondria providing red fluorescence (119). However, if there is a reduction in ΔΨm, the dye cannot aggregate in the mitochondria and thus remains in the cytoplasm in its monomer form, generating green fluorescence (119).

(i) Materials

The Mitotracker kit was purchased from Biocom Biotech Pty Ltd. Clubview, South Africa.

(ii) Method

SNO cells were seeded at 1×10^6 cells per $25cm^2$ flask and exposed to ESE-16 and the appropriate controls. Samples were trypsinized and centrifuged at 13 000 x g and the

supernatant was removed. Samples were resuspended in 1ml diluted Mitocapture solution and incubated at 37°C for 20 min. Samples were centrifuged at 500 x g, the supernatant was removed and was resuspended in 1ml pre-warmed (37°C) incubation buffer. Samples were analysed using an FACS FC500 System flow cytometer equipped with an air-cooled argon laser excited at 488nm (Beckman Coulter South Africa (Pty) Ltd). Apoptotic cells were detected in the FL1 FITC channel showing diffused green fluorescence. Healthy cells were detected in the FL2 channel showing red fluorescence. This experiment was repeated three times with at least 10 000 to 30 000 events being counted for each repeat. Analysis of the data were conducted with the use of Cyflogic version 1.2.1 software (Peru Therho, Turko, Finland).

2.4.5.5) Reactive oxygen species

In the mitochondria, ROS is generated via the electron transport chain and can accumulate as by-products, which can lead to mitochondrial proteins and mitochondrial DNA, causing loss of electron transport, decrease in ATP production and $\Delta\Psi m$ dissipation (44,67,68,132). In addition, ROS accumulation is believed to act as signaling molecules which initiates MMP, causing the release of pro-apoptotic proteins (47,67).

This superoxide anion can be regarded as the precursor for most ROS (44). Suspected O_2^- generation was assessed using hydroethidine (HE), an O_2^--sensitive dye which is oxidized by O_2^- to a red fluorescing compound (67,105).

(i) Materials

HE was purchased from Sigma-Aldrich Co. (St Louis, USA).

(ii) Method

SNO cells were seeded in complete growth medium at 1×10^6 cells per $25cm^2$ flask and exposed to ESE-16 and the appropriate controls. Cells were trypsinized and resuspended in 1ml PBS. Samples were resuspended in 10µM HE for 15 min at 37°C. Fluorescence was measured on the FL2 channel of an FACS FC500 System flow cytometer (Beckman Coulter South Africa (Pty) Ltd equipped with an air-cooled argon laser with an excitation wavelength of 488nm. This experiment was repeated three times with at least 10 000 to 30 000 events

being counted for each repeat. Analysis of the data were conducted with the use of Cyflogic version 1.2.1 software (Peru Therho, Turko, Finland).

2.4.5.6) Cytochrome *c*

Cytochrome *c* is a critical apoptogen that plays an important role in the intrinsic apoptotic pathway (58,59,63). When cytochrome *c* is lost from the mitochondria, the electron transport chain is disrupted, causing ROS production and loss in $\Delta\Psi m$, which may play a role in MMP (60,61). In addition, when released into the cytosol, cytochrome *c* binds to the adapter molecule Apaf-1, allowing dATP to bind onto Apaf-1 inducing conformational changes and causing Apaf-1 to oligomerize into the Apaf-1 apoptosome (27,48,58-61). The FlowCellect Cytochrome *c* kit was used to assess the loss of mitochondrial cytochrome *c* in cells exposed to ESE-16.

(i) Materials

The cytochrome *c* kit was purchased from FlowCellect (Millipore Corporation, Billerica, MA, USA)

(ii) Method

SNO cells were seeded at 1×10^6 cells per $25cm^2$ flask and exposed to ESE-16 and the appropriate controls. Samples were trypsinized and centrifuged at 300 × g for 5 min. Supernatant was removed and samples were resuspended in 200µl PBS. Samples were centrifuged at 300 × g for 5 min and the supernatant was removed before 100µl of permeabilization buffer working solution was added. Samples were incubated for 10 min on ice after which 100µl fixation buffer was added. Samples were incubated at room temperature for 20 min, centrifuged for 5 min at 300 × g and the supernatant was removed. 1 × Blocking buffer (150µl) was added and samples were centrifuged at 300 × g for 5 min. Supernatant was removed and 1 × Blocking buffer (100µl) was added. Samples were incubated at room temperature for 30 min. Anti-cytochrome *c*-FITC antibody (10µl) was added to each sample and samples were incubated at room temperature for 30 min in the dark. 1 × Blocking buffer (100µl) was added to each sample before being centrifuged for 5 min at 300 × g. Supernatant was removed and 200µl 1 × Blocking buffer was added to each sample. FITC fluorescence was measured at FL1 channel with an FACS FC500 system flow cytometer (Beckman Coulter South Africa (Pty) Ltd) equipped with an air-cooled argon laser with an excitation

wavelength of 488nm. According to the user's manual, viable cells demonstrates higher levels of fluorescence while apoptotic cell, which have released their cytochrome *c* from their mitochondria will demonstrate a lower level of fluorescence. This experiment was repeated three times with at least 10 000 to 30 000 events being counted for each repeat. Analysis of the data were conducted with the use of Cyflogic version 1.2.1 software (Peru Therho, Turko, Finland).

2.4.6) Spectrophotometry

2.4.6.1) Redox status

Several studies have suggeted that pyridine nucleotides may be directly involved in cell death (79,81). Due to their critical role in oxidative stress, NAD^+/NADH and $NADP^+$/NADPH ratios can affect cell survival by influencing oxidative stress and the antioxidation systems of the cells (81). It is also believed that the NAD^+/NADH and $NADP^+$/NADPH ratios can modulate PTP openings, significantly influencing the $\Delta\Psi m$ and MMP (79,81,82). In addition, it has been reported that NADH/NADPH depletion is an early event in apoptosis (79,81,82).

NAD^+/NADH and $NADP^+$/NADPH quantification were determined to study the effects of ESE-16 on the redox status of the SNO cells after 24 hours of exposure. BioVision's NAD^+/NADH – and $NADP^+$/NADPH Quantification Kit detect the intracellular nucleotides and their ratio.

(i) Materials

The NAD^+/NADH and $NADP^+$/NADPH Quantification Kits were purchased from BioVision (Mountain View, California, USA).

(ii) Method

SNO cells were seeded in complete growth medium at 1×10^6 per $25cm^2$ flask and exposed to ESE-16 and the appropriate controls. Cells were trypsinized and washed with cold PBS. Samples were transferred to eppendorf tubes and the NAD^+/ NADH or $NADP^+$/NADPH proteins was extracted from the cells with 100µl extraction buffer. Supernatant (50µl) was transferred in duplicate to wells in a 96-well plate to detect the total amount of NAD^+ and NADH (NADt) or $NADP^+$ and NADPH (NADPt). To detect only NADH or NADPH, 200µl

of samples were aliquoted into separate eppendorf tubes and heated at 60°C for 30 min in a waterbath. This causes the NAD^+ or the $NADP^+$ to denature while the NADH or the NADPH remain unchanged. Samples (50µl) were transferred in duplicate to 96-well plates. NADP Cycling Mix (100µl) was added to each well and after a 5 min incubation period at RT, 10µl NADPH developer was also added to each well. After 1 hour incubation, absorbance was determined with the use of an EL_x800 Universal Microplate Reader (Bio-Tek Instruments Inc.Vermont, USA) at a wavelength of 450 nm. The concentration of NADt, NADH, NADPt and NADPH within each sample was calculated with the use of a standard curve. According to the manufacturer's manual, the NAD^+/NADH and $NADP^+$/NADPH ratio can be calculated using the following equations:

Ratio = (NADt - NADH)/NADH and (NADPt – NADPH)/ NADPH

2.4.6.2) Caspase activity

The activation of the initiator and effector caspases will induce the caspase cascade and will lead to cell death through the coordinated cleavage of a specific collection of protein substrates (59,83,85). Caspase 9 is known to be an initiator caspase and caspase 3 an effector caspase in the intrinsic apoptotic pathway (48,59,83).

The activity of caspase 9 and - 3 due to ESE-16-exposure was investigated with the use of a Caspase 9 and - 3 Colorimetric Kit. The assays were based on the detection of the chromophore *p*-nitroanilide (*p*NA) at a wavelength of 405nm via spectrophotometry.

(i) Materials

Caspase 3 and - 9 Colorimetric Kits were purchased from BioVision (Mountain View, California, USA).

(ii) Method

SNO cells were seeded in complete growth medium at 1×10^6 cells per $25cm^2$ flask and exposed to ESE-16 and the appropriate controls. Cells were trypsinized and centrifuged at 250 x g for 10 min. Supernatant was removed and samples were lysed with the addition of cold lysis buffer and were incubated on ice for 10 min. Samples were centrifuged at 10 000 x g for 1 min and supernatant was transferred to new tubes and kept on ice. This was expected to yield a cell lysate with an approximate protein concentration of 2 - 4 mg/ml. Cell lysate

(50µl) were added to wells in a 96-well plate. 2× Reaction Buffer (50µl) containing dithiothreitol (DDT) stock was added to samples along with 5µl of caspase-3/-9 colorimetric substrate. The plate was incubated at 37° C for 1 - 2 hours. Absorbance was determined at a wavelength of 405nm with the use of an EL_x800 Universal Microplate Reader (Bio-Tek Instruments Inc. Vermont, USA).

2.5) Logistics

Experiments were conducted in the cell culture laboratory of the Department of Physiology at the University of Pretoria. All techniques discussed were standardized at the Department of Physiology at the University of Pretoria. Transmission electron microscopy and confocal microscopy were conducted at the Electron Microscopy Unit at the University of Pretoria. Flow cytometry was conducted at the Department of Pharmacology at the University of Pretoria.

2.6) Statistical Analysis

Qualitative analysis was obtained via PlasDIC, light microscopy, confocal microscopy and TEM. Quantitative analysis was obtained via mitotic indices, flow cytometry and spectrophotometry. All experiments conducted were repeated three times. For the techniques that involved flow cytometry, 10 000 to 30 000 events were counted for each repeat and analysis of the data was done with the use of the Cyflogic program, version 1.2.1, created by Perttu Terho and Mika Korkeamäki from CyFlo Ltd. based in Finland. Quantitative data was analysed for significance by using student *t*-test statistics. A *P*-value of < 0.05 was regarded as statistically significant.

Chapter 3
Results

3.1) Polarization-optical differential interference contrast

PlasDIC images were used to visualize morphological changes in the SNO cells after exposure to ESE-16 and the appropriate controls. Cells propogated in medium (Figure 3.1 A) and vehicle-treated cells (Figure 3.1 B) showed normal cell morphology with the majority of the cells being in interphase. The positive control for apoptosis (Figure 3.1 C), cells treated with actinomycin D, showed a decrease in cell density and morphological characteristics of apoptosis such as membrane blebbing and apoptotic bodies. Also present, were bubble-like structures which are believed to indicate apoptotic cells undergoing secondry necrosis. Morphological changes of cells treated with ESE-16 (Figure 3.1 D) included a decrease in cell density, rounding of cells (indicative of mitotic block), membrane blebbing and the presence of apoptotic bodies. Bubble-like structures, indicating secondary necrosis, were also present.

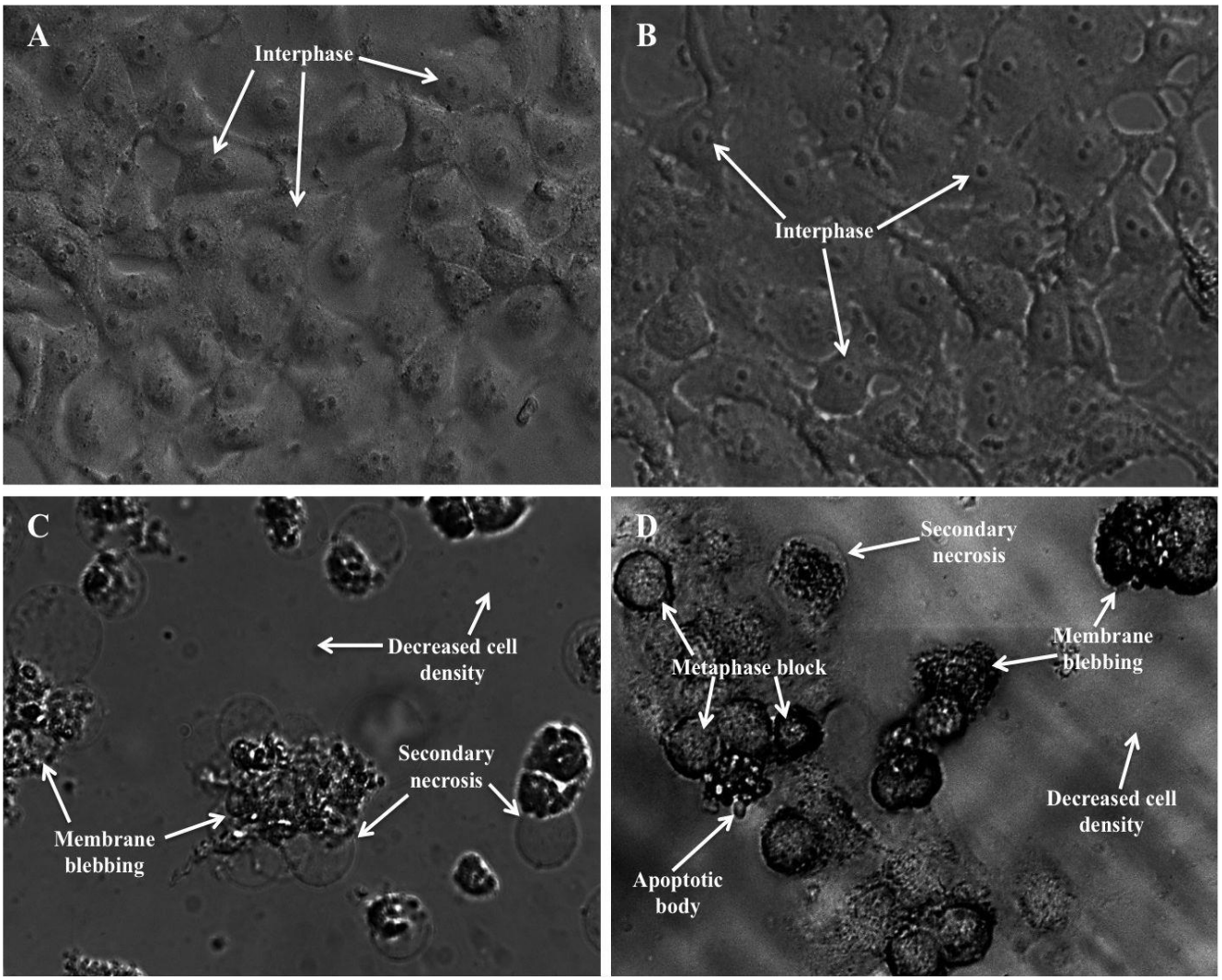

Figure 3.1 : Polarization-optical transmitted light differential interference contrast microscopy images of SNO cells. (A) Cells propogated in medium only, (B) cells exposed to DMSO – vehicle control, (C) cells exposed to actinomycin D – positive control and (D) cells exposed to ESE-16 at a concentration of 0.2µM. Cells propogated in medium and the vehicle-treated cells showed normal cell morphology with the majority of the cells being in interphase. The positive control for apoptosis showed a decrease in cell density and morphological characteristics of apoptosis such as membrane blebbing and apoptotic bodies. Morphological indicators of secondary necrosis (bubble-like structures visible on the membranes of the cells) were also observed. ESE-16-treated cells revealed a decrease in cell density, rounding of cells (indicative of metaphase block), membrane blebbing, apoptotic bodies (indicative of apoptotic cell death) and morphological indicators of secondary necrosis (Magnification: ×40).

3.2) Light microscopy

3.2.1) Haematoxylin and eosin staining

H&E staining was used to visualize morphological changes of the nuclear and cytoplasmic components in SNO cells after exposure to ESE-16 and the appropriate controls. Cells propogated in medium (Figure 3.2 A) and the vehicle-treated cells (Figure 3.2 B) showed normal cell morphology with the majority of the cells being in interphase. The positive control for apoptosis (Figure 3.2 C) and ESE-16-treated cells (Figure 3.2 D) showed a decrease in cell density and morphological characteristics of apoptosis such as membrane blebbing and apoptotic bodies. ESE-16-treated cells also showed an increase in the number of round cells with hypercondensed chromatin indicative of a metaphase block.

In addition to the qualitative data obtained, mitotic indices quantified the observed effects (Table 3.1). H&E staining allows for the identification of cells in interphase, the different mitotic phases and apoptotic cells (124). One thousand cells were counted on each slide of the biological replicates and divided into their different phases (123). Cells that could not be categorized due to excessive fragmentation, unusual nuclear morphology or a lack of clear nuclear material were defined and counted as abnormal (97). Data are expressed as the average percentages of cells in each phase. Mitotic indices revealed a significant increase, with a *P*-value of 0.0003*, in the percentage of cells in metaphase in the ESE-16-treated samples when compared to controls. ESE-16 treated cells also showed a significant increase in the percentage of cells undergoing apoptosis when compared to the appropriate controls (*P*-value of 0.0006)*.

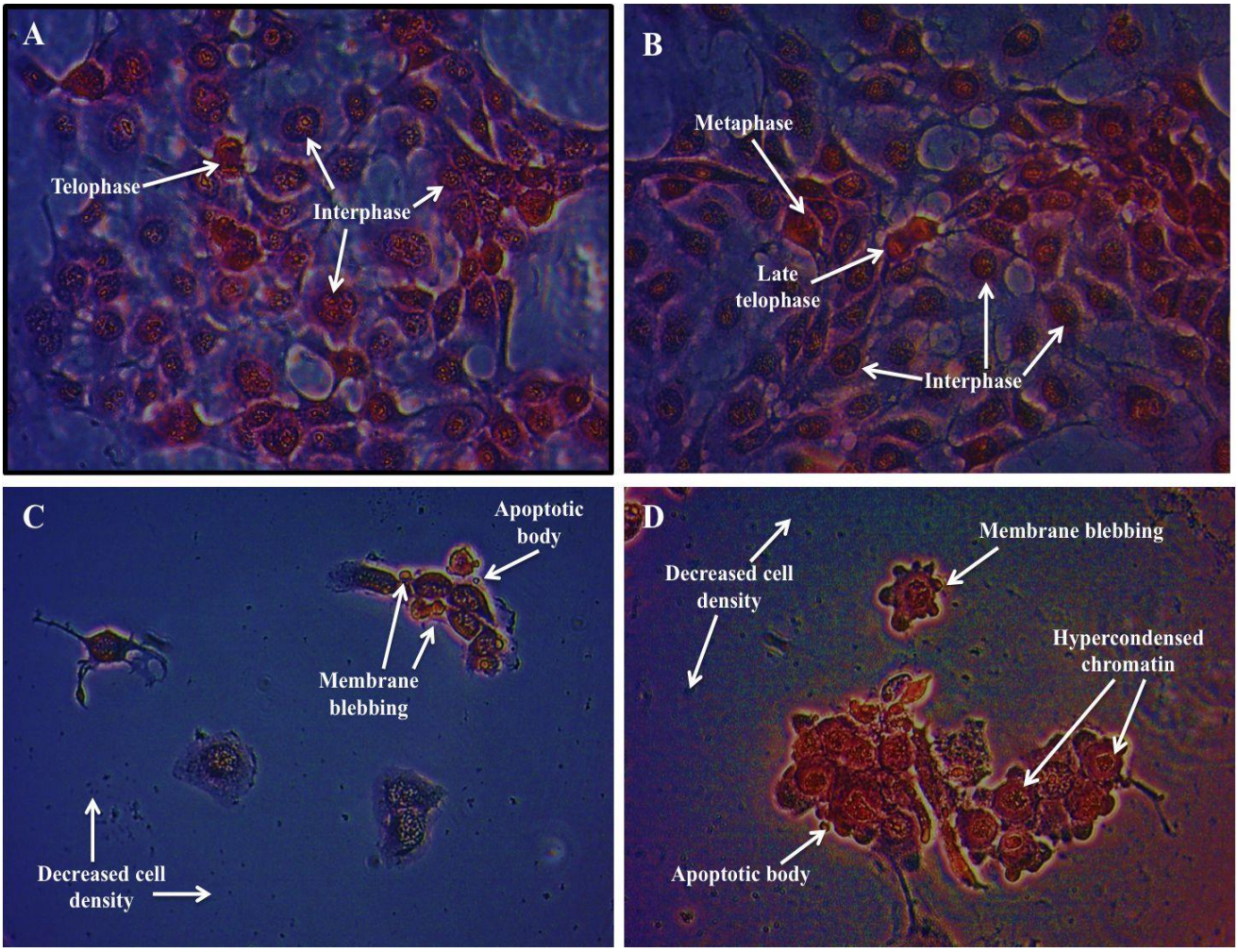

Figure 3.2: Haematoxylin and eosin staining images revealing morphological changes in the nuclear and cytoplasmic components in SNO cells. (A) Cells propogated in medium only, (B) cells exposed to DMSO – vehicle control, (C) cells exposed to actinomycin D – positive control and (D) cells exposed to ESE-16 at a concentration of 0.2µM. Cells propogated in medium and the vehicle-treated cells showed normal cell morphology, with the majority of the cells being in interphase. The positive control for apoptosis and the ESE-16 treated cells showed a decrease in cell density and morphological characteristics of apoptosis such as membrane blebbing and apoptotic bodies. The ESE-16 treated cells also showed an increase in the number of round cells with hypercondensed chromatin indicative of a metaphase block (Magnification: ×20).

Table 3.1: Average percentage of cells in interphase, cells in various stages of mitosis and cells displaying morphological characteristics of apoptosis.

	Interphase	Prophase	Metaphase	Anaphase	Telophase	Apoptosis	Abnormal
Medium	96.1%	0.6%	1.5%	0.4%	0.6%	0.5%	0.4%
DMSO	97.5%	0.2%	1.3%	0.2%	0.6%	0.2%	0.4%
Actinomycin D	60.2%	0.3%	2.5%	0%	0.5%	33.8%	2.3%
ESE-16	27.3%	0.7%	46.0% *	0.2%	0.4%	21.4% *	4.2%

3.3) Transmission electron microscopy

TEM was used to study the internal ultrastructure of the SNO cells after exposure to ESE-16 and the appropriate controls. Results revealed normal infrastructure of cells propogated in medium (Figure 3.3 A) and the vehicle control (Figure 3.3 B). Both revealed microvilli protruding from their cell membrane surface, a smoothly outlined nuclear membrane and well-preserved cytoplasmic organelles. The positive control for apoptosis (Figure 3.4 A and B) showed loss of microvilli, membrane blebbing and the presence of apoptotic bodies. Interestingly, figure 3.4 B showed a rupture of the plasma mebrane. This is believed to be a morphological characteristic of apoptotic cells which has phased into secondary necrosis due to the lack of scavenger cells to remove the dying cells (46,56). ESE-16-treated cell image (Figure 3.5 A) revealed the absence of the nuclear membrane, membrane blebbling and apoptotic body formation. Figure 3.5 B showed the remains of a cell or ghost cell, seen after the cell has been completely destroyed.

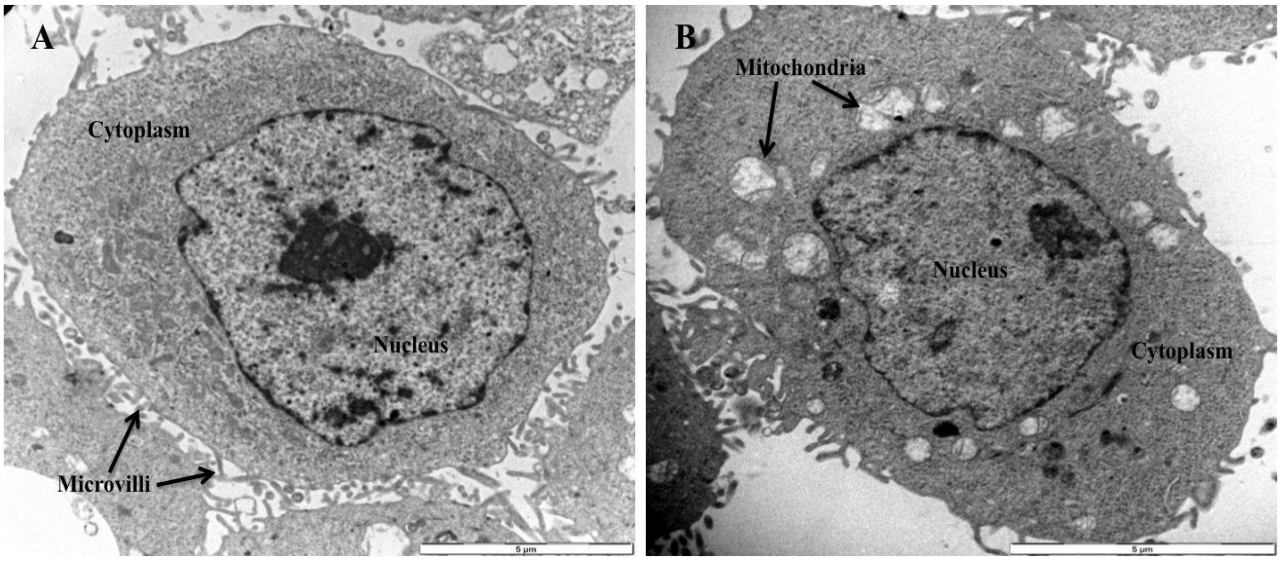

Figure 3.3: Transmission electron microscopy images providing information on the internal ultrastructure of SNO cells propogated in medium only and SNO cells treated with DMSO. (A) Cells propogated in medium only and (B) cells exposed to DMSO – vehicle control. Both the cells propogated in medium and the vehicle control cells showed microvilli protruding from their cell membrane surface. The nuclear membrane is smoothly outlined and well-preserved cytoplasmic organelles are visible. Scale bar: 5µm.

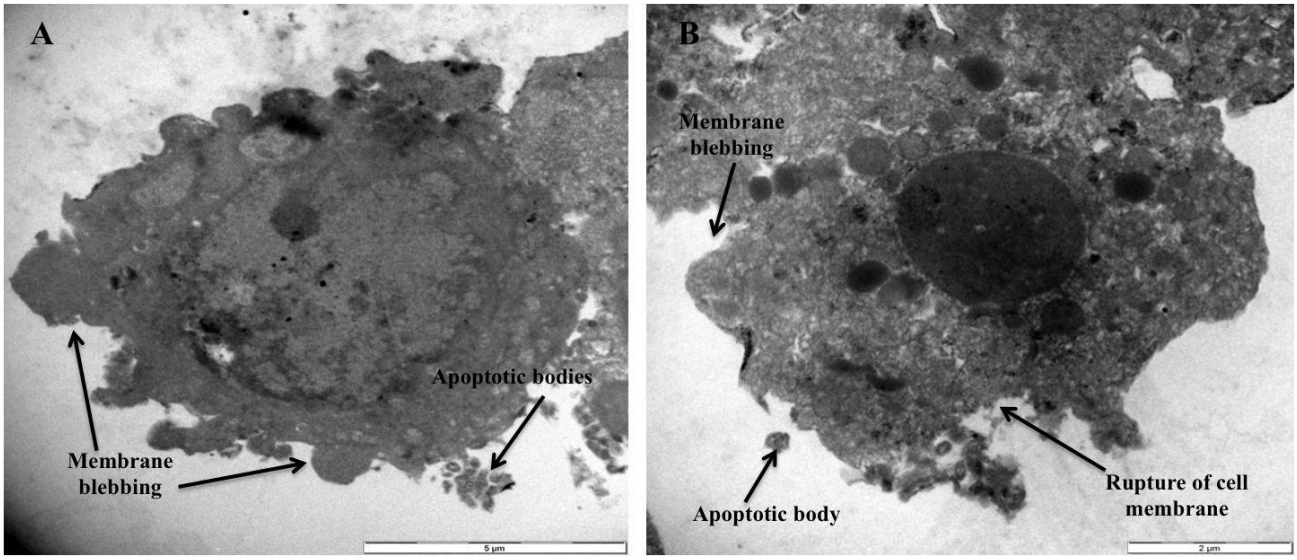

Figure 3.4: Transmission electron microscopy images providing information on the internal ultrastructure of SNO cells after exposure to actinomycin D. The positive control for apoptosis showed loss of microvilli, membrane blebbing and the presence of apoptotic bodies. Interestingly, figure 3.4 B showed a rupture of the plasma mebrane, believed to be a morphological characteristic of apoptotic cells which has phased into secondary necrosis due to the lack of scavenger cells to remove the dying cells (46,56). Scale bar: 5µm for figure 3.4 A and 2µm for figure 3.4 B.

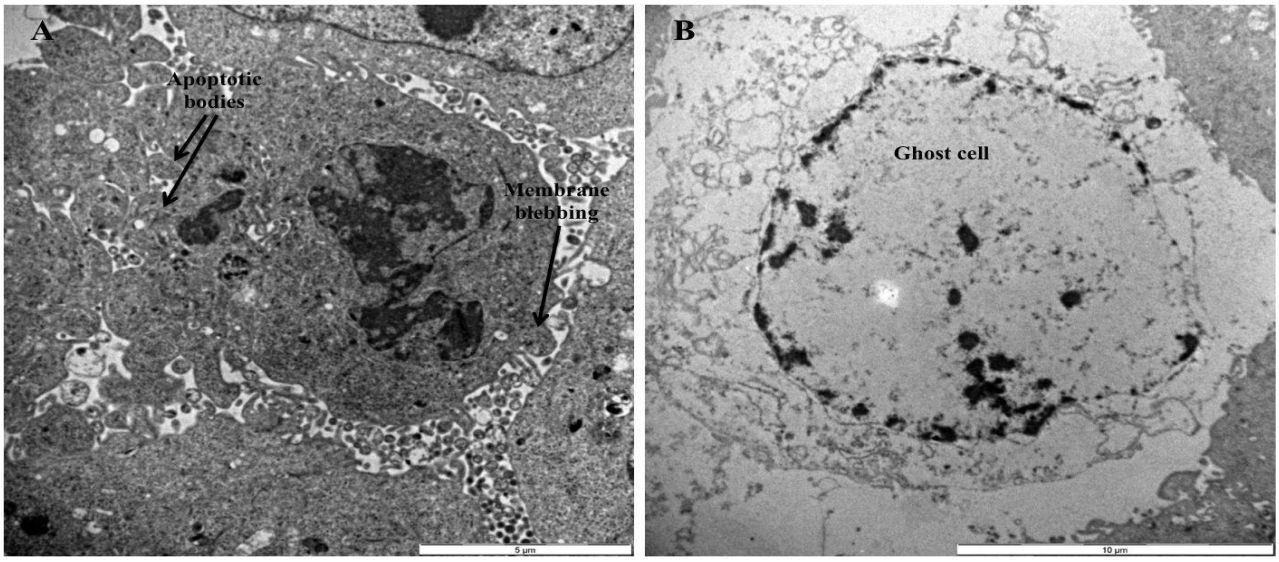

Figure 3.5: Transmission electron microscopy images revealing changes on the internal ultrastructure of SNO cells after exposure to 0.2µM ESE-16. (A) Revealed the absence of a membrane, membrane blebbling and apoptotic body formation while (B) shows the remains of a cell or ghost cell. Scale bar: 5µm for figure 3.5 A and 10µm for figure 3.5 B.

3.4) Confocal microscopy

Confocal microscopy was used determine the influence of ESE-16 on the cytoskeletal microtubule architecture of SNO cells after exposure to ESE-16 and the appropriate controls. Cells were stained with mouse monoclonal antibody against human α-tubulin and a secondary antibody, biotin-conjugated anti-mouse IgG 58 (Fab-specific, developed in goat) in a FITC-conjugate diluent which stained the α-tubulin of the cells green. DAPI was used to stain the nuclei of the cells blue to provide contrast to the green stain. Cells propogated in medium (Figure 3.6 A) and vehicle control cells (Figure 3.6 B) showed normal microtubule architecture. The positive control (Figure 3.6 C) showed a decrease in cell density and revealed shrunken cells. The ESE-16-treated cells (Figure 3.6 D) also showed a decrease in cell density and revealed abnormal spindle formation, indicating cells being blocked in metaphase.

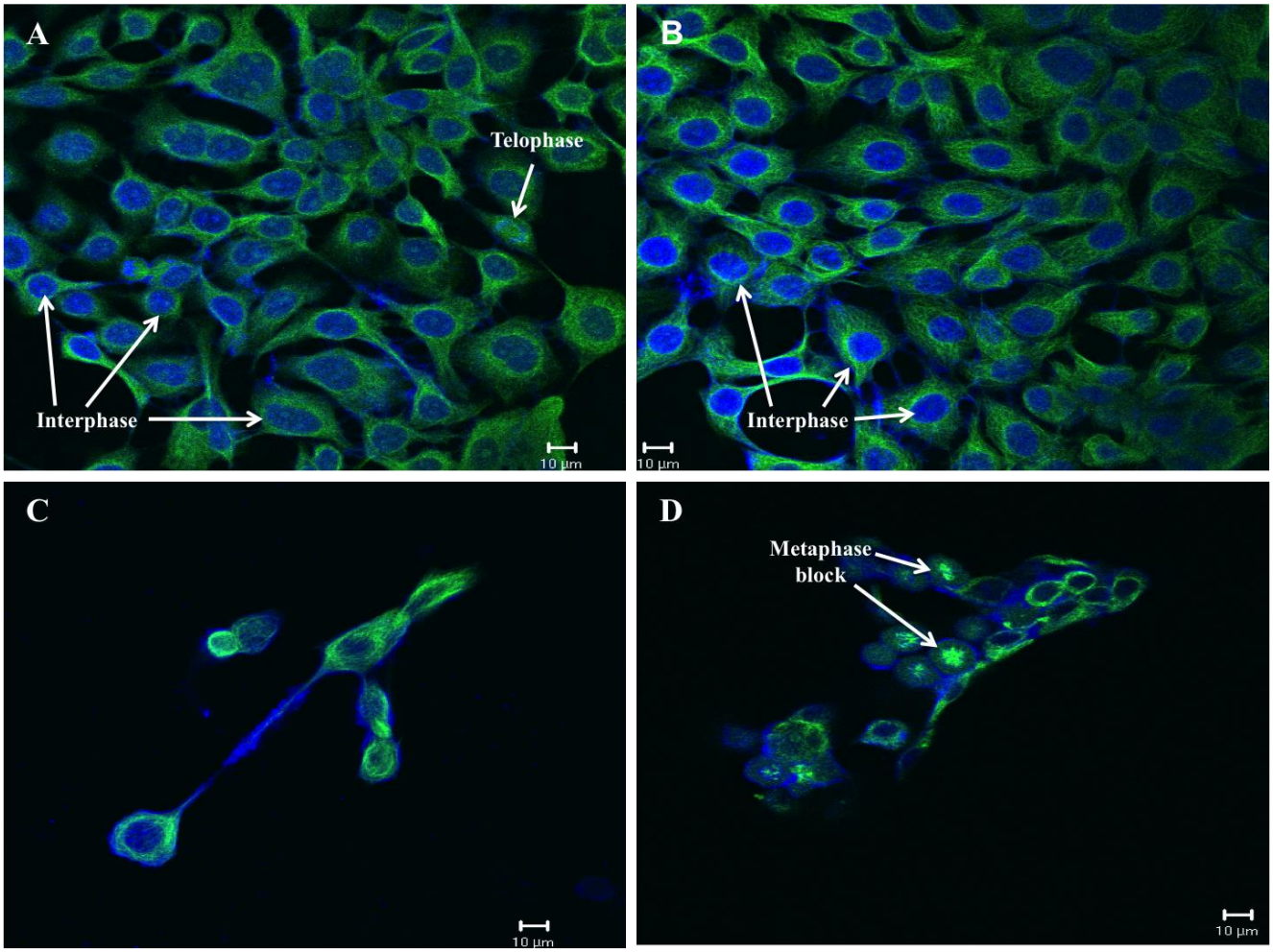

Figure 3.6: Confocal microscopy images of the microtubule architecture of SNO cells with the use of anti-α tubulin antibodies and nuclear stain 4',6-diamidino-2-phenylindole. (A) Cells propogated in medium only, (B) cells exposed to DMSO – vehicle control, (C) cells exposed to actinomycin D – positive control and (D) cells exposed to ESE-16 at a concentration of 0.2µM. The α-tubulin of the cells were stained green by a FITC-conjugate diluent while the nuclei were stained blue by DAPI to provide contrast to the green fluorescence. Cells propogated in medium and vehicle control cells showed normal microtubule architecture. The positive control showed a decrease in cell density and revealed shrunken cells. ESE-16-treated cells showed a decrease in cell density and abnormal spindle formation when compared to the appropriate controls. The abnormal spindle formation is indicative of metaphase block. Scale bar: 10µm.

3.5) Flow cytometry

3.5.1) Cell cycle progression

Cell cycle analysis (Figure 3.7) was performed to view the influence of ESE-16 on cell cycle progression. An increase in the percentage of cells in sub G_1 was observed in the ESE-16-treated cells, having 9.82% cells in sub G_1, when compared to the vehicle control with 2.80% of DMSO-treated cells in sub G_1 (Table 3.2). This is indicative of apoptosis and

quantitatively confirms the qualitative results obtained via PlasDIC, H&E staining and TEM. There was also an increase in the G_2/M phase in cells exposed to ESE-16 (36.10%), compared to vehicle control (20.61%). This is indicative of cells in metaphase block and confirms the qualitative results obtained via PlasDIC, H&E staining and confocal microscopy.

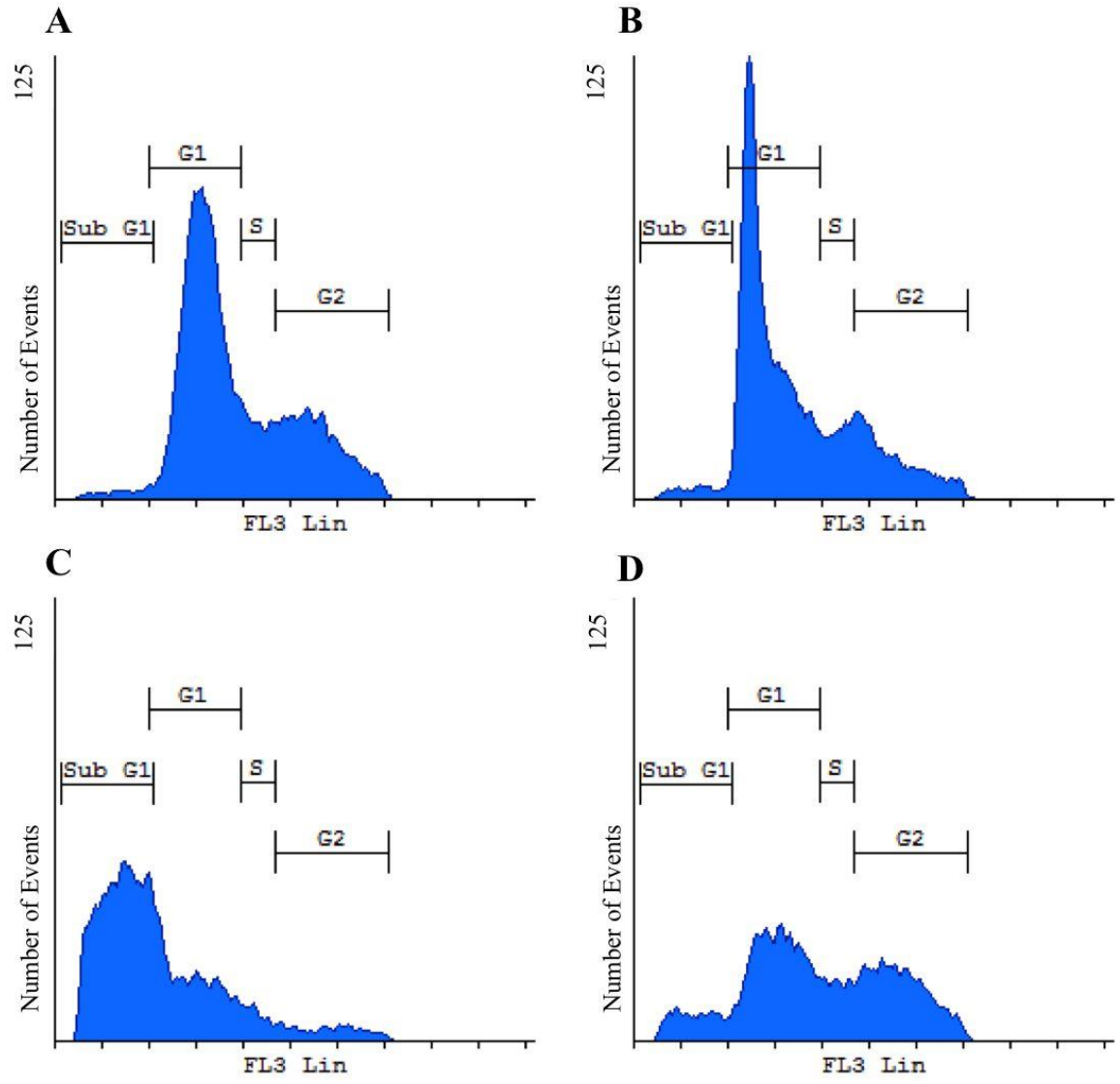

Figure 3.7: Histograms illustrating cell cycle progression of SNO cells after exposure to ESE-16 and various controls. (A) Cells propogated in medium only, (B) cells exposed to DMSO – vehicle control, (C) cells exposed to actinomycin D – positive control and (D) cells exposed to ESE-16 at a concentration of 0.2µM. The percentage of cells present in sub G_1 in ESE-16-treated cells was found to be 9.82% which is significantly higher compared to the 2.80 % cells in sub G_1 in the vehicle-treated control. An increase in the percentage of cells in the G_2/M phase in the ESE-16-treated samples (36.10%) was also found compared to the vehicle control (20.61%).

Table 3.2: Percentage of cells in the different phases of the cell cycle of the ESE-16-treated samples and appropriate controls.

	Medium	DMSO	Actinomycin D	ESE-16
Sub G1	1.7%	2.8%	55.6%	9.8%
G1	60.1%	66.2%	36.1%	42.8%
S	11.2%	10.5%	5.3%	11.6%
G2/M	27.1%	20.6%	6.7%	36.1%

3.5.2) Apoptosis detection assay

Annexin V-FITC, a well-known apoptosis detecting assay, was used to confirm the qualitative and quantitative observations that apoptosis is taking place in the SNO cells after exposure to ESE-16 (Figure 3.8). Results revealed a mean increase in the mean fluorescent intensity (MFI) in the ESE-16-treated (average of 25.50) when compared to the vehicle control with an average MFI of 11.32. The increase in MFI indicates an increase in PS externalization which is an early apoptotic indicator (59). However, the *P*-value obtained for this experiment was 0.0614, which makes this result statistically insignificant. This may be due to the fact that PS externalization is an early sign of apoptosis and that, at the time of experiment termination, the cells may have already surpassed the early apoptotic stage. This may also explain the low MFI value of the positive control (average of 18.82).

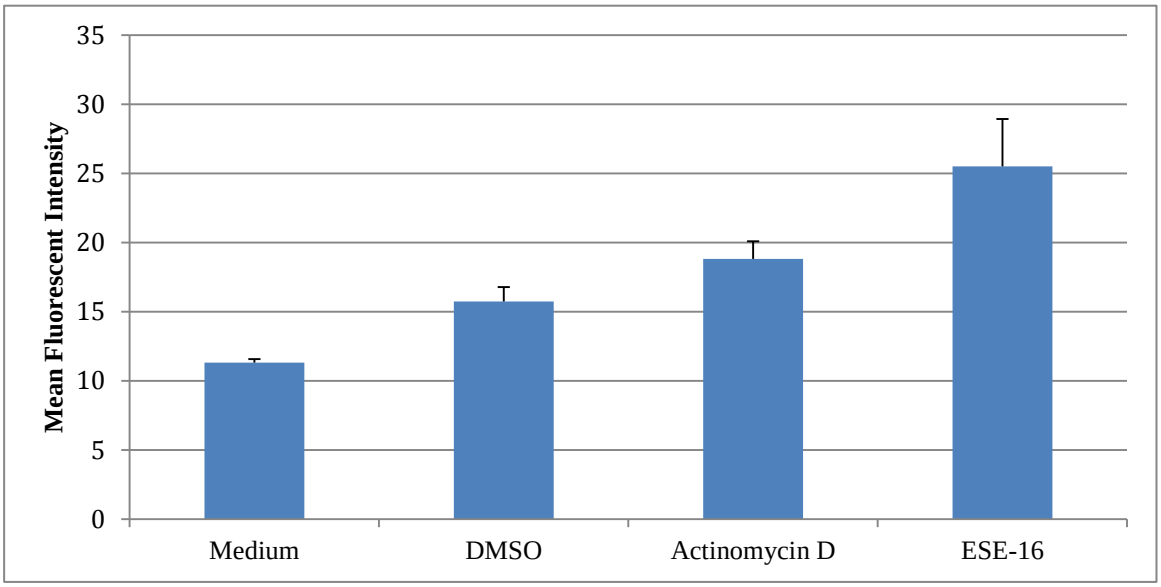

Figure 3.8: Bar graph showing the average mean fluorescent intensity increase in the ESE-16-treated cells compared to the appropriate controls illustrating an increase in phosphatidylserine externalization. This bar graph represents the average MFI of all three repeats done. Cells propogated in medium had an average MFI of 11.31, the vehicle control had an average MFI of 15.74, the positive control had an average MFI of 18.82 while the ESE-16-treated cells an average MFI of 25.50. The increased MFI indicates an increase in PS externalization which is an early apoptotic indicator (59).

3.5.3) Cyclin B levels

As mentioned previously, cyclin B and CDK1 form the MPF which allows the cell to enter the mitotic phase of the cell cycle (18,22,24,31). Defects in spindle assembly or spindle-kinetochore attachment during the mitotic phase are sensed by the spindle checkpoint which will cause metaphase arrest by inhibiting cyclin B degradation (22,28,37-39). Elevated cyclin B levels are thus used as an indicator of metaphase arrest. With the use of a anti-cyclin B conjugated antibody, cyclin B levels in the SNO cells were determined (Figure 3.9). Results revealed an X-mean value of 87.87 for the vehicle control (represented by the green histogram), while ESE-16-treated cells, represented by the red histogram, showed a shift to the right with an X-mean of 100.67. The shift to the right indicates an increase in fluorescence which illustrates an increase in cyclin B levels in the ESE-16-treated cells. The increased cyclin B levels indicates cells blocked in metaphase and confirms the qualitative data obtained via PlasDIC, H&E staining and confocal microscopy.

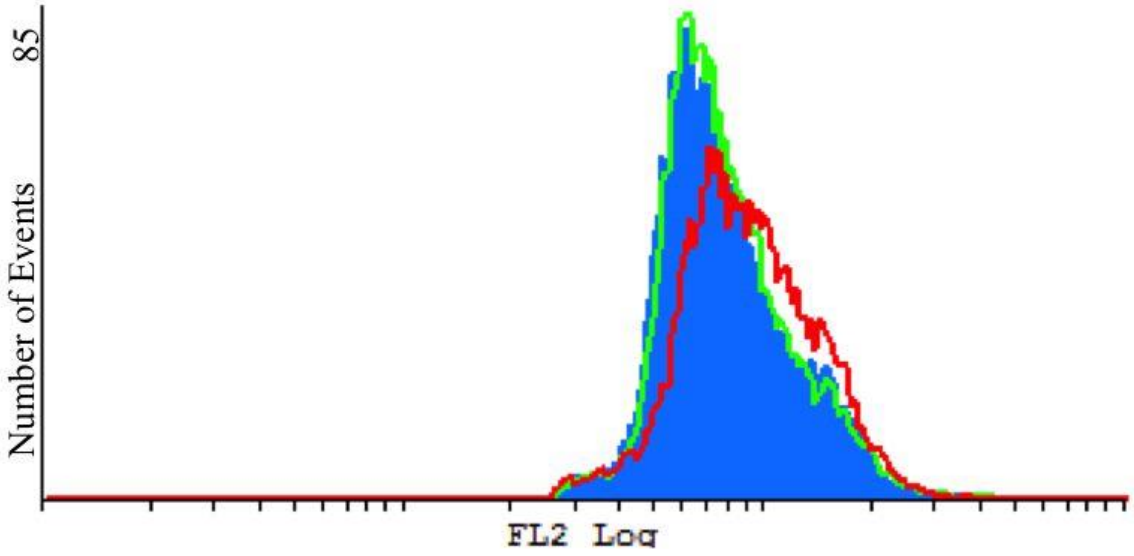

Figure 3.9: Overlay histogram illustrating cyclin B levels in the SNO cells exposed to ESE-16 and various controls. Cells propogated in medium is represented by the blue histogram, the vehicle control is represented by the green histogram and ESE-16-treated cells is represented by the red histogram. Results revealed a shift to the right due to increased fluorescence in the ESE-16-treated cells, having an X-mean of 100.67 when compared to the appropriate controls. Cells propogated in medium had an X-mean of 87.65 while the DMSO-treated cells had an X-mean of 87.87. The results illustrates an increase in cyclin B levels in the ESE-16-treated cells, indicative of metaphase block.

3.5.4) Mitochondrial membrane potential

The Mitotracker kit was used to study the possible influence ESE-16 has on the ΔΨm of the SNO cells. The mitochondria are labelled by a cationic dye named 5,5',6,6'-tetrachloro-1,133'-tetra-ethylbenzimidazolyl-carbocyanine iodide which passively diffuses across the plasma membrane and accumulates in active mitochondria (119). Reduction of the ΔΨm is an another feature of apoptosis due to loss of the electrochemical gradient across the mitochondrial membrane. With the reduction of the mitochondrial membrane potential, the mitotracker dye cannot aggregate in the mitochondria and thus remains in the cytoplasm in its monomer form, generating green fluorescence (119). Results obtained showed a statistcally significant (*P*-value of 0.019)* increase in the MFI of green fluorescence in the ESE-16-treated cells when compared to the appropriate controls (Figure 3.10). These results illustrate that ESE-16 causes a decrease in ΔΨm which may lead to the degradation of the mitochondrial membrane and apoptosis. Findings once again confirm qualitative and quantitative data obtained with regard to ESE-16 causing apoptosis at a concentration of

0.2µM after an exposure time of 24 hours. Results also provides evidence of the degradation of the mitochondrial membrane indicating apoptotic cell death via the intrinsic pathway.

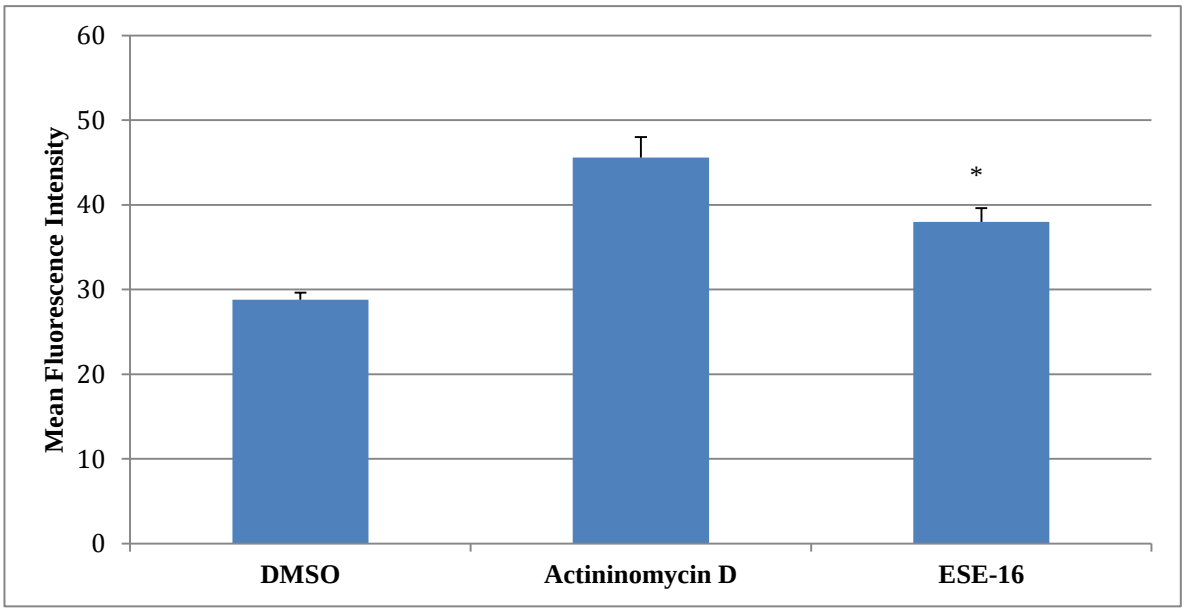

Figure 3.10: Bar graph showing the average mean fluorescent intensity increase in the ESE-16-treated cells compared to the appropriate controls, illustrating a decrease in mitochondrial membrane potential. This bar graph represents the average MFI of all three repeats done. The vehicle control had an average MFI of 28.79 while the postive control had an average MFI of 45.58 and the ESE-16-treated cells an average MFI of 37.995. The increase in the MFI seen in the ESE-16-treated cells is statistically significantly (*P*-value of 0.019)* higher than that of the vehicle control indicating a decrease in ΔΨm and possible mitochondrial membrane degradation.

3.5.3) Reactive oxygen species

An accumulation of ROS can lead to mitochondrial proteins and mitochondrial DNA causing loss of electron transport, decrease in ATP production and ΔΨm dissipation (44,67,68,132). Superoxide anion can be regarded as the precursor for most ROS (44). Thus, flow cytometry was used to measure O_2^- levels in the SNO cells after exposure to ESE-16 and the various controls (Figure 3.11). Viable cells represent the population of cells which showed little or no increase in fluorescence, thus no increase in O_2^- production. Non-viable cells represent the population of cells with an increase in fluorescence thus indicating an increase in O_2^- production. Results revealed an increase in O_2^- production in the ESE-16 treated cells with 38.17% of its population being non-viable when compared to the 21.45% non-viable population of the vehicle control (Table 3.3). Results indicate that ESE-16 does cause an

increase in O_2^- levels which may lead to mitochondrial degradation and cell death. This confirms results obtained from studying the ΔΨm.

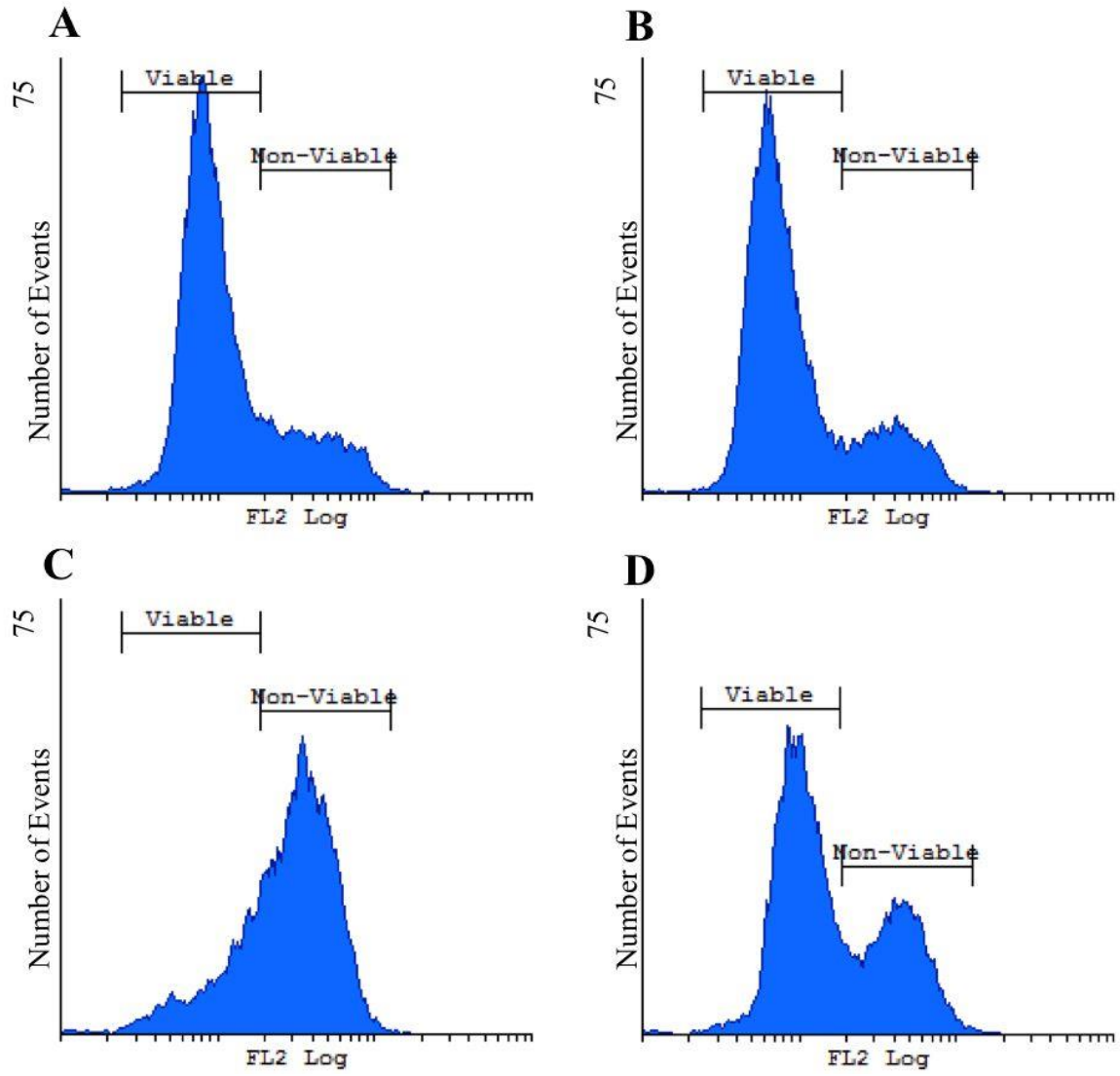

Figure 3.11: Histograms illustrating superoxide levels in SNO cells after exposure to ESE-16 and the appropriate controls. (A) Cells propogated in medium only, (B) cells exposed to DMSO – vehicle control, (C) cells exposed to actinomycin D – positive control and (D) cells exposed to ESE-16 at a concentration of 0.2µM. Viable cells represent the population of cells which showed little or no increase in fluorescence, thus no increase. The non-viable cells represent the population of cells with an increase in fluorescence thus indicating an increase in O_2^- production. The ESE-16-treated cells showed 38.17% of its population to be non-viable compared to the 21.45% non-viable population of the vehicle control.

Table 3.3: Percentages of viable and non-viable cells of the representative repeat, illustrating superoxide levels in SNO cells after exposure to ESE-16 and the appropriate controls.

	Medium	DMSO	Actinomycin D	ESE-16
Viable Cells	75.18%	77.90%	22.61%	60.11%
Non-Viable Cells	23.45%	21.05%	75.29%	38.17%

3.5.4) Cytochrome *c*

Cytochrome *c* is a critical apoptogen that plays an important role in the intrinsic apoptotic pathway (58,59,63). When cytochrome *c* is lost from the mitochondria, the electron transport chain is disrupted causing ROS production and loss in ΔΨm, which may play a role in MMP (60,61). In addition, when released into the cytosol, cytochrome *c* binds to Apaf-1 which will lead to the formation of the apoptosome (27,48,58-61).

Cytochrome *c* levels of SNO cells after exposure to ESE-16 and the appropriate controls were studied with the use of flow cytometry (Figure 3.12). According to the user's manual, viable cells demonstrate higher levels of fluorescence while apoptotic cell, which have released their cytochrome *c* from the mitochondria, will demonstrate a lower level of fluorescence. Results revealed a decrease in fluorescence in the ESE-16-treated cells with an X-mean of 291.88. In comparison, the X-mean of the vehicle control was 406.3, illustrating an increased fluorescence indicative of the presence of cytochrome *c* in the mitochondria of these cells. Results showed a loss of cytochrome *c* from the mitochondria of the ESE-16-treated cells and confirmed mitochondrial membrane degradation in cells treated with ESE-16, as well as the tendency of these cells undergoing apoptosis via the intrinsic pathway.

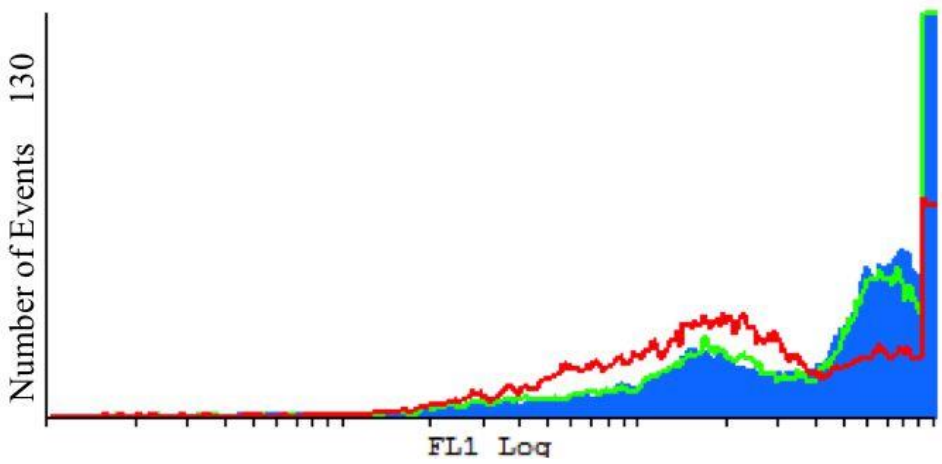

Figure 3.12: Overlay histogram illustrating cytochrome *c* levels in SNO cells exposed to ESE-16 and various controls. Cells propogated in medium is represented by the blue histogram, the vehicle control is represented by the green histogram and ESE-16-treated cells is represented by the red histogram. Results revealed a decrease in fluorescence in the ESE-16-treated cells with an X-mean of 291.88, indicating the release of cytochrome *c* from the mitochondria. In comparison, the X-mean of cells propogated in medium was 504.83 and the X-mean of the vehicle control was 406.3. The increased fluorescence indicates of the presence of cytochrome *c* in the mitochindria of these cells.

3.6) Spectrophotometry

3.6.1) Redox status

Cumulating evidence has suggested that the NAD^+/NADH and $NADP^+$/NADPH ratios may have an influence on oxidative stress and cell death (79,81). The NAD^+/NADH and $NADP^+$/NADPH ratios were quantified via spectrophotometry in order to study the possible influence of these pyridine nucleotides.

Results from quantifying of the NAD^+/NADH ratio (Figure 3.13 A) revealed an increase in ratio in the cells treated with ESE-16 (5.0686) when compared to the vehicle control (4.1145). The increase in NAD^+/NADH ratio in the ESE-16-treated cells is believed to be due to a build up in NADH in the cell which may be due to the inhibition of the respiratory chain in the mitochondria via damage, mutation or loss of cytochrome *c* (67). This is believed to also lead to increased O_2^- formation (67). Results obtained from NAD^+/NADH quantification can be seen as confirmation of cytochrome *c* release and O_2^- production.

In contrast, results from quantifying the $NADP^+$/NADPH ratio (Figure 3.13 B) showed a

decrease in ratio in cells treated with ESE-16 (0.1071) compared to the vehicle control (0.221). It has been reported that NADH and NADPH depletion is an early sign of apoptosis (79,81,82). It is believed to be due to NADH and NADPH being oxidized at the early stages of cell death, before cell shrinkage and PS exposure (79,81,82). This may explain the decreased $NADP^+$/NADPH ratio observed in the ESE-16-treated cells and consequently the decreased NAD^+/NADH – and $NADP^+$/NADPH ratios observed in both positive controls. These results once again confirms apoptotic cell death occuring.

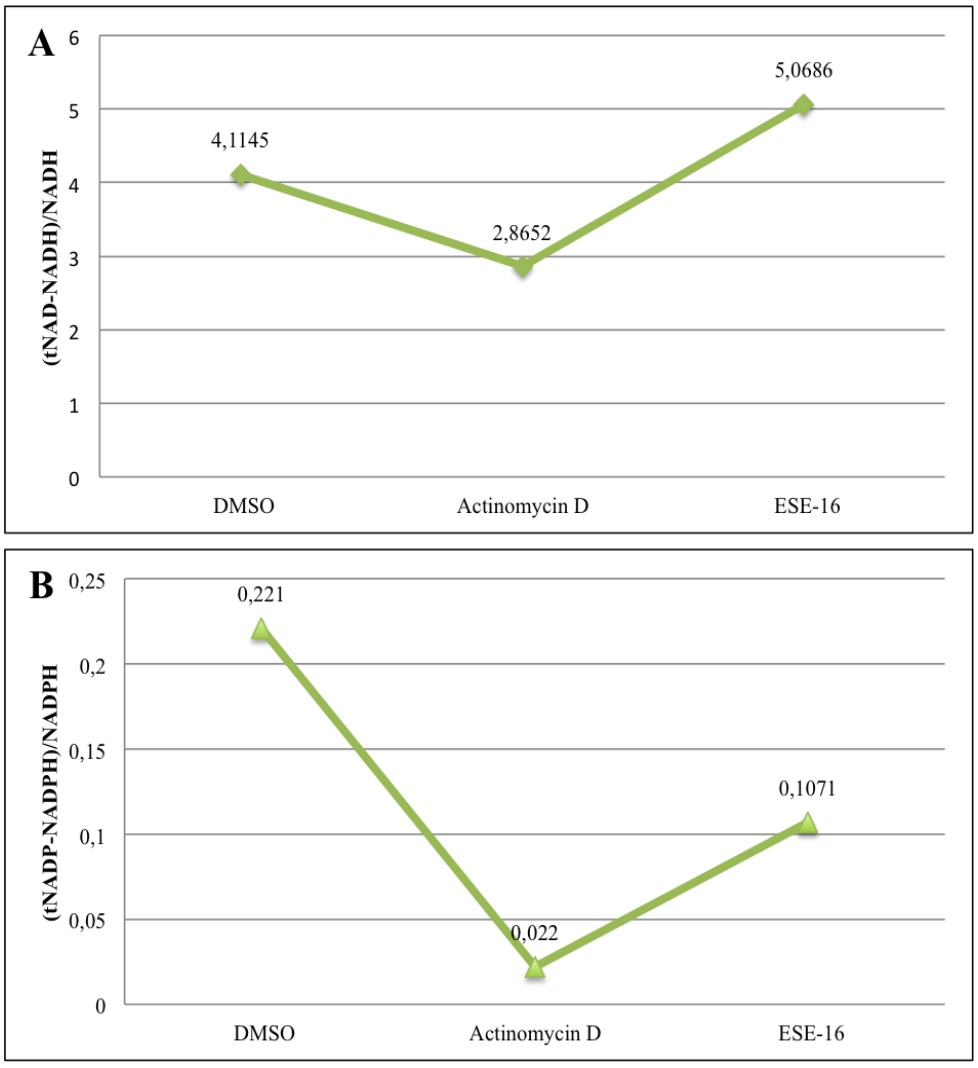

Figure 3.13: Line graphs comparing changes in the NAD^+/NADH and $NADP^+$/NADPH ratios in SNO cells exposed to ESE-16 and various controls. (A) Representative line graph of NAD^+/NADH quantification. Results revealed an increase in ratio in the cells treated with ESE-16 (5.0686) when compared to the vehicle control (4.1145). The positive control, in contrast, showed a decrease in ratio with a ratio value of 2.8652. (B) Representative line graph of $NADP^+$/NADPH quantification. Results revealed a decrease in ratio in ESE-16-treated cells (0.1071) compared to the vehicle control (0.221). The positive control also showed a decrease in ratio with a ratio value of 0.022.

3.6.2) Caspase activity

The activity of initiator caspase 9 and the effector caspase 3 in SNO cells after exposure to ESE-16 or the appropriate controls was studied via spectrophotometry. Results, showing the average ratio to medium, revealed an increase in both caspase 9 and caspase 3 activity in the ESE-16-treated cells when compared to the vehicle control.

The initiator caspase 9 results (Figure 3.14) showed that ESE-16-treated cells had a ratio to medium value of 1.2188, while the vehicle control had a value of 1.0625. This is not a statistically significant increase (*P*-value of 0.238) when compared to the difference in caspase 3 ratio to medium values. The effector caspase 3 results (Figure 3.15) showed ESE-16-treated cells had an average ratio to medium value of 2.9772 while the vehicle control had a value of 1.0681. This is a statistically significant increase with a *P*-value of 0.004*.

The difference in the increase of activity of the two caspases may be explained by the fact that the effector caspase 3 had already, at the time of measurement, begun the degradation phase of apoptosis (59,62) causing a decrease in caspase 9. The caspase activity results show that ESE-16 causes the activation of caspases and reveals that ESE-16 causes cell death in a caspase-dependent manner.

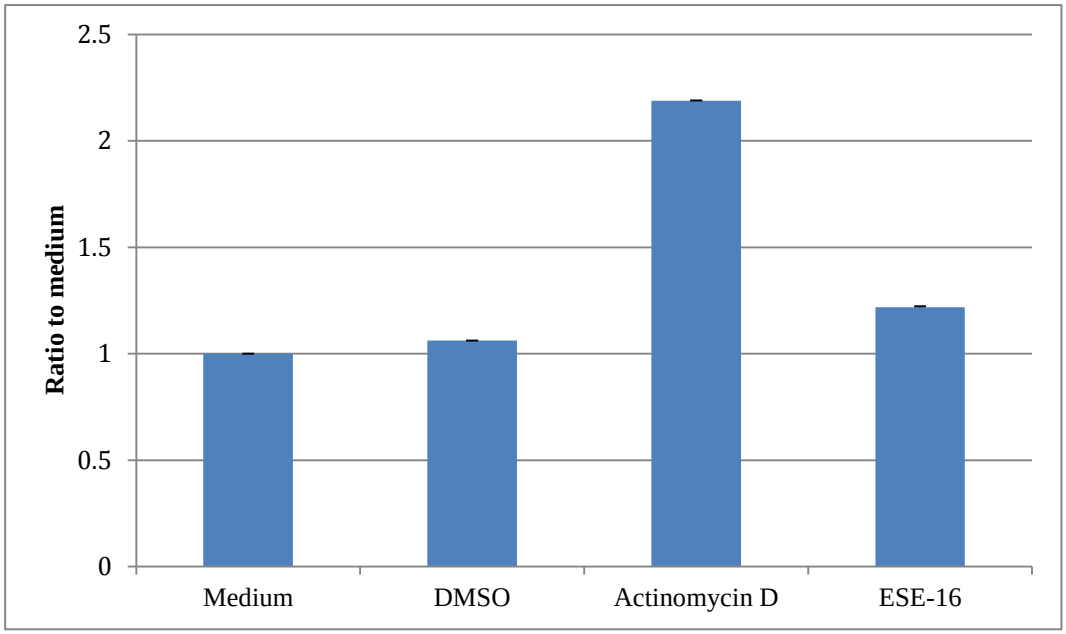

Figure 3.14: Bar graph illustrating the ratio to medium of the initiator caspase 9 levels in SNO cells exposed to ESE-16 and various controls. Results revealed a statistically insignificant increase (*P*-value of 0.238) in caspase 9 activity in the ESE-16-treated cells when compared to the vehicle control. The ESE-16-treated cells had a ratio to medium value of 1.2188, while the vehicle control had a ratio to medium value of 1.0625.

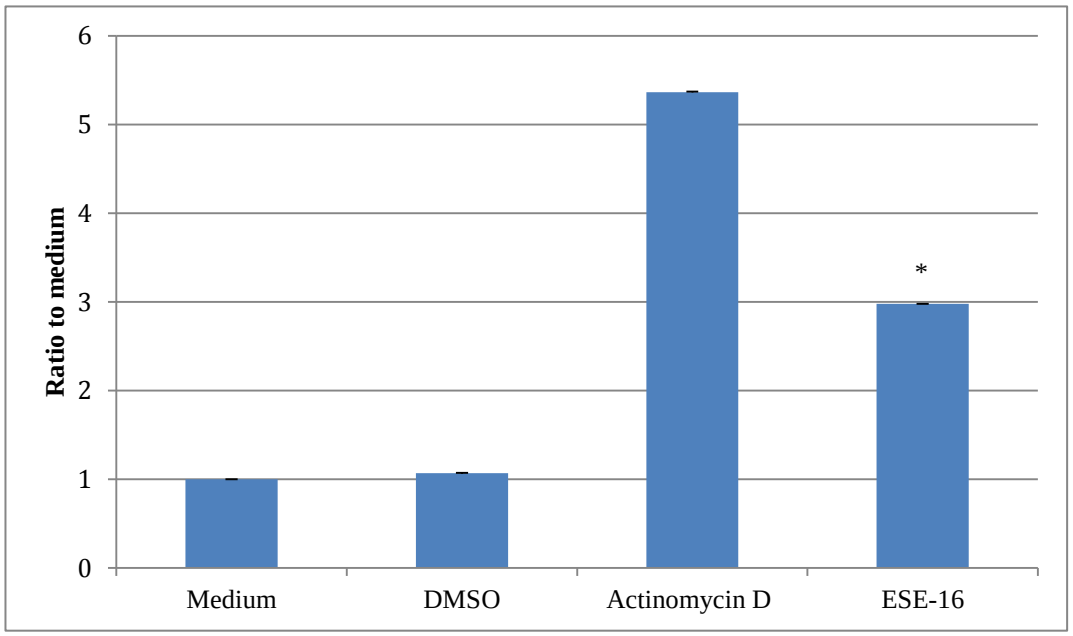

Figure 3.15: Bar graph illustrating the ratio to medium of the effector caspase 3 levels in SNO cells exposed to ESE-16 and various controls. Results revealed a statistically significant increase (*P*-value of 0.004)* in caspase 3 activity in the ESE-16-treated cells when compared to the vehicle control. The ESE-16-treated cells had a ratio to medium value of 2.9772, while the vehicle control had a ratio to medium value of 1.0681.

Chapter 4
Discussion

One of the most promising classes of cancer chemotherapeutic drugs available are MIDs (35,39,87). They have a high ability to induce apoptosis by targeting the cell cycle (22,28,35,89). By binding to and interfering with the assembly and degradation of the microtubule machinery, the MIDs inhibit the normal function of the mitotic spindle and prevent hyperproliferation of cancer cells (22,28,35,89).

Due to the therapeutic success of MIDs, intense search and development of new microtubule-targeting compounds are being conducted by pharmaceutical companies (39). Currently, there are three classes of tubulin-binding drugs: the vincas, the taxanes and the colchicine analogues, all classified by their respective tubulin binding domains (28,35,39,87,88).

A promising compound, known for it antiproliferative, anti-angiogenic and pro-apoptotic characteristics *in vitro* and *in vivo* is 2ME (38,89,94,100,101). This compound is a colchicine analogue (88,94,95,101,104) and causes abnormal spindle formation and activation of the spindle checkpoint which leads to metaphase arrest, inhibition of cell proliferation and cell death (32,89,96,97).

However, studies revealed that 2ME have low bioavailability in the human body due to rapid metabolic degradation (94,99,100,105,106). This lead to the search and creation of 2ME analogues which had improved bioavailability and potency.

Our laboratory joined the search and ESE-16, a unique, *in silico*-designed compound was developed (94). This compound was designed with the dual capability of interfering with microtubule dynamics (which plays a role in the uncontrolled proliferation of cancer cells) (35) and inhibiting CAIX, which is over-expressed in a variety of tumours (94,113). These two targets were chosen because 1) several studies have shown that inhibition of CAIX can lead to decreased invasiveness and may cause cell death under hypoxic conditions (113) and 2) by binding to microtubules there is interference during cell division which may lead to cell death (22,28,35,89).

Potential CAIX inhibitors, capable of interfering with microtubule dynamics were identified in our laboratory with the use of Autodock 4.0 bioinformatics software (94). Docking studies

revealed that ESE-16 had a pronounced preference of CAIX over CAII binding (94). The selective inhibition of CAIX provides a valuable strategy for curtailing the development of metastatic processes associated with acidotic microenvironmental conditions in tumors (94,113).

The second target of ESE-16 is the microtubule network and since ESE-16 is derived from 2ME, it also binds to the colchicine binding site (94). When the chemical structures of ESE-16 and 2ME are compared, it can be noticed that a hydroxyl group was exchange for a sulphamoylated group at position 3 of the ESE-16 compound. The sulphamoylated group increases the bioavailability of the compound since it allows the compound to reversibly bind to CAII and forgo presystemic metabolism (94,99,100,108,109). The removal of a hydroxyl group at position 17 on the ESE-16 compound can also be noticed. Studies have shown that modifications at position 3 and -17 of 2ME has the potential to increase anticancer potency and prolong the half-life of the compound (89,97,100,106-108).

Our laboratory has demonstrated the anti-proliferative action of ESE-16 in a variety of cell lines including: the tumorigenic human epithelial cervical HeLa cell line, MCF-7 breast cancer cell line, esophageal carcinoma SNO cell line, metastatic MDA-MB-231 breast cancer cell line and the non-tumorigenic MCF-12A cell line (94,109,110,133,134). Studies have also revealed that ESE-16 is more potent than its source compound, 2ME (94). Research showed that 2ME exerts antiproliferative effects on a variety of cell lines at concentrations between 1-2µM, whereas ESE-16 showed antiproliferative activity on the variety of cell lines (mentioned above) at nanomolar values, with a GI_{50} value of 180-220nM (94).

However, the exact action mechanism of ESE-16 still remains to be elucidated. In this study ESE-16 was shown to induce apoptosis *in vitro* in the esophageal carcinoma SNO cell line via the intrinsic pathway at a concentration of 0.2µM with an exposure time of 24 hours. The concentration of 0.2µM for ESE-16 was chosen since previous dose-dependent investigations conducted in our laboratory showed ESE-16 inhibiting cell proliferation to 50% from concentrations ranging from 0.18µM to 0.22µM (94). Qualitative and quantitative results were obtained during this study.

Qualitative results were obtained via PlasDIC, H&E staining, TEM and confocal microscopy; providing information on morphological changes, microtubule architecture and internal

ultrastructures of the SNO cells after exposure to ESE-16. PlasDIC and H&E staining images allowed for the study of morphological changes in the SNO cells. The results showed apoptosis taking place in the ESE-16-treated cells with the presence of apoptotic morphological characteristics, such as membrane blebbing and apoptotic bodies. These results were confirmed by studying the internal ultrastructure of the cells via TEM. Results revealed the absence of the nuclear membrane, membrane blebbling and apoptotic body formation in the ESE-16-treated cells when compared to the appropriate controls.

In addition, PlasDIC images also revealed morphological characteristics of secondary necrosis in the positive control and ESE-16-treated cells. This is believed to be due to the absence of phagocytic capacity, which is normally present in the body (43). It is postulated that in the absence of scavenger cell, such as phagocytes, apoptotic cells may proceed to secondary necrosis, characterized by the same features of necrotic cell death such as the rounding and swelling of cells (43,46,47,56). This is a self-sufficient process leading to self-elimination (47,56).

Apoptosis occuring in ESE-16-treated SNO cells was confirmed quantitatively with mitotic indices, cell cycle progression analysis and the Annexin V-FITC apoptosis detection assay. Mitotic indices quantified the observed effects in the H&E staining images. Results revealed a statistically significant increase (*P*-value of 0.0006)* in the percentage of ESE-16-treated cells undergoing apoptosis when compared to the appropriate controls. Cell cycle progression analysis revealed an increase in sub G_1 phase when compared to the vehicle control, indicative of a higher percentage of ESE-16-treated cells undergoing apoptosis when compared the vehicle control. Lastly, the Annxin V-FITC apoptosis detection assay revealed a statistically insignificant increase in the MFI value of the ESE-16-treated cells compared to the appropriate controls (*P*-value 0.0614). The increased MFI value indicates an increase in PS externalization which is an early apoptotic indicator (59). This result shows a insignificant increase that may be due to the fact that PS externalization is an early sign of apoptosis and that at the time of experiment termination, the cells may have surpassed the early apoptotic stage.

When qualitative and quantitative data obtained are combined, results show a strong relationship between ESE-16 and apoptosis taking place in the SNO cells after exposure. This correlates with the findings of Nkandeu *et al.* who tested ESE-16 on MCF-7 breast carcinoma

cell line (133), Theron *et al*. who tested ESE-16 on the tumorigenic human epithelial cervical HeLa cell line (110) and Stander *et al.* who tested ESE-16 on the tumorigenic MCF-7, the metastatic MDA-MB-231 and the non-tumorigenic MCF-12A breast cancer cells (109).

Nkandeu *et al.* tested ESE-16 on the MCF-7 cell line at a concentration of 0.18µM with an exposure time of 24 hours (133). Even at this lower concentration, results obtained showed similar morphological changes in the MCF-7 cell line seen in the SNO cells in this study. Cell cycle progression analysis also revealed an increase in the percentage of cells undergoing apoptosis in the ESE-16-treated MCF-7 cells compared to the appropriate controls (133).

Theron *et al.* tested ESE-16 on the HeLa cell line. In contrast to the findings of Stander *et al.*, which found the IC_{50} of ESE-16 on HeLa cells to be 0.22µM (94), Theron *et al.* reported the IC_{50} of ESE-16 on HeLa cells to be 0.5µM (110). Similar to the results found in this study Theron *et al.* found an increase in apoptotic cells in the ESE-16-treated HeLa cells, when compared to the relevant control, with cell cycle progression analysis and with the use of the Annexin V-FITC apoptosis detection kit (110).

Stander *et al.* found a gradual increase in PS externalization in ESE-16-treated MCF-7 and MDA-MB-231 cells in 24 hours (109). In addition, Stander *et al.* noted that the non-tumorigenic MCF-12A did not show a gradual increase in PS externalization for a 24-hour period after exposure to ESE-16 (109). This shows a possible selectivity of ESE-16 toward the more malignant cell lines when compared to non-malignant cell lines (109).

When comparing the ability of ESE-16 and 2-ME's ability to induce cell death, there are similarities. The effects of 2ME have been studied on cell lines incuding the MCF-7 cell line, the estrogen receptor-negative breast carcinoma cell line MDA-MB-435, the human ovarian adenocarcinoma cell line OVCAR-3, the renal carcinoma cell line SN12-C non-small cell lung adenocarcinoma cell line etc (135). Du *et al.* studied the effects of 2ME on the esophageal carcinoma EC9706 cell line in a time- and dose-dependent study (38). Cell cycle progression analysis and Annexin V-FITC detection showed an increase in apoptosis in the 2ME-treated cells after 24 hours (38). It is important to note however, that these results were obtained at concentrations of 5µM - and 10µM 2ME (38).

Cell death via apoptosis due to 2ME exposure was also found by Stander *et al.* and Thaver *et al.* when testing the effects of 1μM 2ME on the MCF-7 breast cancer cell line and the esophageal carcinoma WHCO3 cell line respectively (136,137). When comparing results obtained after 24 hour by 1μM, 5μM and 10μM 2ME and the 0.2μM ESE-16 used in this study, the increased potency of ESE-16 can clearly be seen.

As mentioned previously, ESE-16 was *in silico*-designed to bind to and disrupt microtubules of cells, thereby inducing cell death. ESE-16 has a similar mechanism to that of 2ME, its source compound, and thus also binds to the colchicine binding site situated between the α - and β-dimers of the tubulin protein (88,94,95,101,104). It is hypothesized that ESE-16 will, like its source compound, cause abnormal spindle formation, activate the spindle checkpoint which leads to metaphase arrest, inhibition of cell proliferation and cell death. Qualitative and quantitative data obtained in this study do indicate that ESE-16 blocks the cell in metaphase during mitosis.

The PlasDIC and H&E staining images provided qualitative data on the effect that ESE-16 had on the microtubule architecture of the cells. PlasDIC images showed the rounding of cells, indicative of metaphase block, while H&E images revealed hypercondensed chromatin in the ESE-16-treated cells. The effect on the microtubule architecture was qualitatively confirmed via confocal microscopy which showed hypercondensed chromatin and abnormal spindle formation in the ESE-16-treated cells when compared to the appropriate controls.

Quantitative confirmation on whether ESE-16 causes metaphase block, was obtained via mitotic indices, cell cycle progression analysis and studying cyclin B levels in the SNO cells after exposure. Mitotic indices revealed a significant increase, with a *P*-value of 0.0003*, in the percentage of cells in metaphase in the ESE-16-treated samples when compared to the controls. Cell cycle progression analysis also showed an increase in cells in metaphase with a high percentage of ESE-16-treated cells in G_2/M phase compared to the vehicle control. In addition, results obtained from studying the cyclin B levels in the SNO cells after exposure revealed an increase in cyclin B levels in the ESE-16-treated cells when compared to the appropriate controls. This indicates the activation of the spindle checkpoint which causes the prevention of degradation of cyclin B.

Results obtained from the cell cycle progression analysis once again correlate with previous studies done on the effects of ESE-16 on various cancer cell lines listed above. This illustrates an increase in the percentage of cells in metaphase in the ESE-16-treated samples.

Similar to the results found in this study, an increase in cyclin B levels via ESE-16 was also found by Theron *et al.* in the HeLa cell line (110). Theron *et al.* also believed that the increased levels of cyclin B in the ESE-16-treated cells were indicative of the activation of the SAC and the prevention of cyclin B degradation (110). In addition, Stander *et al.* collected information about gene expression changes associated with ESE-16 exposure (109). It was found that there was a decreased gene expression of cyclin B and increased protein levels of cyclin B in the MDA-MB-231 cells exposed to ESE-16 (109). Another gene that was also down regulated in all cell lines due to ESE-16 exposure was Bub3 (109).

As discussed in the introduction of this study, until all kinetochores are correctly attached to the spindle fibers and the chromosomes are properly aligned on the metaphase plate, the SAC inhibits APC/C activation and prevents the continuation of the cell cycle (25). The key step in the SAC appears to be the interaction of two complexes at the kinetochore (26). The complexes consist of mitotic checkpoint proteins such as Bub1, Bub3, Mad1 and Mad2 (26,28,37). The down regulation of the Bub3 gene seen by Stander *et al.* may add to the inhibition of the APC/C thus causing metaphase block. The inhibition of APC/C prevents cyclin B degradation which will lead to the arrest of cell division in metaphase (22,28,37-39). This may explain the increased cyclin B levels found in the ESE-16-treated samples.

The ability of 2ME to induce metaphase block and cell cycle arrest has been studied extensively. 2ME has been shown to cause metaphase block in a variety of cell lines (including the MCF-7 cell line, the EC9706 cell line, the WHCO3 cell line and the MDA-MB-435 breast cancer cell line) at concentrations of 1µM, 2µM, 5µM and 10µM after 24 hours (32,38,136,137). In addition, it has also been found that 2ME has the ability to increase cyclin B levels in a variety of cancer cells also at the different concentrations mentioned above (32,38,136). The similarty in the effect of ESE-16 on the SNO cell line, observed in this study, compared to the metaphase arrest ability of 2ME indicates that ESE-16 does have a similar action mechanism to that of its source compound. However, the increased potency of ESE-16 can once again be seen, since it was able to cause metaphase

block in the SNO cell line after 24 hours exposure at a concentration of 0.2µM. This is a much lower concentration than what is needed to induce metaphase block by 2ME.

According to the hypothesized chain of events in this study, the blocking of the cell in metaphase leads to mitochondrial function disruption. The mitochondria's role in the regulation of cell death is well established (44). It is considered to be the central death machinery in the intrinsic apoptotic pathway (58-61) with the key step believed to be MMP (39,58,60-62).

Research has shown that microtubules have the ability to interact with the mitochondria (28,132). The interaction has been suggested to be due to the release of proteins, such as p53 and Bim from the microtubules, which then build molecular bridges between the microtubules and the apoptotic machinery within the mitochondria (39). It has also been suggested that there may be a mechanistic relationship between the activation of the spindle checkpoint and induction of apoptotic cell death due to the activation of proteins involved in the checkpoint (22). This link between the two organelles suggests that damage to microtubules could directly result in an apoptotic response via the mitochondria (28). In parallel with their effects on the microtubule network, MIDs has also been shown to activate the apoptotic pathway through a direct action on the mitochondria with MID-mediated ROS generation (39). MIDs induces early $\Delta\Psi m$ collapse and a subsequent large amplitude swelling of isolated mitochondria (39).

The possible effect that ESE-16 had on the mitochondria of SNO cells after exposure was studied by means of flow cytometry and spectrophotometry by quantitatively analyzing $\Delta\Psi m$, cytochrome *c* levels, ROS production and the redox status of the SNO cells after ESE-16 exposure.

Results obtained from studying the $\Delta\Psi m$ showed a statistcally significant (*P*-value of 0.019)* increase in the MFI of green fluorescence in the ESE-16-treated cells when compared to the vehicle control. The increase in green fluorescence shows that the mitotracker dye cannot aggregate in the mitochondria and thus remains in the cytoplasm in its monomer form, generating green fluorescence (119). These findings illustrate that ESE-16 caused a decrease in $\Delta\Psi m$, which may lead to the degradation of the mitochondrial membrane and apoptosis.

Results also provide evidence of apoptosis via the intrinsic pathway since MMP of the mitochondria is considered a key step in this pathway (39,58,60-62).

The decrease of ΔΨm due to ESE-16 exposure was also found by Stander *et al.* in the tumorigenic MCF-7 and MDA-MB-231 cell lines. In addition, Stander *et al.* once again showed that ESE-16 had a more pronounced effect on the tumorigenic cell lines when compared to the non-tumorigenic MCF-12 cell line (109). This reaffirms possible selectivity of ESE-16 toward the more malignant cell lines when compared to non-malignant cell lines.

Parallel to ΔΨm findings, results obtained from studying cytochrome *c* levels showed a loss of cytochrome *c* from the mitochondria. This confirms the ΔΨm results since, when cytochrome *c* is lost from the mitochondria, the electron transport chain is disrupted causing ROS production and loss in ΔΨm, which may in turn play a role in MMP (60,61). These results once again confirm mitochondrial membrane degradation in cells treated with ESE-16 and the tendency of these cells to undergo apoptosis via the intrinsic pathway.

The mitochondria are both the major source of intracellular ROS and, at the same time, targets of ROS (61,67,68). ROS are natural by-products from the production of ATP which occurs in the mitochondrial matrix via the oxidative phosphorylation pathway (44,68-70). Approximately 1-2% of O_2 consumed during normal cellular respiration is converted to O_2^- via one-electron reduction (44,67). The mitochondrial electron transport chain serves as the primary source of O_2^- due to several redox centers in the transport chain that may leak electrons to O_2 (44).

The accumulation of ROS may lead to oxidative damage to mitochondrial proteins and mitochondrial DNA, causing loss of electron transport, decrease in ATP production and ΔΨm dissipation (44,67). In addition, ROS accumulation is believed to act as signaling molecules which initiate MMP via PTP (discussed above), causing the release of the pro-apoptotic proteins found in the intermembrane space (47,67).

Since O_2^- can be regarded as the precursor for most ROS (44) the levels of O_2^- was measured via flow cytometry in SNO cells after exposure to ESE-16. Results revealed an increase in O_2^- levels in the ESE-16-treated cells when compared to the relevant controls. Results shows that the ESE-16-treated cells are suffering from oxidative stress after 24 hour exposure.

Results also confirm the previously discussed results of ΔΨm dissipitation and cytochrome *c* realease, since it is believed that ROS can cause ΔΨm dissipation (44,67) and act as signaling molecules which initiate MMP and cause the release of pro-apoptotic proteins such as cytochrome *c* (47,67).

The increased O_2^- levels in ESE-16-treated cells were reported by Stander *et al.* which found in a time dependent study that O_2^- formation increased in the MDA-MB-231 cell after 6 hour exposure while MCF-7 cells showed an increase in O_2^- levels after 12 hours (109). The non-tumorigenic MCF-12A cell line only showed increased O_2^- formation after 18 hours (109), once again suggesting the selectivity of ESE-16 towards the malignant cell lines when compared to non-malignant cell lines.

Several studies have linked 2ME with the increase in ROS production, specifically O_2^- (89,132). Chua *et al.* showed, however, that 2ME induced only a moderate increase in cellular superoxide while analogues of 2ME extended stronger ROS production, thus suggesting that ROS induction is not a major mechanism of action for 2ME (89). This correlates with literature by Stander *et al.*, which showed that 2ME-treated MCF-7 cells had no significant increase in O_2^- levels compared to the vehicle control (136).

By studying various analogues of 2ME, Chua *et al.* suggested that the 2-methoxy group at position 2 in the 2ME compound structure is not required for ROS production and may in fact even have an inhibitory effect (89). The increased O_2^- production due to ESE-16 may be due to the conformational changes in the ESE-16 compound structure, as Chua *et al.* also showed an increase in O_2^- levels due to 2ME analogues which also had modifications done on positions 3 and 17 (89).

In addition to measuring O_2^- production in SNO cells, the redox status of cells after ESE-16 exposure was also studied. The redox status is a term used to describe the oxidation and reduction status of the cell and is also commonly used to describe the balance of NAD^+/NADH and $NADP^+$/NADPH within the cell (77,78,80). When the intracellular redox balance shifts towards oxidation, the cell undergoes oxidative stress, due to increased production or insufficient degradation of ROS and may lead to oxidative damage, ΔΨm dissipation and cell death (44,67,77). Accummulating evidence has suggested that the NAD^+/NADH and $NADP^+$/NADPH ratios may also change during oxidative stress (79).

Results revealed an increase in ratio in the cells treated with ESE-16 when compared to the vehicle control. The increase in NAD^+/NADH ratio in the ESE-16-treated cells is believed to be due to a build up in NADH in the cell which may be due to the inhibition of the respiratory chain in the mitochondria via damage, mutation or loss of cytochrome *c* (67). This is believed to also lead to increased O_2^- formation (67). Results obtained from NAD^+/NADH quantification can be seen as confirmation of cytochrome *c* release and O_2^- production. In contrast, results from quantifying the $NADP^+$/NADPH ratio showed a decrease in ratio in the cells treated with ESE-16 compared to the vehicle control. It has been reported that NADH and NADPH depletion is an early sign of apoptosis (79,81,82). It is believed to be due to NADH and NADPH being oxidized at the early stages of cell death, before cell shrinkage and PS exposure (79,81,82). This may explain the decreased $NADP^+$/NADPH ratio observed in the ESE-16-treated cells which, at the time of experiment termination, may have already entered the early stages of apoptosis.

After the key step in the intrinsic pathway, believed to be MMP (39,58,60-62), several pro-apoptotic proteins, such as AIF and cytochrome *c,* are released into the cytosol (27,48,58,60,61,63). Once released, cytochrome *c* binds to Apaf-1, allowing dATP to bind onto Apaf-1 inducing conformational changes and causes the oligomerization of Apaf-1 into the Apaf-1 apoptosome (27,48,58-61). This apoptosome subsequently recruits and activates the initiator procasapase 9, which in turn activates downstream effector caspases such as caspase 3, leading to the execution phase of apoptosis (27,48,58-61).

Caspase activity in the SNO cells after exposure to ESE-16 was quantitatively studied via spectrophotometry. Results revealed a statistically insignificant increase in caspase 9 activity in ESE-16-treated cells when compared to the relevant controls with a *P*-value of 0.238. In comparison, caspase 3 showed a statistically significant increase in activity with a *P*-value of 0.004^* in the ESE-16-treated cells when compared to the appropriate controls. The difference in the increase of activity of the two caspases may be explained by the fact that the effector caspase 3 had already, at the time of measurement, begun the degradation phase of apoptosis (59,62) causing a decrease in caspase 9. The caspase activity results shows that ESE-16 causes the activation of caspases and induces cell death in a caspase-dependent manner.

This was the first study conducted to investigate the action mechanism of the ESE-16 compound on an esophageal carcinoma cell line. In addition to obtaining information of the

action mechanism of ESE-16, this study confirmed the increased potency of this compound compared to its source compound, 2ME.

From this study, it can be concluded that the novel *in silico*-designed compound induces cell death at a concentration of 0.2μM on the esophageal carcinoma SNO cell line by disrupting microtubule function, resulting in a metaphase block. The hypothesized chain of events (Figure 4.1) is as follows: The compound binds to the microtubules of the SNO cells, causing the activation of the spindle checkpoint and subsequent metaphase arrest. This leads to increased ROS production, ΔΨm dissipation, degradation of the mitochondrial membrane and the release of cytochrome *c*. Cytochrome *c* then binds with Apaf-1 to form the apoptosome, which activates the initiator caspase 9. Caspase 9 activates the effector caspase 3, which then lead to the cell undergoing apoptosis. It can also be concluded that the ESE-16 compound uses the intrinsic apoptotic pathway as an action mechanism to cause cell death.

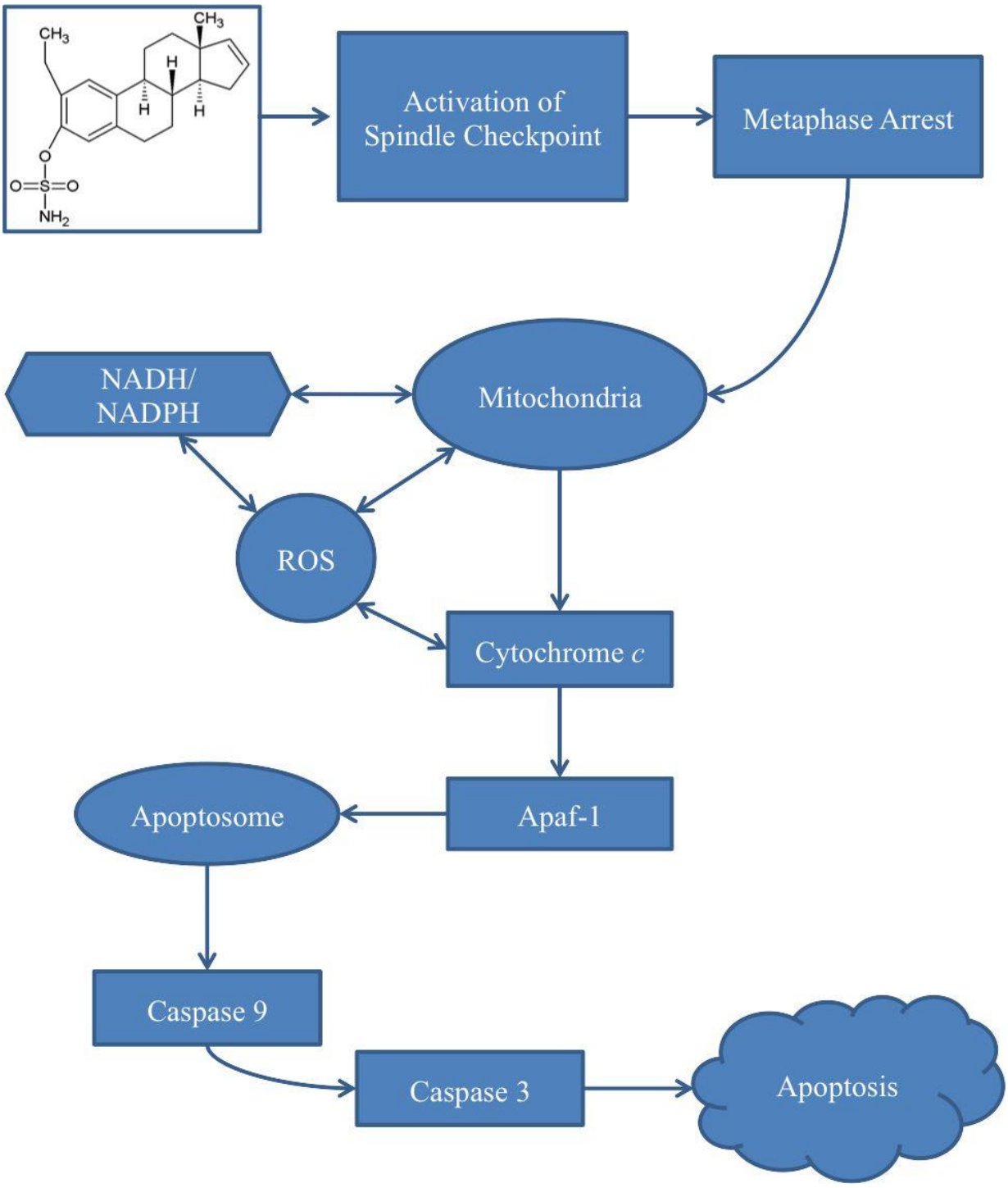

Figure 4.1: The hypothesized mechanism of action of ESE-16 on esophageal carcinoma SNO cells. ESE-16 binds to the microtubules of the SNO cells, causing the activation of the spindle checkpoint and subsequent metaphase arrest. This leads to increased ROS production and changes in the redox status of the cells, $\Delta\Psi m$ dissipation, degradation of the mitochondrial membrane and the release of cytochrome *c*. Cytochrome *c* then binds with Apaf-1 to form the apoptosome, which activates the initiator caspase 9. Caspase 9, in turn, activates the effector caspase 3, which will lead to caspase-dependent cell death. It can be concluded from the results of this study that ESE-16 uses the intrinsic apoptotic pathway as an action mechanism to cause cell death.

Chapter 5

Conclusion

South Africa is one of the areas with the highest incidence rates of EC in the world, making it a cancer of national importance (2,3). The prognosis of EC is generally unfavourable, with an approximated long-term survival rate of only 5% (6). Treatments for EC include surgery, radiation treatments and chemotherapy (14-16). Despite significant progress, cancer treatments have not met expectations and cancer research is focused on new ideas and major innovation to address issues such as bioavailability and delivery methods of anticancer compounds. The field of drug development has been transformed by targeted treatments and their ability to direct treatment at specific molecular targets (14).

Research has shown that effective cancer treatment can be achieved by drugs that target certain processes or proteins capable of causing disruption in the cell cycle machinery (18,35). One of the latest and most promising classes of cancer chemotherapeutic drugs available, with a high ability to induce apoptosis, are MIDs (35,39,87).

The latest promosing MID, is the unique *in silico*-designed ESE-16 compound. This compound was designed with the dual capability of interfering with microtubule dynamics, thus inhibiting uncontrolled proliferation (22,28,35,89) and inhibiting CAIX which is over expressed in a variety of tumours (94,113).

Our laboratory has established the anti-proliferative action of ESE-16 in a variety of cancer cell lines including the tumorigenic human epithelial cervical HeLa cell line, MCF-7 breast cancer cell line and the metastatic MDA-MB-231 breast cancer cell line (94,109,110,133). It was also established that ESE-16 is more more potent than its source compound, 2ME (94). Studies revealed that 2ME had antiproliferative effects at concentrations between 1-2μM, whereas ESE-16 showed antiproliferative activity at nanomolar values, with a GI_{50} value of 180-220nM (94). In addition, the ESE-16 compound was also tested on the non-tumorigenic MCF-12A breast cells and it was found that the compound had a higher affinity for the tumorigenic cell lines when compared to this non-tumorigenic cell line (109).

Data from the previous *in vitro* studies mentioned above support the concept that ESE-16 prevents cancer cell proliferation and may act as a potential anticancer drug. The aim of this

study was to investigate the possible induction of apoptosis *in vitro* via the intrinsic pathway by the ESE-16 compound on the esophageal carcinoma SNO cell line.

Results revealed qualitative and quantitative evidence that ESE-16 caused apoptosis in the SNO cells. Qualitative and quantitative results also revealed abnormal spindle formation in the ESE-16-treated SNO cells, causing metaphase block. Further, results revealed the effect ESE-16 had on the mitochondria of the SNO cells with a dissipation in $\Delta\Psi m$, an increase in O_2^- levels, the changes in the redox status of the cells, the increase in cytochrome *c* levels in the cytosol; showing that cell death occurs via the mitochondria, which is considered to be the central death machinery in the intrinsic apoptotic pathway (58-61). In addition, results revealed an increase in both the initiator caspase 9 and effector caspase 3 activities, which shows that ESE-16 causes cell death in a caspase-dependent manner.

This was the first study conducted to investigate the action mechanism of the ESE-16 compound on an esophageal carcinoma cell line. In addition to obtaining information of the action mechanism of ESE-16, this study confirmed the increased potency of this compound compared to its source compound, 2ME. From this study, it can be concluded that the novel *in silico*-designed compound, ESE-16, exerts its anti-proliferative effect on the esophageal carcinoma SNO cell line by disrupting microtubule function, resulting in a metaphase block. It can also be concluded that the ESE-16 compound uses the intrinsic apoptotic pathway as an action mechanism to cause cell death.

This study unraveled the action mechanism of this novel compound and provides cellular targets for future *in vivo* studies to establish its efficacy as a clinically usable anticancer agent. Future studies will investigate the action mechanism of this compound on areas such as angiogenesis, will test whether it exerts any significant side effects and test whether the *in silico*-design has increased the compounds' bioavailability.

References

(1) World Health Organization. Cancer. Accessed at www.who.int/media-centre/facsheets/fs297/en/index.html on July 10, 2013.

(2) Jemal A, Bray F, Center MM, Ferlay J, Ward E, Forman D. Global Cancer Statistics. CA Cancer J Clin. 2011;61:69-90.

(3) Kamangar F, Dores GM, Anderson WF. Patterns of cancer incidence, mortality, and prevalence across five continents: defining priorities to reduce cancer disparities in different geographic regions of the world. J Clin Oncol. 2006;24(14):2137-2150.

(4) Kamangar F, Chow WH, Abnet CC, Dawsey SM. Environmental causes of esophageal cancer. Gastroenterol Clin North Am. 2009;38(1):27-57.

(5) IARC Monographs on the Evaluation of Carcinogenic Risks to Humans. Accessed at monographs.iarc.fr/ENG/Classification/ on July 10, 2013.

(6) Kollarova H, Machova L, Horakova D, Janoutova G, Janout V. Epidemiology of esophageal cancer--an overview article. Biomed Pap Med Fac Univ Palacky Olomouc Czech Repub. 2007;151(1):17-20.

(7) Mao WM, Zheng WH, Ling ZQ. Epidemiologic risk factors for esophageal cancer development. Asian Pac J Cancer Prev. 2011;12(10):2461-2466.

(8) Hendricks D, Parker MI. Oesophageal cancer in Africa. IUBMB Life. 2002;53:263-268.

(9) Myburg RB, Dutton MF, Chuturgoon AA. Cytotoxicity of fumonisin B1, diethylnitrosamine and catechol on the SNO esophageal cancer cell line. Environ Health Perspect. 2002;110(8):813-815.

(10) Digklia A, Voutsadakis IA. Targeted treatments for metastatic esophageal squamous cell cancer. World J Gastrointest Oncol. 2013;5(5):88-96.

(11) Morita M, Kumashiro R, Kubo N, Nakashima Y, Yoshida R, Yoshinaga K, et al. Alcohol drinking, cigarette smoking, and the development of squamous cell carcinoma of the

esophagus: epidemiology, clinical findings, and prevention. Int J Clin Oncol. 2010;15(2):126-134.

(12) Noori P, Hou SM. Mutational spectrum induced by acetaldehyde in the HPRT gene of human T lymphocytes resembles that in the p53 gene of esophageal cancers. Carcinogenesis. 2001;22(11):1825-1830.

(13) Chu FS, Li GY. Simultaneous occurrence of fumonisin B1 and other mycotoxins in moldy corn collected from the People's Republic of China in regions with high incidences of esophageal cancer. Appl Environ Microbiol. 1994;60(3):847-852.

(14) Tew WP, Kelsen DP, Ilson DH. Targeted therapies for esophageal cancer. Oncologist. 2005;10(8):590-601.

(15) Chen SB, Weng HR, Wang G, Yang JS, Yang WP, Liu DT, et al. Surgical treatment for early esophageal squamous cell carcinoma. Asian Pac J Cancer Prev. 2013;14(6):3825-3830.

(16) Hofstetter W. Current and future options for treating esophageal cancer: a paradigm shift toward organ-sparing therapies. Tex Heart Inst J. 2012;39(6):846-847.

(17) Schafer KA. The cell cycle: a review. Vet Pathol. 1998;35(6):461-478.

(18) Bayliss R, Fry A, Haq T, Yeoh S. On the molecular mechanisms of mitotic kinase activation. Open Biol. 2012;2(11):120136.

(19) McIntosh JR, Molodtsov MI, Ataullakhanov FI. Biophysics of mitosis. Q Rev Biophys. 2012;45(2):147-207.

(20) Nakayama KI, Nakayama K. Ubiquitin ligases: cell-cycle control and cancer. Nat Rev Cancer. 2006;6(5):369-381.

(21) Zhang ZY, Zhou B, Xie L. Modulation of protein kinase signaling by protein phosphatases and inhibitors. Pharmacol Ther. 2002;93:307-317.

(22) Luch A. Cell cycle control and cell division: implications for chemically induced carcinogenesis. Chembiochem. 2002;3(6):506-516.

(23) Manchado E, Guillamot M, Malumbres M. Killing cells by targeting mitosis. Cell Death Differ. 2012;19(3):369-377.

(24) Lundberg AS, Weinberg RA. Control of the cell cycle and apoptosis. Eur J Cancer. 1999;35(14):1886-1894.

(25) Bassermann F, Eichner R, Pagano M. The ubiquitin proteasome system - Implications for cell cycle control and the targeted treatment of cancer. Biochim Biophys Acta. 2014;1843(1):150-162.

(26) Murray AW. Recycling the cell cycle: cyclins revisited. Cell. 2004;116(2):221-234.

(27) Van Cruchten S, Van den Broeck W. Morphological and Biochemical Aspects of Apoptosis, Oncosis and Necrosis. 2002;31:214-223.

(28) Mollinedo F, Gajate C. Microtubules, microtubule-interfering agents and apoptosis. Apoptosis. 2003;8(5):413-450.

(29) Okada H, Mak TW. Pathways of apoptotic and non-apoptotic death in tumour cells. Nat Rev Cancer. 2004;4(8):592-603.

(30) Fisher D, Krasinska L, Coudreuse D, Novak B. Phosphorylation network dynamics in the control of cell cycle transitions. J Cell Sci. 2012;125:4703-4711.

(31) Musacchio A. Spindle assembly checkpoint: the third decade. Philos Trans R Soc Lond B Biol Sci. 2011;366(1584):3595-3604.

(32) Choi HJ, Zhu BT. Critical role of cyclin B1/Cdc2 up-regulation in the induction of mitotic prometaphase arrest in human breast cancer cells treated with 2-methoxyestradiol. Biochim Biophys Acta. 2012;1823(8):1306-1315.

(33) Moser SC, Swedlow JR. How to be a mitotic chromosome. Chromosome Res. 2011;19(3):307-319.

(34) Santaguida S, Musacchio A. The life and miracles of kinetochores. EMBO J. 2009;28(17):2511-2531.

(35) Zhou J, Giannakakou P. Targeting microtubules for cancer chemotherapy. Curr Med Chem Anticancer Agents. 2005;5(1):65-71.

(36) Abraham RT. Cell cycle checkpoint signaling through the ATM and ATR kinases. Genes Dev. 2001;15(17):2177-2196.

(37) Baker DJ, Dawlaty MM, Galardy P, van Deursen JM. Mitotic regulation of the anaphase-promoting complex. Cell Mol Life Sci. 2007;64(5):589-600.

(38) Du B, Zhao Z, Sun H, Ma S, Jin J, Zhang Z. Effects of 2-methoxyestradiol on proliferation, apoptosis and gene expression of cyclin B1 and c-Myc in esophageal carcinoma EC9706 cells. Cell Biochem Funct. 2012;30(2):158-165.

(39) Rovini A, Savry A, Braguer D, Carre M. Microtubule-targeted agents: when mitochondria become essential to chemotherapy. Biochim Biophys Acta. 2011;1807(6):679-688.

(40) Burns TF, El-Deiry WS. The p53 pathway and apoptosis. J Cell Physiol. 1999;181(2):231-239.

(41) Igney FH, Krammer PH. Death and anti-death: tumour resistance to apoptosis. Nat Rev Cancer. 2002;2(4):277-288.

(42) Assuncao Guimaraes C, Linden R. Programmed cell deaths. Apoptosis and alternative deathstyles. Eur J Biochem. 2004;271(9):1638-1650.

(43) Vanden Berghe T, Vanlangenakker N, Parthoens E, Deckers W, Devos M, Festjens N, et al. Necroptosis, necrosis and secondary necrosis converge on similar cellular disintegration features. Cell Death Differ. 2010;17(6):922-930.

(44) Orrenius S, Gogvadze V, Zhivotovsky B. Mitochondrial oxidative stress: implications for cell death. Annu Rev Pharmacol Toxicol. 2007;47:143-183.

(45) Christofferson DE, Yuan J. Necroptosis as an alternative form of programmed cell death. Curr Opin Cell Biol. 2010;22(2):263-268.

(46) Kepp O, Galluzzi L, Lipinski M, Yuan J, Kroemer G. Cell death assays for drug discovery. Nat Rev Drug Discov. 2011;10(3):221-237.

(47) Wickman GR, Julian L, Mardilovich K, Schumacher S, Munro J, Rath N, et al. Blebs produced by actin-myosin contraction during apoptosis release damage-associated molecular pattern proteins before secondary necrosis occurs. Cell Death Differ. 2013;20(10):1293-1305.

(48) Galluzzi L, Zamzami N, de La Motte Rouge T, Lemaire C, Brenner C, Kroemer G. Methods for the assessment of mitochondrial membrane permeabilization in apoptosis. Apoptosis. 2007;12(5):803-813.

(49) Pyo JO, Nah J, Jung YK. Molecules and their functions in autophagy. Exp Mol Med. 2012;44(2):73-80.

(50) Hitomi J, Christofferson DE, Ng A, Yao J, Degterev A, Xavier RJ, et al. Identification of a molecular signaling network that regulates a cellular necrotic cell death pathway. Cell. 2008;135(7):1311-1323.

(51) Xie Z, Klionsky DJ. Autophagosome formation: core machinery and adaptations. Nat Cell Biol. 2007;9(10):1102-1109.

(52) Maiuri MC, Zalckvar E, Kimchi, A, Kroemer, G. Self-eating and Self-killing: crosstalk between autophagy and apoptosis. Molecular Cell Biology. 2007;8(9):741-752.

(53) Gozuacik D, Kimchi A. Autophagy as a cell death and tumor suppressor mechanism. Oncogene. 2004;23(16):2891-2906.

(54) Garcia-Mata R, Gao YS, Sztul E. Hassles with taking out the garbage: aggravating aggresomes. Traffic. 2002;3(6):388-396.

(55) Galluzzi L, Kroemer G. Necroptosis: a specialized pathway of programmed necrosis. Cell. 2008;135(7):1161-1163.

(56) Silva MT. Secondary necrosis: the natural outcome of the complete apoptotic program. FEBS Lett. 2010;584(22):4491-4499.

(57) Wlodkowic D, Skommer J, Darzynkiewicz Z. Cytometry of apoptosis. Historical perspective and new advances. Exp Oncol. 2012;34(3):255-262.

(58) Movassagh M, Foo RS. Simplified apoptotic cascades. Heart Fail Rev. 2008;13(2):111-119.

(59) Blatt NB, Glick GD. Signaling pathways and effector mechanisms pre-programmed cell death. Bioorg Med Chem. 2001;9(6):1371-1384.

(60) Pradelli LA, Beneteau M, Ricci JE. Mitochondrial control of caspase-dependent and -independent cell death. Cell Mol Life Sci. 2010;67(10):1589-1597.

(61) Wu CC, Bratton SB. Regulation of the intrinsic apoptosis pathway by reactive oxygen species. Antioxid Redox Signal. 2013;19(6):546-558.

(62) Brentnall M, Rodriguez-Menocal L, De Guevara RL, Cepero E, Boise LH. Caspase-9, caspase-3 and caspase-7 have distinct roles during intrinsic apoptosis. BMC Cell Biol. 2013;14:32-2121-14-32.

(63) Cregan SP, Dawson VL, Slack RS. Role of AIF in caspase-dependent and caspase-independent cell death. Oncogene. 2004;23(16):2785-2796.

(64) Soriano ME, Scorrano L. Traveling Bax and forth from mitochondria to control apoptosis. Cell. 2011;145(1):15-17.

(65) Donovan M, Cotter TG. Control of mitochondrial integrity by Bcl-2 family members and caspase-independent cell death. Biochim Biophys Acta. 2004;1644:133-147.

(66) Cottet-Rousselle C, Ronot X, Leverve X, Mayol JF. Cytometric assessment of mitochondria using fluorescent probes. Cytometry A. 2011;79(6):405-425.

(67) Murphy MP. How mitochondria produce reactive oxygen species. Biochem J. 2009;417(1):1-13.

(68) Mammucari C, Rizzuto R. Signaling pathways in mitochondrial dysfunction and aging. Mech Ageing Dev. 2010;131:536-543.

(69) Kussmaul L, Hirst J. The mechanism of superoxide production by NADH:ubiquinone oxidoreductase (complex I) from bovine heart mitochondria. Proc Natl Acad Sci U S A. 2006;103(20):7607-7612.

(70) Giorgio M, Migliaccio E, Orsini F, Paolucci D, Moroni M, Contursi C, et al. Electron transfer between cytochrome c and p66Shc generates reactive oxygen species that trigger mitochondrial apoptosis. Cell. 2005;122(2):221-233.

(71) Matsunami T, Sato Y, Hasegawa Y, Ariga S, Kashimura H, Sato T, et al. Enhancement of reactive oxygen species and induction of apoptosis in streptozotocin-induced diabetic rats under hyperbaric oxygen exposure. Int J Clin Exp Pathol. 2011;4(3):255-266.

(72) Mesquita FS, Dyer SN, Heinrich DA, Bulun SE, Marsh EE, Nowak RA. Reactive oxygen species mediate mitogenic growth factor signaling pathways in human leiomyoma smooth muscle cells. Biol Reprod. 2010;82(2):341-351.

(73) O'Donnell BV, Tew DG, Jones OT, England PJ. Studies on the inhibitory mechanism of iodonium compounds with special reference to neutrophil NADPH oxidase. Biochem J. 1993;290:41-49.

(74) Hawkins BJ, Madesh M, Kirkpatrick CJ, Fisher AB. Superoxide flux in endothelial cells via the chloride channel-3 mediates intracellular signaling. Mol Biol Cell. 2007;18(6):2002-2012.

(75) Liu Y, Fiskum G, Schubert D. Generation of reactive oxygen species by the mitochondrial electron transport chain. J Neurochem. 2002;80(5):780-787.

(76) Seo BB, Marella M, Yagi T, Matsuno-Yagi A. The single subunit NADH dehydrogenase reduces generation of reactive oxygen species from complex I. FEBS Lett. 2006;580(26):6105-6108.

(77) Pollak N, Dolle C, Ziegler M. The power to reduce: pyridine nucleotides--small molecules with a multitude of functions. Biochem J. 2007;402(2):205-218.

(78) Sun F, Dai C, Xie J, Hu X. Biochemical issues in estimation of cytosolic free NAD/NADH ratio. PLoS One. 2012;7(5):e34525-e34534.

(79) Ying W. NAD+/NADH and NADP+/NADPH in cellular functions and cell death: regulation and biological consequences. Antioxid Redox Signal. 2008;10(2):179-206.

(80) Oka S, Hsu CP, Sadoshima J. Regulation of cell survival and death by pyridine nucleotides. Circ Res. 2012;111(5):611-627.

(81) Xia W, Wang Z, Wang Q, Han J, Zhao C, Hong Y, et al. Roles of NAD(+) / NADH and NADP(+) / NADPH in cell death. Curr Pharm Des. 2009;15(1):12-19.

(82) Gendron MC, Schrantz N, Metivier D, Kroemer G, Maciorowska Z, Sureau F, et al. Oxidation of pyridine nucleotides during Fas- and ceramide-induced apoptosis in Jurkat cells: correlation with changes in mitochondria, glutathione depletion, intracellular acidification and caspase 3 activation. Biochem J. 2001;353:357-367.

(83) Bao Q, Shi Y. Apoptosome: a platform for the activation of initiator caspases. Cell Death Differ. 2007;14(1):56-65.

(84) Abraham MC, Shaham S. Death without caspases, caspases without death. Trends Cell Biol. 2004;14(4):184-193.

(85) Boatright KM, Salvesen GS. Mechanisms of caspase activation. Curr Opin Cell Biol. 2003;15(6):725-731.

(86) Lorenzo HK, Susin SA. Mitochondrial effectors in caspase-independent cell death. FEBS Lett. 2004;557:14-20.

(87) Calligaris D, Verdier-Pinard P, Devred F, Villard C, Braguer D, Lafitte D. Microtubule targeting agents: from biophysics to proteomics. Cell Mol Life Sci. 2010;67(7):1089-1104.

(88) Downing KH. Structural basis for the interaction of tubulin with proteins and drugs that affect microtubule dynamics. Annu Rev Cell Dev Biol. 2000;16:89-111.

(89) Chua YS, Chua YL, Hagen T. Structure activity analysis of 2-methoxyestradiol analogues reveals targeting of microtubules as the major mechanism of antiproliferative and proapoptotic activity. Mol Cancer Ther. 2010;9(1):224-235.

(90) Tevaarwerk AJ, Holen KD, Alberti DB, Sidor C, Arnott J, Quon C, et al. Phase I trial of 2-methoxyestradiol NanoCrystal dispersion in advanced solid malignancies. Clin Cancer Res. 2009;15(4):1460-1465.

(91) Matei D, Schilder J, Sutton G, Perkins S, Breen T, Quon C, et al. Activity of 2 methoxyestradiol (Panzem NCD) in advanced, platinum-resistant ovarian cancer and primary peritoneal carcinomatosis: a Hoosier Oncology Group trial. Gynecol Oncol. 2009;115(1):90-96.

(92) Harrison MR, Hahn NM, Pili R, Oh WK, Hammers H, Sweeney C, et al. A phase II study of 2-methoxyestradiol (2ME2) NanoCrystal(R) dispersion (NCD) in patients with taxane-refractory, metastatic castrate-resistant prostate cancer (CRPC). Invest New Drugs. 2011;29(6):1465-1474.

(93) Bruce JY, Eickhoff J, Pili R, Logan T, Carducci M, Arnott J, et al. A phase II study of 2-methoxyestradiol nanocrystal colloidal dispersion alone and in combination with sunitinib malate in patients with metastatic renal cell carcinoma progressing on sunitinib malate. Invest New Drugs. 2012;30(2):794-802.

(94) Stander A, Joubert F, Joubert A. Docking, synthesis, and in vitro evaluation of antimitotic estrone analogs. Chem Biol Drug Des. 2011;77(3):173-181.

(95) Kamath K, Okouneva T, Larson G, Panda D, Wilson L, Jordan MA. 2-Methoxyestradiol suppresses microtubule dynamics and arrests mitosis without depolymerizing microtubules. Mol Cancer Ther. 2006;5(9):2225-2233.

(96) C, Lottering ML, Steffens F, Joubert A. In vitro effects of 2-methoxyestradiol on MCF-12A and MCF-7 cell growth, morphology and mitotic spindle formation. Cell Biochem Funct. 2008;26(5):632-642.

(97) Voster CJJ, Joubert AM. In vitro effects of 2-methoxyestradiol-bis-sulphamate on the non-tumorigenic MCF-12A cell line. Cell Biochem Funct. 2010;28:412-419.

(98) Joubert A, Marais S. Influence of 2-methoxyestradiol on cell morphology and Cdc2 kinase activity in WHCO3 esophageal carcinoma cells. Biomed Res. 2007;28(1):9-16.

(99) Purohit A, Hejaz HA, Walden L, MacCarthy-Morrogh L, Packham G, Potter BV, et al. The effect of 2-methoxyoestrone-3-O-sulphamate on the growth of breast cancer cells and induced mammary tumours. Int J Cancer. 2000;85(4):584-589.

(100) Newman SP, Ireson CR, Tutill HJ, Day JM, Parsons MF, Leese MP, et al. The role of 17beta-hydroxysteroid dehydrogenases in modulating the activity of 2-methoxyestradiol in breast cancer cells. Cancer Res. 2006;66(1):324-330.

(101) Zhu BT, Conney AH. Is 2-methoxyestradiol an endogenous estrogen metabolite that inhibits mammary carcinogenesis? Cancer Res. 1998;58(11):2269-2277.

(102) Joubert A, Maritz C, Joubert F. Bax/Bcl-2 expression levels of 2-methoxyestradiol-exposed esophageal cancer cells. Biomed Res. 2005;26(3):131-134.

(103) Joubert A, Marais S. In vitro effects of 2-methoxyestradiol on cell morphology and Cdc2 Kinase activity in SNO oesophageal carcinoma cells. Cell Biochem Funct. 2007;25(3):357-362.

(104) Mooberry SL. Mechanism of action of 2-methoxyestradiol: new developments. Drug Resistance Updates. 2003;6(6):355-361.

(105) Visagie MH, Joubert AM. In vitro effects of 2-methoxyestradiol-bis-sulphamate on reactive oxygen species and possible apoptosis induction in a breast adenocarcinoma cell line. Cancer Cell Int. 2011;11(1):43-49.

(106) Liu Q, Jin W, Zhu Y, Zhou J, Lu M, Zhang Q. Synthesis of 3'-methoxy-E-diethylstilbestrol and its analogs as tumor angiogenesis inhibitors. Steroids. 2012;77(5):419-423.

(107) Leese MP, Leblond B, Newman SP, Purohit A, Reed MJ, Potter BV. Anti-cancer activities of novel D-ring modified 2-substituted estrogen-3-O-sulfamates. J Steroid Biochem Mol Biol. 2005;94:239-251.

(108) Chander SK, Foster PA, Leese MP, Newman SP, Potter BV, Purohit A, et al. In vivo inhibition of angiogenesis by sulphamoylated derivatives of 2-methoxyoestradiol. Br J Cancer. 2007;96(9):1368-1376.

(109) Stander BA, Joubert F, Tu C, Sippel KH, McKenna R, Joubert AM. Signaling pathways of ESE-16, an antimitotic and anticarbonic anhydrase estradiol analog, in breast cancer cells. PLoS One. 2013;8(1):e53853-e53869.

(110) Theron AE, Nolte EM, Lafanechere L, Joubert AM. Molecular crosstalk between apoptosis and autophagy induced by a novel 2-methoxyestradiol analogue in cervical adenocarcinoma cells. Cancer Cell Int. 2013;13(1):87-105.

(111) Supuran CT, Scozzafava A. Carbonic anhydrases as targets for medicinal chemistry. Bioorg Med Chem. 2007;15(13):4336-4350.

(112) Chiche J, Ilc K, Laferriere J, Trottier E, Dayan F, Mazure NM, et al. Hypoxia-inducible carbonic anhydrase IX and XII promote tumor cell growth by counteracting acidosis through the regulation of the intracellular pH. Cancer Res. 2009;69(1):358-368.

(113) Genis C, Sippel KH, Case N, Cao W, Avvaru BS, Tartaglia LJ, et al. Design of a carbonic anhydrase IX active-site mimic to screen inhibitors for possible anticancer properties. Biochemistry. 2009;48(6):1322-1331.

(114) Thiry A, Dogne JM, Masereel B, Supuran CT. Targeting tumor-associated carbonic anhydrase IX in cancer therapy. Trends Pharmacol Sci. 2006;27(11):566-573.

(115) Helmlinger G, Sckell A, Dellian M, Forbes NS, Jain RK. Acid production in glycolysis-impaired tumors provides new insights into tumor metabolism. Clin Cancer Res. 2002;8(4):1284-1291.

(116) Bey E, Alexander J, Whitcutt JM, Hunt JA, Gear JH. Carcinoma of the esophagus in Africans: establishment of a continuously growing cell line from a tumor specimen. In Vitro. 1976;12(2):107-114.

(117) Strober W. Trypan blue exclusion test of cell viability. Curr Protoc Immunol. 2001;DOI: 10.1002/0471142735.ima03bs21.

(118) Mqoco T, Marais S, Joubert A. Influence of estradiol analogue on cell growth, morphology and death in esophageal carcinoma cells. Biocell. 2010;34(3):113-120.

(119) Visagie MH, Joubert AM. The in vitro effects of 2-methoxyestradiol-bis-sulphamate on cell numbers, membrane integrity and cell morphology, and the possible induction of apoptosis and autophagy in a non-tumorigenic breast epithelial cell line. Cell Mol Biol Lett. 2010;15(4):564-581.

(120) Stander XX, Stander BA, Joubert AM. In vitro effects of an in silico-modelled 17beta-estradiol derivative in combination with dichloroacetic acid on MCF-7 and MCF-12A cells. Cell Prolif. 2011;44(6):567-581.

(121) Fischer AH, Jacobson KA, Rose J, Zeller R. Hematoxylin and eosin staining of tissue and cell sections. CSH Protoc. 2008:pdb.prot4986.

(122) Van Zijl C, Lottering ML, Steffens F, Joubert A. In vitro effects of 2-methoxyestradiol on MCF-12A and MCF-7 cell growth, morphology and mitotic spindle formation. Cell Biochem Funct. 2008;26(5):632-642.

(123) Visagie M, Mqoco T, Joubert A. Sulphamoylated estradiol analogue induces antiproliferative activity and apoptosis in breast cell lines. Cell Mol Biol Lett. 2012;17(4):549-558.

(124) Visagie MH, Joubert AM. 2-Methoxyestradiol-bis-sulfamate induces apoptosis and autophagy in a tumorigenic breast epithelial cell line. Mol Cell Biochem. 2011;357:343-352.

(125) Hurbain I, Sachse M. The future is cold: cryo-preparation methods for transmission electron microscopy of cells. Biol Cell. 2011;103(9):405-420.

(126) Krysko DV, Vanden Berghe T, D'Herde K, Vandenabeele P. Apoptosis and necrosis: detection, discrimination and phagocytosis. Methods. 2008;44(3):205-221.

(127) Semwogerere D, Weeks ER. Confocal Microscopy. Encyclopedia of Biomaterials and Biomedical Engineering. 2005;1-10.

(128) Ibrahim SF, van den Engh G. Flow cytometry and cell sorting. Adv Biochem Eng Biotechnol. 2007;106:19-39.

(129) Shvets E, Elazar Z. Flow cytometric analysis of autophagy in living mammalian cells. Methods Enzymol. 2009;452:131-141.

(130) Brown M, Wittwer C. Flow cytometry: principles and clinical applications in hematology. Clin Chem. 2000;46:1221-1229.

(131) Pozarowski P, Darzynkiewicz Z. Analysis of cell cycle by flow cytometry. Methods Mol Biol. 2004;281:301-311.

(132) Chauhan D, Li G, Sattler M, Podar K, Mitsiades C, Mitsiades N, et al. Superoxide-dependent and -independent mitochondrial signaling during apoptosis in multiple myeloma cells. Oncogene. 2003;22(40):6296-6300.

(133) Nkandeu DS, Mqoco TV, Visagie MH, Stander BA, Wolmarans E, Cronje MJ, et al. In vitro changes in mitochondrial potential, aggresome formation and caspase activity by a novel 17-beta-estradiol analogue in breast adenocarcinoma cells. Cell Biochem Funct. 2013;31(7):566-574.

(134) Wolmarans E, Mqoco TV, Stander A, Nkandeu SD, Sippel K, McKenna R, et al. Novel estradiol analogue induces apoptosis and autophagy in esophageal carcinoma cells. Cell Mol Biol Lett. 2014;Epub ahead of print.

(135) Pribluda VS, Gubish ER,Jr, Lavallee TM, Treston A, Swartz GM, Green SJ. 2-Methoxyestradiol: an endogenous antiangiogenic and antiproliferative drug candidate. Cancer Metastasis Rev. 2000;19:173-179.

(136) Stander BA, Marais S, Vorster CJ, Joubert AM. In vitro effects of 2-methoxyestradiol on morphology, cell cycle progression, cell death and gene expression changes in the tumorigenic MCF-7 breast epithelial cell line. J Steroid Biochem Mol Biol. 2010;119:149-160.

(137) Thaver V, Lottering M-, van Papendorp D, Joubert A. In vitro effects of 2-methoxyestradiol on cell numbers, morphology, cell cycle progression, and apoptosis induction in oesophagealcarcinoma cells. Cell Biochem Funct. 2009;27(4):205-210.